DOLOMIZATION OF THE CATOCHE FORMATION, DANIEL'S HARBOUR, WESTERN NEWFOUNDLAND, CANADA

EBUBE AZOMANI

DOLOMITIZATION OF THE CATOCHE FORMATION, DANIEL'S HARBOUR, WESTERN NEWFOUNDLAND, CANADA

By

© Ebube Azomani

A thesis submitted to the

School of Graduate Studies

In partial fulfillment of the

Requirements for the degree of

Master of Science

Department of Earth Science

Memorial University

June, 2012

St. John's, Newfoundland

ABSTRACT

The Catoche Formation of the St. George Group in western Newfoundland consists of early Ordovician (Arenigian) shallow marine platform carbonates (~ 160 m thick), which were extensively dolomitized during the course of their diagenetic history. The dolomite occurs as both replacement and pore-filling cements and are a major control on porosity distribution in the formation. The origin and diagenetic history of the Catoche dolomites at Daniel's Harbour were analyzed in comparison to equivalent successions at Port au Choix and Port au Port Peninsula to assay the reservoir potential of Catoche dolomites in western Newfoundland. Petrographic examination identified at least three generations of dolomite in the Catoche Formation, which are: (1) an early replacement sub- to euhedral micritic dolomite (< 4 μm – 30 μm, D1), (2) eu- to subhedral dolomite (70 μm – 1 mm) often with cloudy cores and clear rims (D2), and (3) subhedral to anhedral saddle dolomite cement (200 μm – 3 mm, D3). The micritic dolomite (D1) exhibits dull cathodoluminescence (CL) under the cathodoluminoscope, whereas dolomite D2 exhibits consistent concentric CL zonation. Some subhedral crystals of D3 appear zoned both in plane polarized light and cathodoluminoscope, otherwise D3 exhibits a dull CL. Stoichiometric dolomite occurs in all three generations with D2 as the dominant dolomite by abundance.

The low strontium (47 ± 25 ppm) content coupled with depleted $\delta^{18}O$ value of dolomitizing fluids (–10 to –11.2‰VSMOW) and near-micritic grain size, suggests an early precipitation of dolomite D1 at low temperatures in near-surface conditions from solutions likely formed by mixing of early Ordovician sea and meteoric waters. In contrast, microthermometric measurements of primary two-phase fluid inclusions in dolomite D2 (homogenization temperatures (T_h), of 102 to 168°C with a salinity range of 19.8 to 25 eq. wt% NaCl) and dolomite D3 (T_h of 158 to 190°C with a salinity range of 20.2 to 22.2 eq. wt% NaCl), suggest

that both dolomite generations were generated in mid to deep burial settings from high salinity, low-temperature hydrothermal fluids likely under suboxic conditions. This is consistent with the low Sr concentrations for dolomites D2 (36.4 ± 8 ppm) and D3 (38.7 ± 9 ppm), $\delta^{18}O$ values of dolomitizing fluids for D2 (+2.1 to +8.1‰, VSMOW) and D3 (+6 to +8.1‰, VSMOW), coupled with Fe contents of D2 (1684 ± 1096 ppm) and D3 (1783.7 ± 618 ppm) and Mn for D2 (131.2 ± 50) and D3 (197.5 ± 55 ppm).

ΣREE and shale normalized values of Catoche carbonates indicate enrichment in rare earth element (REE) concentration of the earliest calcite (C1) relative to those of Arenig seawater, and the REE_{SN} profiles of the dolomite generations mimic that of calcite C1. Evaluation of shale normalized Cerium (Ce) and Lanthanum (La) anomalies of the Catoche dolomite(s) indicate they precipitated in equilibrium with slightly oxic to suboxic source fluids and chondrite normalized Europium (Eu) anomalies suggest similar source fluids for D2 and D3 dolomites regardless of differential in mean homogenization temperatures. Results of fluid inclusion gas analysis are consistent with petrographic features and geochemical compositions and support the exclusion of magmatic fluids during dolomitization.

Visual estimates of porosity (ϕ) from thin sections indicate that it varies from < 1 to about 12 % with four porous ($\phi \geq 4$) horizons at approximately 6m, 70m, 120m and 150m from the top of the succession and about 4m, 40m, 4m and 4m thick respectively. Vugs and intercrystalline pores are two types of porosity associated with the dolomites with the latter being the dominant type and associated mainly with dolomite D2. The porosity coupled with appropriate thermal maturation, occurrence of suitable traps, and evidence of hydrocarbon accumulation, suggests that the Catoche dolomites are potential reservoirs and suitable hydrocarbon targets.

This work is dedicated to;

Mrs. A.U Azomani., Dr. Hosan, M. Azomani and Esther, A. Azomani.

ACKNOWLEDGEMENTS

The author wishes to express his sincere appreciation to Prof. Karem Azmy for his supervision of this study, field assistance and critical reading of the thesis. Thanks are extended to the Petroleum Exploration Enhancement Program (PEEP) for funding this project. Special thanks also goes to Dr. Nigel Blamey of Memorial University (Newfoundland), for his assistance in the analysis of fluid inclusion gases used in this study and Prof. Uwe Brand from Brock University (Ontario), for his constructive comments that contributed to the improvement of the manuscript.

The author also wishes to thank Allison Pye (Stable Isotope Lab) and Pam King (trace element lab) for technical assistance in chemical analyses. Gillespie Helen (ultraviolet-fluorescence microspectrophotometry Lab) also provided assistance with UV micro-spectrometry.

TABLE OF CONTENTS

LIST OF FIGURES

LIST OF TABLES

CHAPTER ONE

INTRODUCTION

1.1 Scope and Purpose of Study

The Lower Ordovician St. George Group in western Newfoundland is a succession of alternating subtidal to peritidal platform carbonates (~ 500 m thick), which were affected by multiphase dolomitization events during the course of its diagenetic history. The St George Group consists of four formations and unconformably overlies the Berry Head Formation of the Port au Port Group. The St. George unconformity represents the upper boundary of the St. George Group which is overlain by the Table Head Group. Hydrothermal fluids played an important role in the dolomitization process and the resulting hydrothermal dolomites exhibit a major control on the distribution of porosity in the St. George Group carbonates (knight and James, 1987; Knight et al., 1991; Azmy et al., 2008, 2009; Conliffe et al., 2009, 2010; Azmy and Conliffe, 2010). Hydrothermal dolomites are formed under mid- to deep burial conditions from high salinity fluids at temperatures higher than those of the host formation (e.g. Davies and Smith, 2006).

Dolomitization of carbonates in sedimentary sequences has been the focus of many studies particularly in the last few decades as it is a significant diagenetic process that influences porosity development in carbonate reservoirs. Several models have been put forth to explain the mechanism(s) via which dolomitization occurs as no consensus exists regarding the general chemical conditions required for dolomitization. However, all models must explain the source of magnesium and method(s) of pumping dolomitizing fluids through the pore spaces of rocks.

The occurrence of major hydrocarbon accumulations in Paleozoic hydrothermal dolomites on the eastern Laurentian margin have recently directed studies to western Newfoundland (cf. Haywick., 1984; Lane., 1990; Cooper et al., 2001; Lavoie et al., 2005; Azmy et al., 2008, 2009; Conliffe et al., 2009; Azmy and Conliffe, 2010). The current study focuses on the dolomitization of the Catoche Formation (upper St. George Group) at Daniel's Harbour on the Northern Peninsula in western Newfoundland and the main objectives are:

1. To investigate the petrographic and geochemical attributes of the Catoche dolomites
2. To decipher and describe the origin and diagenetic history of the dolomites in the formation.
3. To better understand the porosity – dolomitization relationship in the succession, and
4. To correlate results of this study with results from other sections of the Catoche Formation across western Newfoundland to better understand the pattern of porosity distribution.

1.2 Geological Setting

The St. George Group of western Newfoundland extends approximately 400 km from the Port au Port Peninsula in the south to Cape Norman on the Great Northern Peninsula (Fig 1.1). It consists mainly of an alternating succession of dolomitized early Ordovician (Tremadocian to Arenigian) subtidal to peritidal carbonates (limestones and dolostones). These warm, shallow-water early Ordovician carbonates are divided into two third-order sequences (Knight and James, 1987).

The Laurentian paleoplate developed by active rifting during the late Precambrian around 570 to 550 Ma (Cawood et al., 2001) and formed a passive pre-platform shelf that was covered

by clastics (James et al., 1989; Cawood et al; 2001). A major transgression along the eastern platform margin of Laurentia during the early Ordovician resulted in the accumulation of thick carbonate deposits which formed a carbonate platform (Wilson et al., 1992; Smith, 2006; Knight et al., 2007, 2008). High-energy Cambrian carbonates of the Port au Port Group were buried by low-energy early Ordovician carbonates of the St. George Group in western Newfoundland (Knight et al., 2007, 2008). The St. George Group from bottom to top consists of the Watts Bight, Boat Harbour, Catoche and Aguathuna Formations (Fig 1.2) and represents an alternating succession of subtidal-peritidal-subtidal-peritidal carbonate sediments respectively (Haywick, 1984; Lane, 1990; Knight et al., 2008). The Watts Bight and Boat Harbour Formations represent the lower Tremadocian megacycle whereas the Catoche and Aguathuna Formations represent the upper Arenigian megacycle (Knight and James, 1987; Conliffe et al., 2010; Azmy and Conliffe, 2010). Subsequent tectonic activity led to the uplift, exposure and erosion of the carbonate platform resulting in the St. George and Boat Harbor unconformities, with the former marking the upper boundary of the St. George Group and a shift from a passive margin to an active foreland basin (James et al., 1989; Cooper et al., 2001; Knight et al., 1991, 2007;). Both unconformities also mark the end of two megacycles (Knight and James, 1987).

The Catoche Formation rests conformably on the Barbace Cove Member of the Boat Harbour Formation and is overlain by the Aguathuna Formation. It is about 160 m thick at Port au Choix (its type area) and consists of well-bedded, fossiliferous, bioturbated gray lower limestone about 120 m thick and an upper dolostone about 40 m thick. However, on the Port au Port Peninsula, the Catoche Formation in ascending order, consists of a lower limestone (~70 m), a middle dolostone (~ 50 m), and the Costa Bay Member (~ 40 m). The Costa Bay Member of the Catoche Formation is an interval of distinctively white limestone which occurs on the Port au

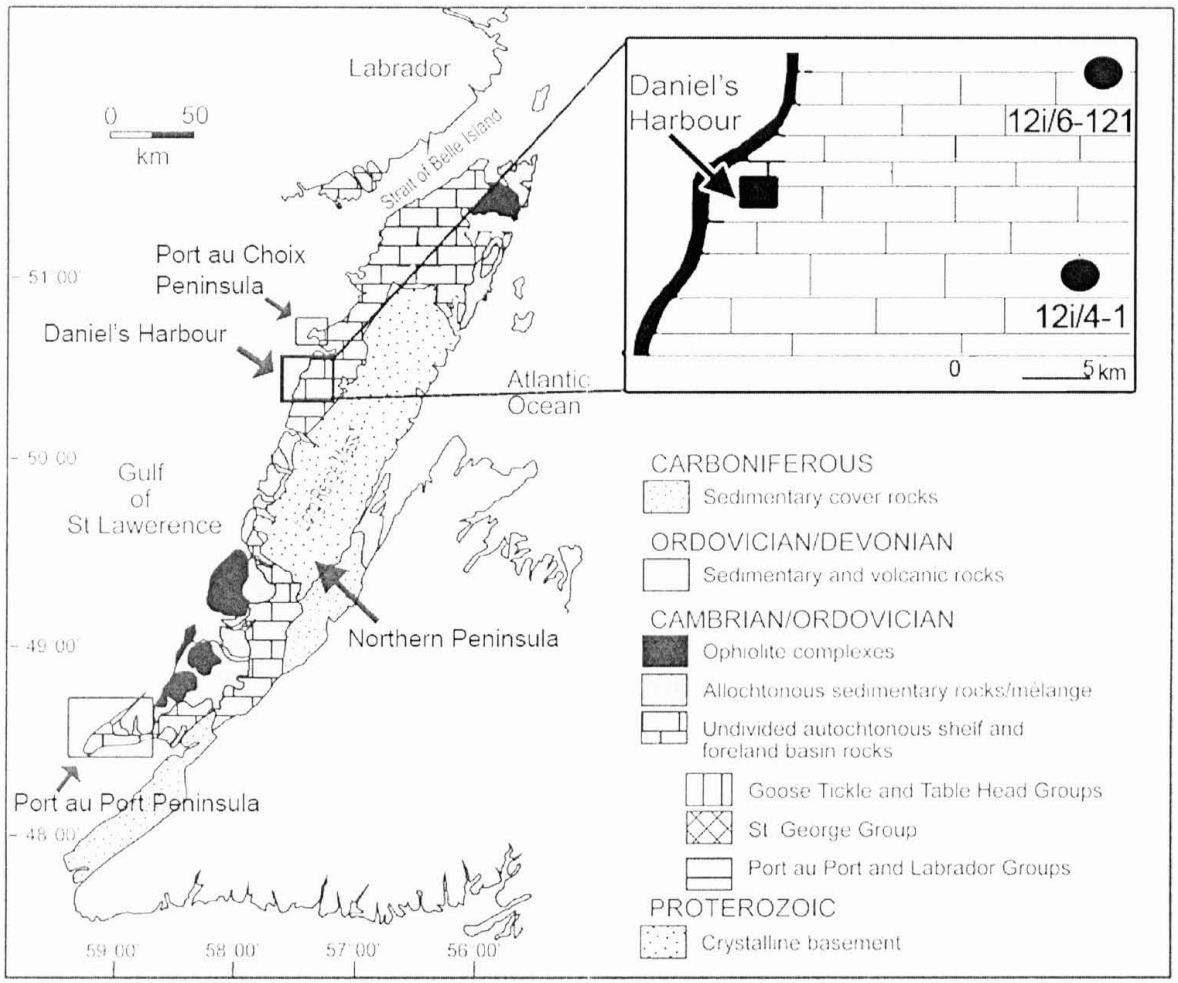

Fig 1.1 Regional geologic map of western Newfoundland showing approximate locations of investigated cores 12i/4-1 and 12i/6-121 near Daniels Harbour and the locations of the counterpart sections in Port au Choix and Port au Port Peninsula (modified from Zhang and Barnes, 2004)).

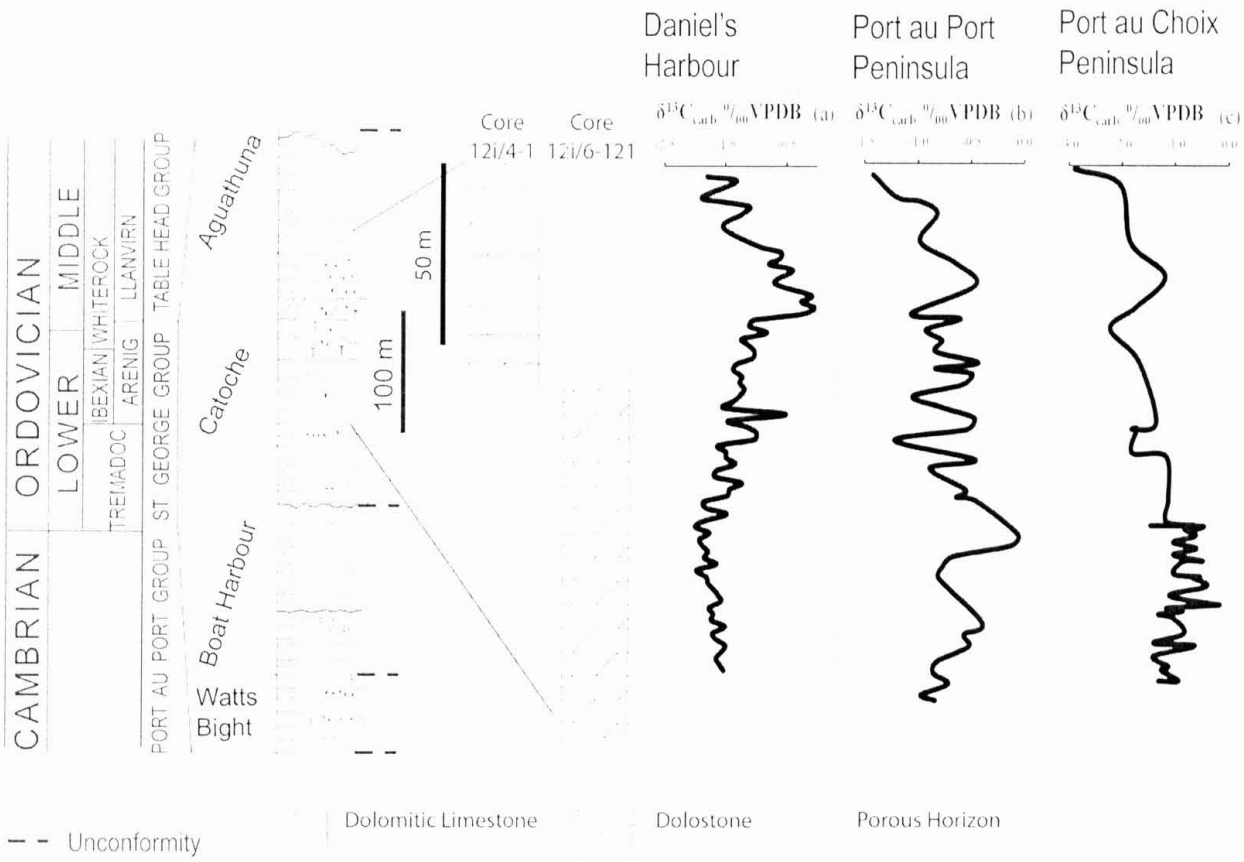

Fig 1.2 Simplified stratigraphic diagram of the St George Group (in part after Knight et a., 2007 and Azmy and Conliffe, 2010), showing the $\delta^{13}C$ profiles and porosity variations within the Catoche carbonates at (A) Daniel's Harbour (current study), (B) Port au Port Peninsula (Conliffe et al, 2012), (C) Port au Choix (Greene, 2008).

Port Peninsula (and adjacent areas) and on the three thrust stacks that deform the shelf rocks (Knight et al., 2007). It has been mapped across western Newfoundland and correlated with the upper (~ 40 m) dolostone of the succession at Port au Choix (Knight, 1986, 1987, 1994, 1997; Baker and Knight, 1993; Knight et al., 2007). The upper ~40 m of the Catoche Formation at Port au Choix is a series of cyclic, shallowing upward, meter-scale grainstones interpreted as peloidal sand shoals that have been extensively dolomitized (Knight, 1991; Knight, et al., 1991; Baker and Knight, 1993; Knight et al., 2007). The Catoche Formation is believed to be Arenigian in age (Knight et al., 2007; Ji, 1989; Ji et al., 1989; Boyce, 1989; Lane, 1990; Greene, 2008).

1.3 Chemistry of Dolomite (Overview)

Dolomite is a highly ordered calcium-magnesium carbonate mineral with crystals built up of layers of cations (Ca^{2+}, Mg^{2+}) alternating with anions (CO_3^{2-}) perpendicular to the c-axis direction with half of the cation layers as magnesium layers (Tucker and Wright, 1990). Dolomite is chemically represented as $CaMg(CO_3)_2$ with equal molar proportions of calcium and magnesium (stoichiometric dolomite), but its composition varies from $Ca_{1.16}Mg_{0.84}(CO_3)_2$ to $Ca_{0.96}Mg_{1.04}(CO_3)_2$ (Land, 1985). Three factors contribute to this non-stoichiometric departure from ideal composition: (1) the degree to which calcium (Ca) and magnesium (Mg) are segregated into their respective layers, (2) presence of excess Ca which is accommodated in the Mg layers, (3) other cations (Fe, Sr, Na, and Mn) substitute for Ca in dolomites (Veizer et al., 1978). Departures from ideal composition diminish the ordering of the crystals (Carpenter, 1980) and increase the solubility of the mineral (Boggs, 2009).

Dolomites form either by direct precipitation from aqueous solutions or by alteration of calcium bearing carbonate mineral as represented by the following chemical equations:

1. $Ca^{2+}_{(aq)} + Mg^{2+}_{(aq)} + 2CO_3^{2-}{}_{(aq)} \rightarrow CaMg(CO_3)_{2\,(solid)}$ Direct Precipitation

(Dolomite)

2. $2CaCO_{3\,(SOLID)} + Mg^{2+}_{(aq)} \rightarrow CaMg(CO_3)_{2(solid)} + Ca^{2+}_{(aq)}$ Alteration of carbonate

(Dolomite)

Though direct precipitation of dolomite from aqueous solution is possible, it rarely occurs at surface temperatures and pressure even though seawater (the main source of magnesium) is supersaturated with respect to dolomite (Tucker and Wright, 1990; Boggs, 2009). Limitations to direct precipitation of dolomite at surface temperature and pressure include;

1. Rapid crystallization from super saturated solutions impede the segregations of Ca^{2+} and Mg^{2+} into their respective layers such that magnesium layers are contaminated with Ca^{2+} and vice versa which results in the precipitation of disordered Ca-Mg carbonate (Folk, 1975)
2. High ionic strength of seawater (Folk and Land, 1975)
3. Mg^{+2} hydration (Lippman, 1973)
4. Low activity of (CO_3^{2-}) relative to Ca^{2+} and Mg^{2+} in most natural solutions (Lippman, 1973)
5. Dolomite precipitates from CO_3^{-2} and not HCO^{3-} like calcite or aragonite (Tucker and Wright, 1990)
6. Aragonite and calcite are precipitated preferentially because dolomite is highly ordered (Tucker and Wright, 1990).

However, these limitations to dolomite precipitation from seawater can be overcome by evaporation, lowering the SO_4^{2-} content, and increase in temperature (Tucker and Wright, 1990).

Dilution of natural aqueous solutions such as mixing of seawater or brine with meteoric water can produce dolomites (Tucker and Wright, 1990). Though simple dilution of seawater or brine with meteoric water is not enough to precipitate dolomite directly from solution, the resulting solution is potent enough to alter deposited carbonate minerals it comes in contact with and thus produce dolomites as represented by chemical equation 2 above. This process of altering prior carbonates to produce dolomites is known as dolomitization. Also the mixing of natural aqueous solutions, which invariably causes dilution of the supersaturated solution, reduces the rate of crystallization which creates conditions that favour the development of highly ordered dolomite crystals (Morrow, 1982; Tucker and Wright, 1990). The occurrence of dolomite in organic-rich marine sediments (organogenic dolomite) made scientists believe that chemical processes triggered by sulfate reducing bacteria could cause precipitation of dolomite. However, the actual role of the sulfate reducing bacteria in the low temperature formation of dolomite and the specific mechanism of dolomitization involving sulfate reducing bacteria is yet to be demonstrated (Compton, 1988; Yvonne et al, 2000)

Dolomites contain elements such as strontium (Sr), iron (Fe) and manganese (Mn) which can provide useful insight to the nature of dolomitizing fluids and environmental conditions during precipitation. Also, the isotopic composition of elements like carbon (C), and oxygen (O) in dolomite can be used to infer the nature of dolomitizing fluids, redox conditions and degree of organic productivity in environment of deposition. Sr and O-isotope composition of dolomites reflects the nature of the dolomitizing fluids whereas Fe, Mn, and C may reflect redox conditions and degree of organic productivity in environment of deposition (Tucker and Wright, 1990; Boggs, 2009). However the sole use of elements in the interpretation of paleoenvironmental conditions is discouraged, instead geochemical data must be supported by data from other

approaches in geology such as petrography, microthermometry, cathodoluminescence, and fluid inclusion gas analyses. Theoretical considerations suggest that dolomite precipitation is favored by high Mg^{2+}/Ca^{2+} ratios, low Ca^{2+}/CO_3^{2-} ratios, low salinity, concentration of dissolved SO_4^{2-} and high temperatures (Baker and Kastner, 1981; Machel and Mountjoy, 1986).

1.4 Dolomite and Dolomitization

Dolomite is a highly ordered mineral that is very difficult to precipitate at temperatures below 100°C. It can precipitate directly from aqueous solutions (primary dolomite) or formed by the alteration of calcium bearing carbonate minerals (diagenetic dolomite), via a process known as dolomitization. Dolomitization involves the partial replacement of Ca^{2+} by Mg^{2+} in the crystal lattice of the precursor mineral, hence availability of Mg^{2+} is a prerequisite for dolomitization. Though direct precipitation of dolomite from aqueous solution is possible, it rarely precipitates at near-surface temperatures due to kinetic limitations discussed earlier. Consequently, a huge proportion of dolomite in the geologic record is diagenetic and several models have been put forth to explain how these diverse diagenetic dolomites formed as several methods of dolomitization exists, hence there is no one unique model to explain all dolomite.

Dolomitization models are based mainly on various conditions under which dolomites form in modern environments. However, all models must account for the source of Mg^{2+} and mechanism for delivering Mg^{2+} to dolomitization sites. Six models have been proposed, namely; sabkha, seepage-reflux, meteoric-marine mixing zone, Coorong, burial and seawater. Each model involves a different type of dolomitizing fluids, mode of flow and geologic settings but there is overlap between the models and several could apply to one setting. The sabkha and Coorong models are specific to well defined geologic settings whereas the other models are more generalized and emphasize particular aspects of the dolomitization process that may be

operational in a variety of geologic settings. As the product of a particular model may not be very distinctive petrographyically and/or geochemically, the application of these models to individual dolostone masses depends on inferences derived from the attributes of these dolostones such as petrographic features, geochemical data, internal facies relationship, major stratigraphic and paleogeographic features, scale and distribution. Therefore, the interpretation of the origins of a particular dolostone is dependent on inferences that are derived mainly from comparisons with a variety of dolomitization models.

1.4.1 Sabkha model

Sabkhas are coastal supratidal mudflats that are common in arid regions. Sabkha sediments often consist of evaporites, carbonates and possible siliciclastics in a capillary zone above a saline water table. Seawater is mainly supplied by periodic flood recharge which carries water onto the supratidal flats particularly along old channels (McKenzie et al., 1980). This flood recharge leads to a relatively short lived downward movement of water via the sediment to join the net seaward flow of groundwater (Fig 1.3). Intense heat over the sabkhas results in evaporation from the capillary zone above the water table and induces an upward flow of water from the saturated groundwater zone to replace the water lost by capillary evaporation until the water table falls below a level where capillary evaporation can operate. This process is known as evaporative pumping (Hsu and Siegenthaler, 1969). Water lost from sabkha sediments via evaporation is replaced by periodic flood recharge from seawater which also provides Mg for dolomitization (Fig 1.3). Evaporation of water from the sediments causes the salinity of seawater to be elevated beyond gypsum saturation within the supratidal flats, which increases the Mg / Ca ratio, reduces Mg^{2+} hydration and invariably precipitates dolomite. The resulting brines then reflux through the sabkha sediments similar to downward flow in the reflux model.

Sabkha dolomites are usually syngenetic, Ca-rich, often occur in association with evaporite minerals and poorly ordered with the degree of order increasing with distance from the shoreline (McKenzie and Piggott, 1981; Tucker and Wright, 1990). The Abu Dhabi Sabkha dolomite is perhaps the best known example of sabkha dolomitization.

1.4.2 Seepage-reflux model

This model (Fig 1.4), involves the generation of dolomitizing fluids through evaporation of lagoon water or tidal flat pore waters and then the decent of these fluids into underlying carbonate sediments (Tucker and Wright, 1990; Boggs, 2009). Evaporative concentration leads to precipitation of aragonite and gypsum which preferentially removes Ca^{2+} from the water and increases the Mg / Ca ratio of the resultant brine. Subsequent decent of these dense, often hot highly alkaline Mg^{2+}-rich hypersaline brine through deposited calcium carbonate sediment, will displace less dense seawater in the pores of the sediment and move seawards by seepage through the seaward dipping beds. Flushing underlying carbonate sediments with large volumes of this Mg^{2+} rich brine would bring about dolomitization via seepage refluxion (Boggs, 2009). In the seepage-reflux model, evaporated seawater is the source of Mg^{2+} whereas density difference drives the pump mechanism. Dolomitization occurs due to increased Mg / Ca ratio in dolomitizing fluids. Dolomites formed via this model are usually associated with evaporites and are enriched in trace elements and ^{18}O. Although there are no good modern analogues of this model, it has been frequently applied to ancient dolomite sequences. However, seepage-reflux dolomitization is confined to the platform and cannot be invoked to explain dolomitization beyond platform margins (Boggs, 2009). The Cretaceous Edward Formation in Texas is an example of seepage-reflux dolomitization (Tucker and Wright, 1990).

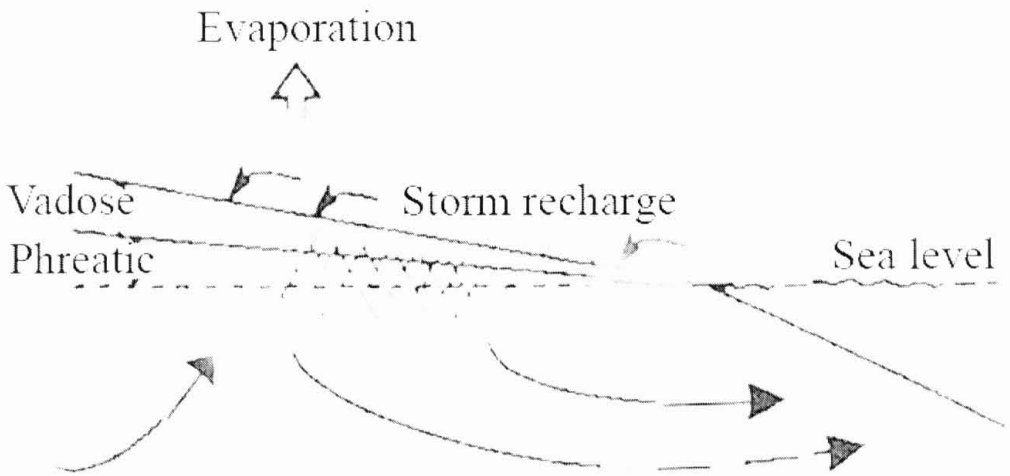

Fig 1.3 Illustration of the sabkha model of dolomitization, arrows indicate directions of fluid flow. In part after Land (1985).

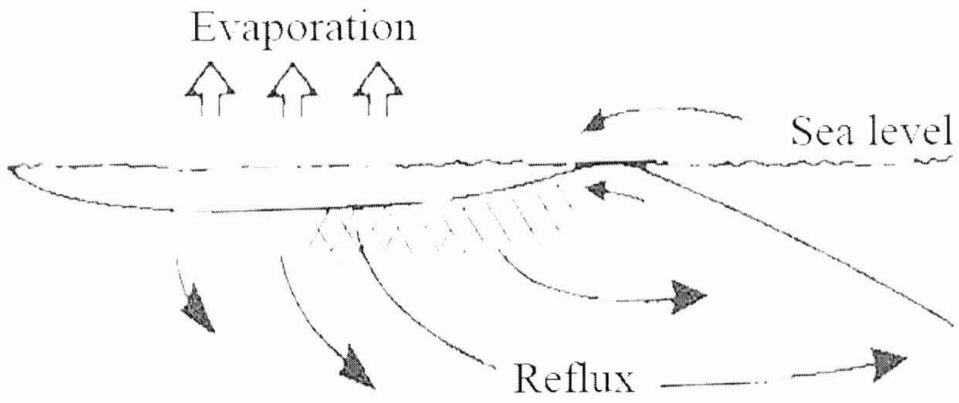

Fig 1.4 Illustration of the seepage-reflux model of dolomitization, arrows indicate directions of fluid flow. In part after Land (1985).

1.4.3 Meteoric-Marine mixing zone model

In the meteoric- marine mixing zone model, dolomitization occurs within the zone of mixing of confined or unconfined meteoric water with phreatic seawater (Fig 1.5a-b). The Mg^{2+} ions for dolomitization are derived primarily from seawater and the delivery mechanism is the continual circulation of seawater induced by the flow of fresh groundwater (Land, 1973). This model applies largely to dolomite bodies that are not associated with evaporite minerals. Mixing of meteoric water with seawater causes under saturation with respect to calcite whereas dolomite saturation increases, resulting in dolomitization. Folk and Land (1975) maintained that dolomite could form from solutions of low salinity and low ionic strength even with Mg / Ca ratios as low as 1:1. When seawater or evaporated brine with high Mg / Ca ratios is diluted by mixing with fresh water, the resultant mixture will retain the high Mg/Ca ratio but not the high salinity of the saline water. Thus, the resultant waters become special waters capable of forming ordered dolomite as dilution also reduces the crystallization rate which allows for the ordered crystals of dolomite to develop. Hence, dolomites formed via this model are usually perfectly clear with plane mirror like faces and are more resistant to solutions compared to dolomites formed via other models (Folk and Land, 1975). Meteoric-marine mixing zone dolomites also have low trace element concentrations and depleted ^{18}O. The Hope Gate Formation of Jamaica is an example of mixing zone dolomitization (Tucker and Wright, 1990).

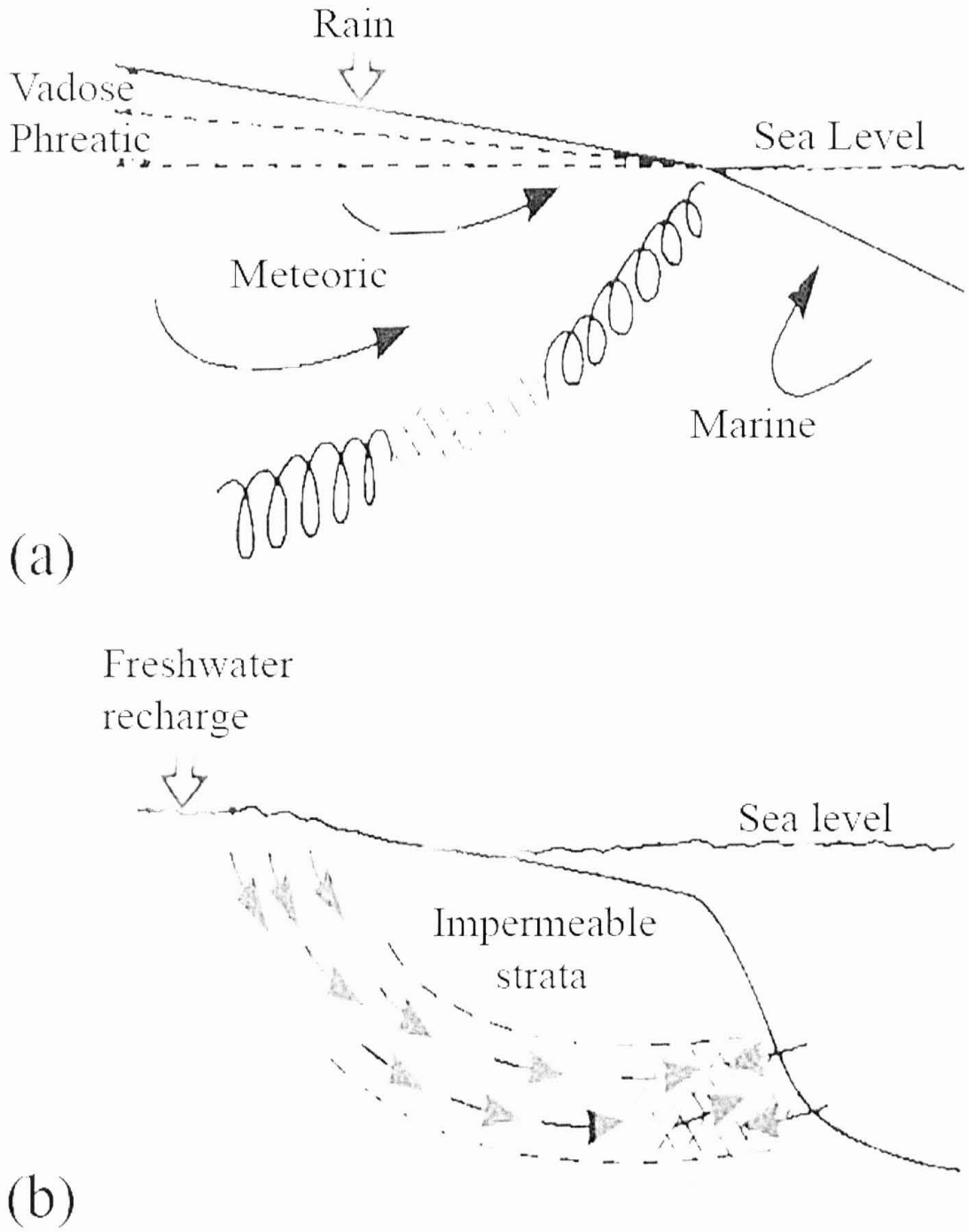

Fig 1.5. Illustration of the meteoric-marine mixing zone model of dolomitization for; (a) unconfined coastal aquifer, (b) deep confined aquifer. Arrows indicate directions of fluid flow. In part after Land (1985).

1.4.4 Seawater model

In the seawater model, dolomitization occurs by active pumping of large amounts of normal unmodified seawater through the pores of sediments (Fig 1.6) such that pore water in the sediments is constantly being renewed with seawater. Movements of large volumes of normal seawater through sediments provide a constant source of Mg and remove replaced Ca that might affect the dolomite crystal structure. Thus, any mechanism that provides a means of forcing large amounts of seawater through sediments can presumably bring about dolomitization with seawater as the source of Mg^{2+} and tidal pumping, thermal convection and density reflux (Whitaker et al., 1994) as mechanism for pumping seawater through sediments. The Cenozoic dolomites of the Bahamas platform are probably the best examples of seawater dolomitization.

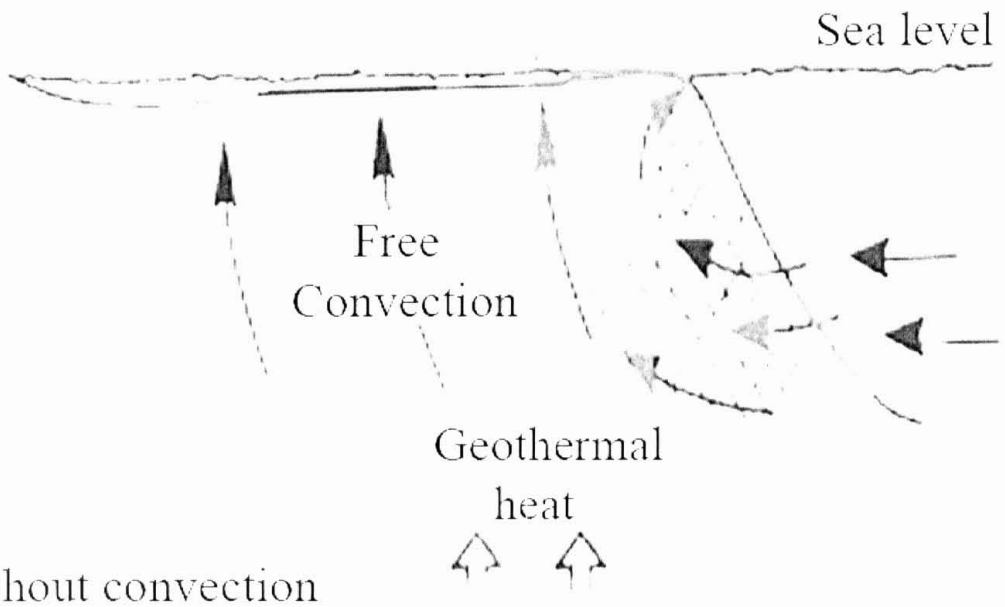

Fig 1.6. Illustration of the seawater model of dolomitization, arrows indicate directions of fluid flow. In part after Land (1985).

1.4.5 Burial model

In the burial model (Fig 1.7), the principal mechanism for dolomitization is the compactional dewatering of basinal mudrocks during burial and the expulsion of Mg^{2+} rich fluids into adjacent carbonate sediments or rocks. Pore-water and transformational changes of clay minerals provide the source of Mg^{2+}. Dolomitization should proceed more easily at depth because higher temperatures, lower proportions of hydrated Mg^{2+} ions, longer time and increased reactions rates favour dolomite precipitation. However, the effectiveness of compaction flow in dolomitization is constrained by the small volume of fluids expelled by compaction. Other mechanisms proposed for moving Mg^{2+} bearing waters through subsurface carbonates include topography driven flow, thermal convection and hydrothermal flows. The burial model basically advocates that if a sufficient volume of essentially normal or modified seawater can be forced through carbonate sediment during burial, dolomitization may occur. The dolomites of the Upper Devonian Miette buildup in Alberta, is an example of burial dolomitization (Mattes and Mountjoy, 1980)

1.4.6 Coorong model

The Coorong model (Fig 1.8) named after the Coorong lagoon in South Australia is believed be a hybrid of the sabkha and mixing zone models (Tucker and Wright, 1990; Morrow, 1982). Research work (Von der Borch and Jones, 1976; Von der Borch, 1976; Von der Borch and Lock, 1979; and Muir et al 1980) established the Coorong lagoon as a model for early dolomitization in many ancient sequences of aphanitic dolomites that are not associated with evaporites. The Coorong lagoon and a series of ephemeral alkaline lakes extend for about 200 km parallel to the South Australian coast. Surface drainage follows the existing topography whereas subsurface

groundwater flow seaward perpendicular to surface drainage (Fig 1.8). The ephemeral lakes are filled during the winter months by seawater and seeping groundwater which are subsequently evaporated to partial or complete dryness during the summer months.

The mechanism for dolomitization in the Coorong lagoon is not fully understood as it could relate to the mixing of seawater with groundwater, the evaporation of the resultant solution and also to the high alkalinity of the lake waters (Tucker and Wright, 1990; Morrow, 1982). Likewise, the source of Mg^{2+} ions could be directly from seawater or from groundwater containing Mg^{2+} ions derived from the weathering of basic volcanic rocks (Von der Borch and Jones, 1976). However, the delivery mechanism is the continual subsurface groundwater flow. Successive regression of the Coorong model on subsiding continental margin could build sequences of evaporite free peritidal to subtidal dolomites (Muir et al., 1980). The dolomites of the Yalco Formation of the McArthur Group in northern Australia, is an example of Coorong dolomitization (Tucker and Wright, 1990).

Fig 1.7 Illustration of the burial model of dolomitization, arrows indicate directions of fluid flow. In part after Land (1985).

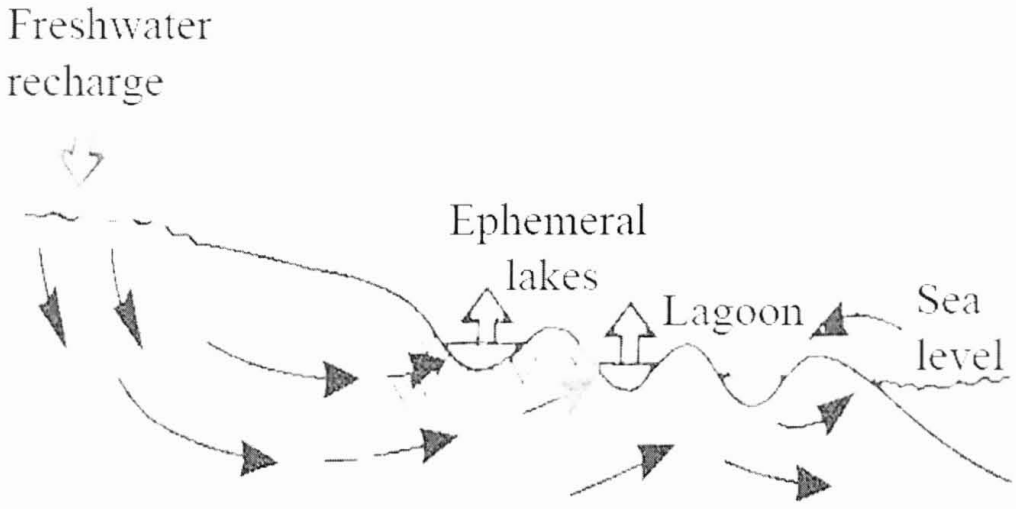

Fig 1.8 Illustration of the Coorong model of dolomitization, arrows indicate directions of fluid flow. In part after Land (1985).

CHAPTER TWO

METHODS AND THEORY

2.1 Methodology

The procedures applied in this study for petrographic and geochemical analysis are the same used in Azmy and Conliffe (2010), Conliffe et al., (2012), Azmy et al., (2007), Azmy et al., (2008), Azmy et al., (2011).

2.1.1 Sampling protocol

The Catoche Formation was examined in core 12i/4-1 (50.93 m, spanning the Upper Catoche) and core 12i/6-121 (103.7 m, spanning the Lower Catoche) both drilled near Daniel's Harbour on the Northern Peninsula (Fig. 1.1; 50°14′31″ N, 57°30′52″ W; NAD 83 and 50°17′38″ N, 57°27′50″ W; NAD 83). Core 12i/4-1 was drilled by US Borax and Chemical Corporation in 1981 whereas core 12i/6-121 was drilled by NFLD Zinc mines in 1989 (http://gis/geosurv.gov.nl.ca). The composite core represents a complete section of the Catoche Formation (154.63 m thick). Ninety-two samples were taken for analysis at 2 m or less intervals (Appendix 1, Fig 1.2).

2.1.2 Petrographic analysis

Thin sections were stained with Alizarin Red-S and potassium ferricyanide solutions (Lindholm and Finkelman, 1974) and examined under standard polarizing microscope and cathodoluminoscope for petrographic features. A mirror-image slab of each thin section was also polished and cleaned with de-ionized water to be utilized for micro sampling and geochemical analyses of the different carbonate generations. Cathodoluminescence was performed using a

Technosyn cold cathodoluminoscope operated at ~12 kV accelerating voltage and ~0.7 mA gun current intensity, whereas ultraviolet luminescence was performed using a CRAIC-QDI 202 UV unit mounted on a Zeiss imager D1m microscope.

Microthermometric fluid-inclusion analyses were performed on double polished wafers (approximately100 μm thick) using a Linkam THMSG600 heating-freezing stage. Calibration with precision of ±0.2°C at –56.6°C and ±1°C at 300°C was conducted using synthetic H_2O and CO_2 fluid inclusion standards. The initial melting temperatures (T_i), last ice melting (T_m (ice)) and the homogenization temperatures (T_h) were measured in primary two-phase fluid inclusions following procedures outlined by Shepherd et al., (1985). Aqueous fluid salinities were calculated using T_m (ice) and the equation of Bodnar (2003).

2.1.3 Geochemical analysis

Polished slabs were washed with deionized water and dried overnight at 50°C prior to microsampling. Approximately 4 mg were microsampled from the cleaned slabs with a low-speed microdrill. For Carbon and Oxygen isotope analyses, about 200 μg of samples was reacted in an inert atmosphere with ultra-pure concentrated orthophosphoric acid at 50°C in a Thermo-Finnigan Gas bench II. The CO_2 produced from the reaction was automatically flushed through a chromatographic column and delivered to the source of a ThermoFinnigan DELTA V plus isotope ratio mass spectrometer in a stream of helium, where the gas was ionized and measured for isotope ratios. Uncertainties of better than 0.1‰ (2σ) for the analyses were determined by repeated measurements of NBS-19 ($\delta^{18}O$ = –2.20‰ and $\delta^{13}C$ = +1.95‰ vs. VPDB) and L-SVECS ($\delta^{18}O$ = –26.64‰ and $\delta^{13}C$ = –46.48‰ vs. VPDB) as well as internal standards during each run. For elemental analyses, ~ 4 mg of sample powder was digested in 2.5% (v/v) pure HNO_3 acid (Coleman et al., 1989) and analyzed for Ca, Mg, Sr, Mn and Fe as well as Rare Earth

Elements (REE) using a HP 4500plus ICP-MS at Memorial University of Newfoundland. The relative uncertainties of these measurements are better than 4% using DLS 88a-4 and CCH-1-4 as standards. Calculations of major and trace element concentrations are based on an insoluble residue-free basis (100% soluble dolomite or calcite). REE concentrations are normalized based on Post-Archean Australian Shale (McLennan, 1989) and chondrite values (Bau and Dulski, 1996), whereas anomalies of Cerium $(Ce/Ce^*)_{SN} = Ce_{SN}/(0.5La_{SN} + 0.5Pr_{SN})$, Lanthanum $(Pr/Pr^*)_{SN} = Pr_{SN}/(0.5Ce_{SN} + 0.5Nd_{SN})$, and Europium $(Eu/Eu^*)_{CN} = Eu_{CN}/(0.67Sm_{CN} + 0.33Tb_{CN})$ were calculated with the formulas of Bau and Dulski (1996).

2.1.4 Fluid inclusion gas analysis

The procedure applied for fluid-inclusion gas analysis was described by Norman et al. (1996, 1997, 2002), Norman and Blamey (2001), Norman and Moore (2003), and Parry and Blamey (2010). Approximately 2 g of samples were mildly crushed by hand and sieved in a 30-mesh sieve with the −30-mesh fraction discarded. The +30 mesh size fraction was then washed in 20% KOH, agitated then decanted. The grains were washed several times in excess amount of 18 MΩ deionized water and air-dried. Gas analyses were conducted with a dual quadrupole mass spectrometer system (two prisma spectrometers) using the crush-fast scan method (Norman et al., 1996, 1997, 2002; Norman and Blamey, 2001; Norman and Moore, 2003; Parry and Blamey, 2010). The method requires 150 mg of prepared samples and uses 6 to 10 incremental crushes in a vacuum ~10^{-8} Torr to open multiple fluid inclusions thereby releasing gases which are analyzed with the mass spectrometers. Species measured includes H_2, He, CH_4, H_2O, N_2, O_2, H_2S, Ar, CO_2, SO_2, C_2–C_4 alkanes and alkenes, and C_6H_6. The system is calibrated with commercial gas mixtures, internal standards, and natural fluid inclusion standards. Precision and accuracy vary with species. H_2 could be reliably detected at 50 ppm, He at <0.5 ppm. Precision

for the major gas species CO_2, CH_4, N_2, and Ar is better than 5 %, whereas it is ~10 % for the minor species.

2.2 Cathodoluminescence

Cathodoluminescence (CL) is the emission of photons of characteristic wavelengths by minerals that are under high-energy electron bombardment. In simple terms, it is luminescence caused by irradiation with cathode rays. Photons emitted by most minerals have wavelengths within the visible-light range of the electromagnetic spectrum but emissions can also occur in the ultraviolet and infrared ranges. When a crystal is bombarded by electrons with sufficient energy, the electrons become energized and move from the lower-energy valence band to the higher-energy conduction band leaving behind an electron hole. When the energized electrons attempt to return to the valence band (i.e. electron and an electron hole recombine), they are temporarily held by electron traps and energy in the form of photons is emitted when the electron vacate such traps. If the wavelength of emitted photons is within the visible portion of the electromagnetic spectrum, luminescence occurs (Boggs Jr and Krinsley, 2006). Electron traps (also called luminescence centers) are defects or chemical impurities in the mineral which temporarily capture mobile electrons. There are two types of electron traps; intrinsic and extrinsic traps. Intrinsic traps are characteristic of the crystal lattice of the mineral and is often due to non-stoichiometry, structural imperfections (poor ordering in the crystal etc.) and impurities that distort the crystal lattice. Extrinsic traps results from impurities in the composition of the mineral often derived from the medium in which the mineral formed. Such impurities are usually transition elements, rare earth elements and actinide elements and are generally the most common source of CL in minerals. Thus, extrinsic traps in carbonates reflect the characteristic nature of the mineralizing fluids.

Activators are ions of trace elements that promote CL in a mineral whereas quenchers are trace element ions that inhibit or eliminate CL. Sensitizers (co-activators) are ions that must coexist with another activator to enhance the CL response of that activator. Thus, the nature of CL in a mineral is a complex function of composition, crystal structure and superimposed strain or damage on the structure of the mineral (Boggs Jr and Krinsley, 2006). Common activators in carbonates are Mn^{2+}, Pb^{2+}, Cu^{2+}, Zn^{2+}, Ag^{+} and most rare earth elements with Mn^{2+} as the most common activator whereas common quenchers include Fe^{2+}, Ni^{2+} and Co^{2+} with Fe^{2+} as the most important quencher (Machel, 1985). The intensity of CL depends on the mineral examined, the voltage and current density of the electron beam used. However in carbonates, the intensity of CL is also influenced by the Mn^{2+}/Fe^{2+} ratios (Boggs Jr and Krinsley, 2006). Common CL applications in carbonate rocks are:

1. To provide general information on the trace element content,
2. To study crystal growth and replacement.
3. To identify different cement generations and study the effects of diagenetic processes,
4. To provide details of internal structures of fossils,
5. To determine the occurrence and distribution of impurities in crystals, and
6. To provide clues on redox conditions, pH and nature of fluids which deposited the carbonate (Choquette and James, 1987; Machel and Burton, 1991; Machel et al., 1991)

2.3 Trace Elements

Minor and trace concentrations of elements occur in carbonates. The simplest method of incorporating these trace constituent elements into crystal lattice is by direct substitution of a host ion by a guest ion of similar charge and radius. However, trace constituents may occur between lattice planes, occupy lattice defects, be absorbed into lattice, become occluded as solid

or liquid inclusions and occupy planes along crystal boundaries (Tucker and Wright, 1990). The concentrations of trace elements in carbonates are determined by (1) the concentration of the minor elements in the pore fluids, (2) the degree of openness of the diagenetic system, and (3) the effective distribution coefficient (k_e) of the trace element between diagenetic solutions and the carbonate precipitate (Tucker and Wright, 1990). Research work abound over the actual values of trace element distribution coefficients (k) and its use in interpreting the chemistry of carbonates (e.g Land, 1980; Kretz, 1982; Veizer 1983). However, differences between theoretical distribution coefficient (k) and effective distribution coefficient (k_e) present a huge problem to this approach as effective distribution coefficient is dependent on temperature, rate of precipitation and other kinetic factors (Tucker and Wright, 1990). In dolomites, the experimental values of distribution coefficient are difficult to obtain as dolomites cannot be precipitated directly from natural waters at surface temperatures in the laboratory (Warren, 2000).

Trace elements usually studied in carbonates are Sr, Na, Fe, Pb, Zn and Mn and data derived from these elements often aid interpretations of the origin of source fluids and/or dolomitizing fluids, redox and general conditions in the diagenetic environment during deposition, and nature of diagenetic system. However, the sole use of trace elements as indicators of conditions in diagenetic environments is not the ideal approach because it provides more conclusive and reliable interpretations when combined with other tools such as petrographic, fluid inclusion, and isotopic analyses. The Sr content in dolomites have been used to place constraints on the composition of dolomitizing fluids and dolomitization models (e.g. Viezer et al., 1978, 1983; Tucker and Wright, 1990) whereas Fe and Mn generally indicate redox conditions (Tucker and Wright, 1990).

2.4 Stable Isotopes

Isotopes of elements vary slightly in mass and energy which results in differences in physical and chemical properties. These differences in properties are generally greater in elements of lower atomic numbers. In a molecule of two or more isotopes, the isotope of lighter mass is more reactive as it possesses weaker bonds compared to the heavier isotope. Fractionation is a change in the ratio of any two isotopes during a reaction or a process and is indicated by a fractionation factor (α) (Tucker and Wright, 1990; Boggs, 2009). The fractionation factor is represented as:

$$\alpha = R_A / R_B \quad \ldots\ldots (1)$$

Where R_A = ratio of heavy to light isotopes in phase A and R_B = ratio of heavy to light isotopes in phase B.

The fractionation factor is also temperature dependent as shown by the following inverse relationship;

$$\alpha \propto 1/T \quad \ldots\ldots (2).$$

Stable isotopes are increasingly used in the interpretations of origins of dolomites particularly in conjunction with trace elements and petrography and they also provide clues to conditions that dominated in a particular diagenetic environment. Stable isotopes often studied in dolomites are those of carbon and oxygen, although strontium, sulphur and recently Mg are useful for some other specific investigations. Quantitative analysis of isotopic data is only possible if isotopic equilibrium is established, isotopic fractionation is insignificant, or the kinetics of the reaction is fully understood (Tucker and Wright, 1990).

2.4.1 Carbon isotopes

Carbon has two isotopes (^{12}C and ^{13}C) and processes that affect the cycling of carbon compounds (carbon cycle) also involve isotopic fractionation of carbon. Global carbon can be divided into two reservoirs namely the oxidized reservoir (principally of CO_2, HCO_3^{2-} and carbonate minerals) and the reduced reservoir (principally of organic compound, fossil fuels and native elements) with a constant exchange of carbon between both reservoirs (Tucker and Wright, 1990). Photosynthetic plants are mainly responsible for carbon fractionation in sedimentary conditions with atmospheric CO_2 as a link between relatively ^{12}C-enriched organic compounds (through photosynthesis) and carbonates (via exchange reactions with aqueous HCO_3^{2-}) causing relative enrichment in ^{13}C (Tucker and Wright, 1990, Faure and Mensing, 2005). Isotopic composition of carbon is measured with a mass spectrometer and expressed relative to Pee Dee Belemnite (PDB) or the synthetic international standard, Vienna PDB (VPDB). Distribution of carbon isotopes in marine and lacustrine carbonates of any age depend on:

1. The isotopic fractionation between atmospheric CO_2 and precipitated carbonates,
2. Isotope fractionation among the aqueous species ($CO_{2\,(aq)}$, $H_2CO_{3\,(aq)}$, HCO_3^{2-}, CO_3^{2-}),
3. Water temperatures or temperatures of diagenetic fluids and salinity,
4. Stability of initial mineral composition carbonate relative to diagenetic environment (calcite vs. aragonite),
5. Non-atmospheric CO_2 formed by oxidation of organic matter,

6. Vital effect (metabolic processes controlling fractionation) of organisms (Coral, mollusk, foram, brachiopods),

7. Subsequent alteration of carbonates during diagenesis,

8. Deposition of secondary carbonates in fractures or cavities by groundwater or subsurface brines, and

9. The openness of the diagenetic system.

The carbon isotopic composition of dolomite reflects the nature of the precursor carbonate or degree of primary productivity unless the process of dolomitization occurs in conditions of high water/rock interaction ratios (under open system conditions) such that solutions have enough dissolved CO_2 to reset the C-isotope signature of the precursor carbonate (Tucker and Wright, 1990; Boggs, 2009).

2.4.2 Oxygen isotopes

Oxygen has three stables isotopes (^{16}O, ^{17}O and ^{18}O) that readily combine with hydrogen to form water and like carbon, the processes that operate in the water cycle also involve fractionation of oxygen. Lighter water molecules ($H_2{}^{16}O$) are preferentially evaporated from seawater as lower isotope masses tend to be enriched in the lighter phase. This has the resultant effect of rain (meteoric water) being about 4 ‰ lower in its $\delta^{18}O$ value relative to the parent seawater (Tucker and Wright, 1990, Faure and Mensing, 2005). Like carbon, the isotopic composition of oxygen is measured with a mass spectrometer but expressed relative to Standard Mean Ocean Water (SMOW) or VSMOW and in carbonate analyses, relative to VPDB. Factors that influence the isotopic distribution of oxygen in diagenetic conditions include:

1. The openness of the system (water / rock ratio),

2. The isotopic composition of both seawater and the evolving diagenetic water,

3. The exchange reactions of isotopic oxygen between fluid and mineral,

4. The temperature and salinity of ambient seawater and the diagenetic fluid,

5. Regional changes in the composition of meteoric waters due to latitude, altitude and seasonal variations, and

6. Secular variations in the ^{18}O composition in global seawater.

Dolomitization requires large volumes of seawater to supply the Mg^{2+} needed for the process. Thus, the oxygen isotopic composition of dolomites reflects the temperature of precipitation and the oxygen isotopic composition of the dolomitizing fluids (Tucker and Wright, 1990). However, the isotopic composition of the dolomitizing fluids can be influenced by that of the precursor carbonate being replaced. But precursor minerals generally only have an effect on the oxygen isotopic composition of dolomites in low water / rock ratios or closed diagenetic systems (Tucker and Wright, 1990).

2.5 Rare Earth Elements

The suite of rare earth elements (REE) is a useful tool for the identification of the origin of fluids, the state of equilibrium in rock-water interactions and changes in fluid composition, which is fundamental in understanding fluid-rock systems. The suite consists of fifteen lanthanides and is traditionally classified into light rare earth elements (LREE; La to Nd), medium rare earth elements (MREE: Sm to Dy) and heavy rare earth elements (HREE; Ho to Lu). REEs have relatively short residence time in oceans (several hundred years; Alibo and

Nozaki, 1999) and are lithophile elements that invariably occur together naturally because all are trivalent (except for Ce^{+4} and Eu^{+2} in certain environments) and have similar ionic radii with chemical characteristics that change systematically along the series, which results in the preferential absorption of LREE relative to MREE and HREE in seawater (Sholkovitz and Shen, 1995). Their incorporation into calcite (biogenic and abiogenic) lies within a relatively narrow range of partition coefficient values (Zhong and Mucci, 1995), and thus observed variation in the series is a reflection of oceanic composition and/or nature of fluids that deposited the carbonates and other processes. Redox conditions control the conversion and distribution of Cerium (Ce) and to a lesser degree Europium (Eu) (Sholkovitz et al., 1994); hence both elements provide further information on process controlling parameters. The earlier concept that limestone was a poor choice for seawater REE proxy due to the effects of diagenesis in ancient carbonates (e.g., Scherer and Seitz, 1980; Shaw and Wasserburg, 1985), was replaced by the current paradigm, which suggests that diagenesis, particularly meteoric and mixed water, has no effect on the pattern, composition and/or distribution of REEs in carbonates (limestones and dolomites) except in diagenetic systems with extremely large water-rock ratios (e.g., Banner et al., 1988; Barton et al., 2006; Webb and Kamber, 2000; Kamber and Webb, 2001; Nothdurft et al., 2004; Webb et al., 2009).

The ratios of Th/U and V/Sc in sediments can be used as a proxy to estimate redox conditions in the depositional environment. Thorium (Th) is unaffected by redox conditions in sedimentary environments and remains insoluble as Th^{4+}. In contrast, uranium (U) is reduced to the insoluble uranous (U^{4+}) fluoride complex and is preserved in sediments under anoxic conditions, whereas in oxidizing conditions, it is converted to the soluble uranyl (U^{6+}) carbonate, which is removed in solution (Wignall and Twitchett, 1996; Kimura and Watanabe, 2001). Thus,

suboxic-anoxic sediments are typically more enriched in U (with Th/U ratios < 2) compared to oxic sediments (with Th/U ratios > 2). Vanadium (V) is another redox-sensitive element that is preferentially concentrated in sediments underlying anoxic or near-anoxic waters (Emerson and Huested, 1991; Wignall, 1994; Kimura and Watanabe, 2001). The degree of V enrichment is most efficiently expressed if the V concentration is normalized by scandium (Sc) abundance, because both V and Sc are insoluble and V varies in proportion to Sc, rather than other insoluble elements such as aluminum. Therefore, suboxic-anoxic sediments have higher V/Sc ratios compared to oxic sediments (Kimura and Watanabe, 2001).

2.6 Fluid Inclusion Gas Analysis

Analysis of gases trapped in fluid inclusions provides yet an additional tool to ascertain the oxidation state and discriminate the origin of source fluids in geologic systems. Giggenbach (1986) introduced the concept that N_2-Ar-He ratios of geothermal gases may identify the source of volatiles in geothermal fluids. Norman and Moore (1999) introduced the use of methane (i.e. ratio of N_2-Ar-CH_4) as a tracer species because; CH_4 provides an indication of the crustal component in thermal fluids, there is no ambiguity about the origin of methane as there is with helium and it is easier to analyze. Norman and Moore (1999) also introduced the concept of CO_2/CH_4 versus N_2/Ar diagram that can differentiate fluids bearing significant organic nitrogen, which could lead to errors in interpretation. The CO_2/CH_4 versus N_2/Ar diagram of Norman and Moore (1999) classified source fluids into three basic groups; magmatic, meteoric and crustal fluids. Meteoric fluids refer to near-surface recharge waters while crustal fluids refer to meteoric fluids that have interacted with crustal rocks and may have species derived from the wall rock. The ratio of CO_2/CH_4 indicates the redox state while N_2/Ar provides an indication of fluid source(s).

2.7 Diagenesis of Carbonates

Diagenesis encompasses all the processes of physical, chemical and biological change that modify sediments after deposition, but excludes changes to sediments caused by weathering and metamorphism. (Choquette and James, 1987; Tucker and Wright, 1990). Diagenesis can begin almost immediately after deposition, while sediments are still on the ocean or other basin floors, and may continue through deep burial and eventual uplift (Boggs, 2009; Tucker and Wright, 1990; Choquette and James, 1987; James and Choquette, 1988). The effects of diagenesis vary from obvious changes like dissolution to form cave systems to subtle changes like modification of trace element and isotopic signatures (Tucker and Wright, 1990). In siliciclastics, the net effect of diagenetic modifications is to move initially incompatible assemblages of siliciclastic minerals towards a state of greater equilibrium with the diagenetic environment without wholesale alteration or replacement of the depositional mineral assemblages. However, this does not hold true for carbonates which can undergo complete or almost complete change in depositional mineralogy during diagenesis (Boggs, 2009). Major controls on diagenesis include:

1. The composition and mineralogy of the sediments,
2. Pore fluid chemistry and flow rate,
3. Geological history of the sediments in terms of burial, uplift and sea level changes,
4. Prevailing climate conditions,
5. Grain size and texture, and
6. Timing of cement precipitation (Degree of lithification).

Diagenesis in carbonates brings about important physical, chemical and mineralogical changes in sediments via six major processes, which are cementation, microbial micritization, neomorphism, dissolution, compaction and dolomitization (Tucker and Wright, 1990). These

processes will be discussed briefly below except for dolomitization which was discussed in detail in chapter one because it is the focus of the current study.

2.7.1 Cementation

The precipitation of cements is a diagenetic process that occurs when pore fluids are supersaturated with respect to the cement phase and there are no kinetic factors inhibiting the precipitation (Tucker and Wright, 1990). In some cases, organic geochemical influences on the cementation process can be significant. Common cements in carbonates include aragonite, low-magnesium calcite, high-magnesium calcite and dolomite whereas cements of siderite, ankerite, gypsum, anhydrite and halite are less common. Cementation can occur in all environments for carbonate diagenesis. The petrographic and geochemical studies of carbonate cements enables deductions to be made on the environment and conditions of cementation (Tucker and Wright, 1990).

2.7.2 Microbial micritization

During this process, skeletal grains of carbonate sediments are bored around the margins by microboring organisms and the bored holes are subsequently filled with fine grained sediments or cement to form micritic envelop or complete micritized grains (Tucker and Wright, 1990). Microbial micritization generally occurs in the early stages of diagenesis usually while sediments are still on the sea floor or just below.

2.7.3 Neomorphism

This term refers to the processes of recrystallization and replacement of carbonate sediments that may result in mineralogical and textural changes whereas recrystallization refers solely to

changes in crystal size without any change of mineralogy (Tucker and Wright, 1990). Neomorphism occurs in the presence of water via dissolution-reprecipitation and hence, dry solid state processes such as inversion of aragonite and recrystallization of calcite are most unlikely to occur in carbonates as diagenetic environments are always wet (Bathurst, 1975; Tucker and Wright, 1990). Neomorphism can be of aggrading type (resultant minerals general increase in crystal size) or of degrading type (resultant minerals general decrease in crystal size) and like cementation, it can occur in all environments for carbonate diagenesis. Calcitization (the replacement of other carbonate minerals by calcite) is a common neomorphic process that affects carbonates.

2.7.4 Dissolution

Dissolution of carbonate sediments and cements is a diagenetic process that occurs when pore fluids are under saturated with respect to carbonate grains or cement (Tucker and Wright, 1990; Boggs, 2009). Dissolution occurs in response to changes in the chemistry of pore fluids such as changes in salinity, temperature or partial pressure of CO_2 and results in the complete or partial dissolution of carbonate grains or cement, particularly if they are of metastable mineralogy like aragonite and high magnesium calcite. Dissolution can occur in all environments for carbonate diagenesis but is particularly important in the near surface meteoric environment due to the presence of meteoric water (Tucker and Wright, 1990).

2.7.5 Compaction

Compaction of carbonate sediments is a diagenetic process that occurs when sediments are buried by younger strata. Compaction occurs in response to changes in temperature, pressure and hydrostatic pressure of pore fluids caused by overburden load. Initial changes to sediments that

are not cemented include dewatering, decrease in porosity (due to closer grain packing and reorientation), decrease in sediment thickness and grain fractures at grain contacts. This is known as mechanical compaction and cementation inhibits its effects by increasing the bearing strength of sediments (Tucker and Wright, 1990; James and Choquette, 1988; Boggs, 2009). Regardless of whether sediments are cemented or not, further compaction will eventually cause grains to dissolve at points of contacts (pressure dissolution) to produce sutured and concavo-convex contacts, stylolites and dissolution seams, which is known as chemical compaction (Tucker and Wright, 1990; James and Choquette, 1988; Boggs, 2009). Compaction can occur in all environments for carbonate diagenesis but is particularly important in the deep burial environment.

2.8 Diagenetic Environments for Carbonates

Since water-rock interactions are the basic driving force for carbonate diagenesis, three major diagenetic environments are recognized based on the composition and nature of water/fluids that can modify carbonate sediments. These environments are the marine, the meteoric and the burial environment (James and Choquette, 1984, 1988; Tucker and Wright, 1990). The respective diagenetic environments pass laterally and vertically one into another and carbonate sediments may move from one environment to another with time, deposition and burial, sea level changes and vertical tectonic movements (Tucker and Wright, 1990; James and Choquette, 1988).

2.8.1 Marine Environments

The marine environment is characterized by marine waters and comprises of the sea floor, shallow marine phreatic zone and the strandline bathed in mixed marine and meteoric waters (Fig. 2.1). In the marine environment, diagenetic processes on the sea floor and marine phreatic

zones depend on water depth and latitude whereas it depends on climatic conditions along the shoreline (Tucker and Wright, 1990; James and Choquette, 1984, 1988).

In low latitude shallow marine environments, the dominant diagenetic processes are cement precipitation and microbial micritization by organisms. Cementation is widespread in areas of high current activity (such as along shoreline and shelf margins) and evaporation (e.g. tidal flats and beaches) due to pumping of seawater through sediments. In contrast, microbial micritization occurs everywhere in the shallow marine environment, but it is most prevalent in quiet water locations due to little or no sediment movement (Tucker and Wright, 1990). In mid to high latitude shallow marine environments, cement precipitation rarely occurs as shallow seawater becomes under saturated with respect to $CaCO_3$ away from the subtropics, thus carbonate grains are more liable to dissolution while microbial borings are usually empty rather than filled with micrite or cement (Tucker and Wright, 1990; Boggs, 2009). Hence, the shallow marine can be divided in three sub environments namely: the active marine phreatic (where pore waters are constantly being replenished and cementation is common), the stagnant marine phreatic (there is little or no movements of sediments or pore water fluids thus cementation is limited and microbial micritization is prevalent), and the marine vadose (where cementation mainly occurs via evaporation of seawater and there may be microbial effects, Tucker and Wright, 1990; James and Choquette, 1984, 1988).

In deep marine settings, the effect of latitude is negligible and the dominant diagenetic processes are neomorphism and marine dissolution due to increased pressure and reduced temperatures (James and Choquette, 1988; Boggs, 2009).

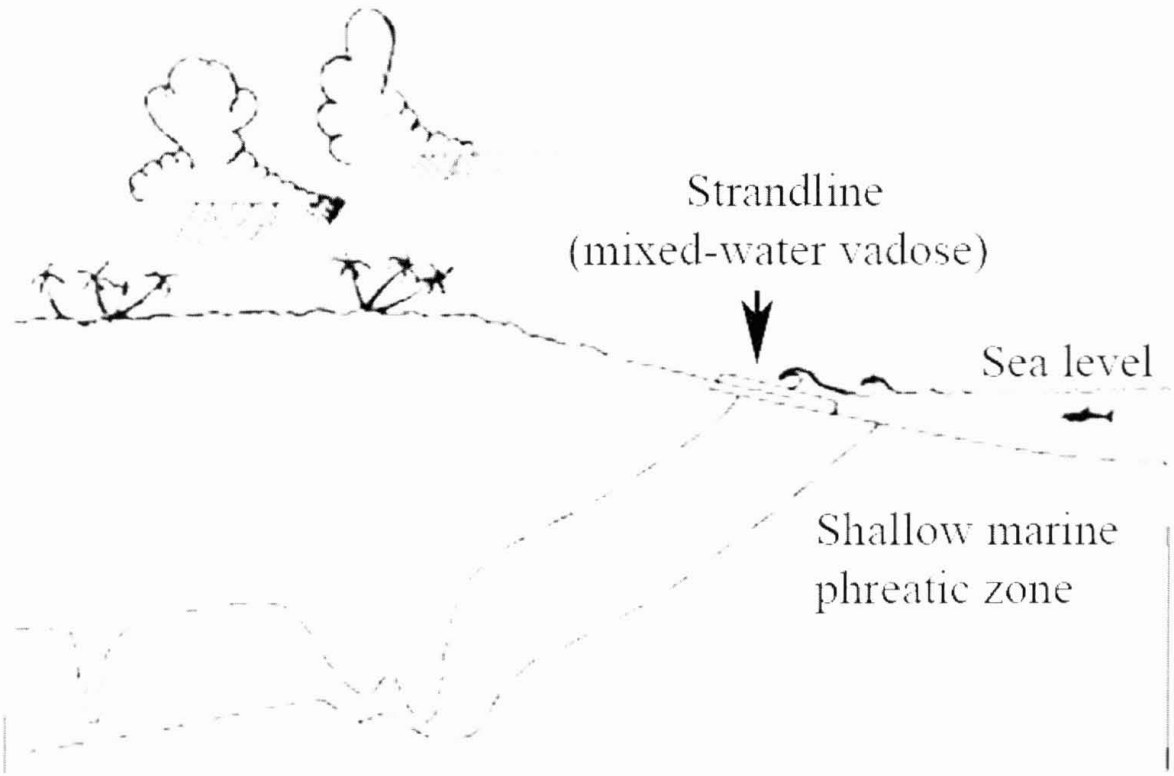

Fig 2.1 The marine diagenetic environment (modified from James and Choquette, 1984)

2.8.2 Meteoric Environment

The meteoric zone is characterized by meteoric waters and consists of the vadose zone, the phreatic zone and the shallow phreatic mixing zone of marine and meteoric waters (Fig 2.2). The water table is the boundary between the meteoric vadose and phreatic zones and represents a surface where atmospheric and hydrostatic pressures are equal (Tucker and Wright, 1990; James and Choquette, 1984, 1988). The meteoric vadose zone is above the water table and opens to the atmosphere. It consists of the zone of infiltration directly below the sediment / atmosphere interface and the zone of gravity percolation which lies above the water table but below the zone

on infiltration (Fig 2.2). The phreatic zone lies below the water table and consists of the shallow phreatic and deep phreatic zones whereas the shallow phreatic mixing zone is a transition zone composed of mixed marine-meteoric waters.

In the meteoric environment, diagenetic processes are controlled by mineralogy, grain size, porosity and permeability, vegetation, climate and time. The first three factors are intrinsic to carbonate sediments whereas the last three are extrinsic (James and Choquette, 1988; Boggs, 2009). The dominant diagenetic processes in this environment are dissolution, cement precipitation and neomorphism (Tucker and Wright, 1990). Dissolution occurs in meteoric environments due to the aggressive nature of meteoric waters caused by the absorption of atmospheric and soil CO_2 (as well as soil acids) and the under saturation of meteoric water with respect to $CaCO_3$. Dissolution invariably leads to super saturation of pore fluids with respect to $CaCO_3$ and prompts the precipitation of low magnesium calcite in meteoric waters with low Mg/Ca ratios, thus carbonates sediments are able to undergo dissolution while there are being cemented (Tucker and Wright, 1990; Boggs, 2009). The removal of CO_2 (by plants and degassing), evaporation and evapotranspiration are the major causes of cement precipitation in the vadose zone whereas the mechanism for cement precipitation in the phreatic zone is poorly understood (Tucker and Wright, 1990; James and Choquette, 1984, 1988). Dissolution coupled with cement precipitation in carbonate sediments ultimately causes neomorphism with textural, mineralogical and geochemical changes (Tucker and Wright, 1990; Boggs, 2009).

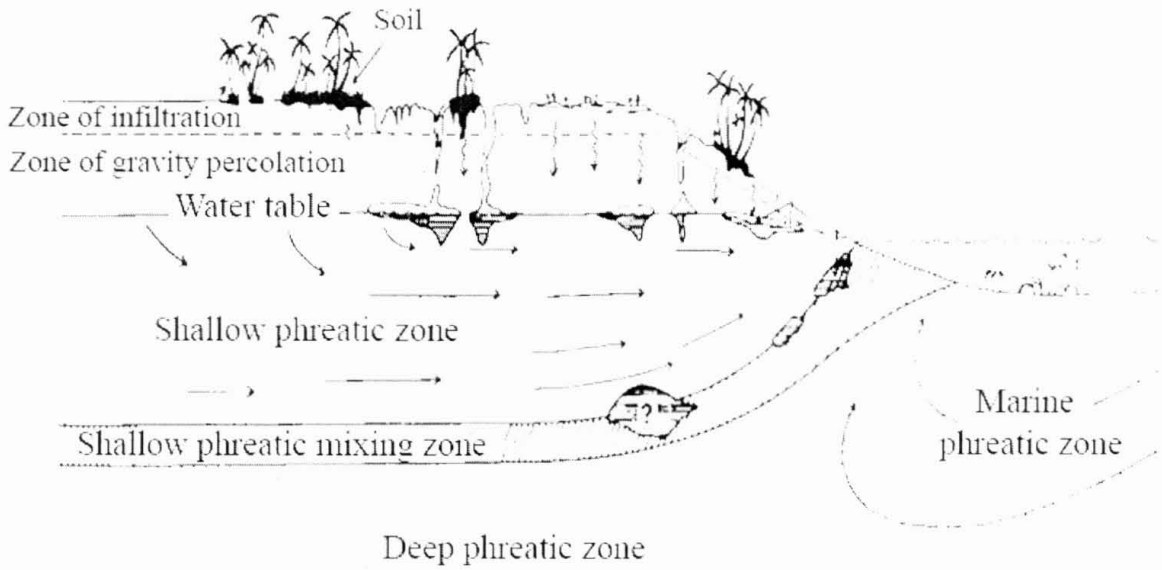

Fig 2.2 The meteoric diagenetic environment (modified from James and Choquette, 1984)

2.8.3 Burial Environment

The burial diagenetic environment is characterized by pore waters that where once marine or meteoric but have been modified during burial, by circulation through basinal rocks, and is defined as the zone between near-surface diagenesis and the onset of low-temperature metamorphism (James and Choquette, 1988, Boggs, 2009). The burial environment consists of shallow and deep burial environments (Fig 2.3; Tucker and Wright, 1990). Intrinsic factors that control diagenesis in the burial environment are, mineralogy, grain size and texture, pore-water

chemistry, porosity and permeability, and early precipitated cement whereas extrinsic factors include; temperature, pressure and solubility of minerals.

The dominant diagenetic processes in the burial environment are; cementation, compaction and dissolution (Tucker and Wright, 1990). With burial and increasing over burden sediments and pore fluids are subjected to increased temperatures and pressure with temperature increase dependent on the geothermal gradient. Increase in temperatures reduces the solubility of $CaCO_3$, which should precipitate carbonate cements more easily at depth. The CO_2 derived from the breakdown of organic compounds increases the acidity of pore ware fluids and hence, causes the dissolution of carbonate grains whereas pressure by over burden load leads to mechanical and eventually chemical compaction. The long-term trend of burial diagenesis is the progressive reduction of porosity by compaction and cementation at higher temperatures and pressures in the presence of pore waters that become increasingly saline.

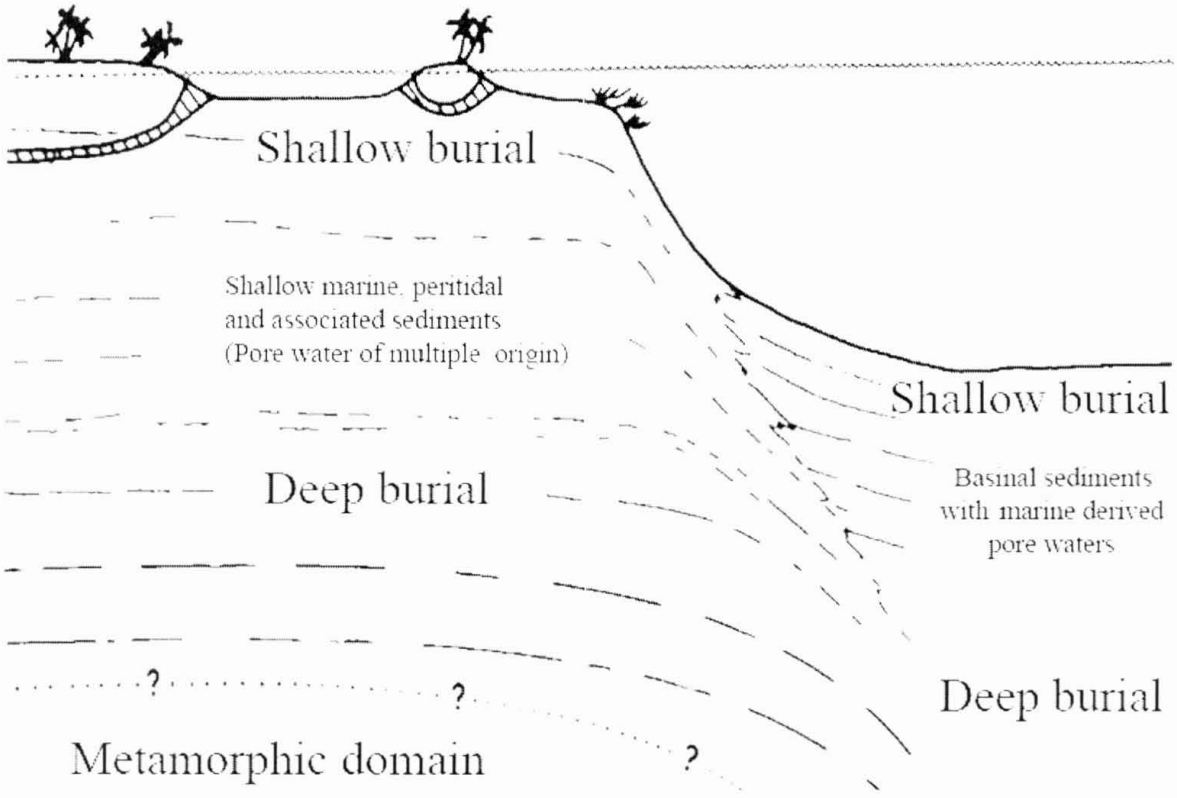

Fig 2.3 The burial diagenetic environment (modified from James and Choquette, 1984)

CHAPTER THREE

RESULTS OF ANALYSIS ON CATOCHE CARBONATES

3.1 Petrography

The Catoche Formation at Daniel's Harbour as reconstructed from core 12i/6-121 and 12i/4-1 (Fig 1.2), is ~ 155 m thick, consists of limestone and dolostone lithofacies and in ascending order, comprises of a lower dolostone (~121 m), a middle limestone (~30 m) and an upper dolostone (~14 m). The limestone lithofacies is a succession of well-bedded, grey, fossiliferous, dolomitic limestone that ranges from mudstone through wacke- to packstone with lenses and beds of boundstone. Porosity is generally low (visual estimates < 2 %) in the limestone lithofacies. The dolostone lithofacies are dark-grey and vary from coarse to fine grained with some zebra texture in the former. Stylolites with amplitudes up to 0.5 cm and some joints also occur in the carbonates.

Petrographic examinations of the Catoche Formation carbonates at Daniel's Harbour indicate that both calcite and dolomite phases are similar to their counterparts at Port au Choix and Port au Port Peninsula (Knight et al. 2007; Greene 2008; Conliffe et al. 2012). The calcite cement generations, from the oldest to the youngest are: marine micrite and microbial mud (C1), pore-filling equant calcite sparite (C2, 50-200 μm) and coarse blocky calcite (C3, 150-650 μm) often filling vugs and joints (Plate.3.1a- c). Calcites C1 and C2 are dull to non-luminescent under the cathodoluminoscope, but calcite C3 exhibits bright orange CL (Plate. 3.1f). The dolomite generations (Plate. 3.1d-f and Plate 3.2a-b), also in the same order, are: dolomicrite (D1), stylolite-associated dolomites (Ds), equant replacive dolomite (D2) and large equant pore-filling replacive saddle dolomite (D3). However, the iron-rich (≥20,000 ppm) pore-filling saddle

dolomite reported by Greene (2008) and Knight et al. (2007) at Port au Choix (referred to by them as D5) was not found in the Catoche Formation at Daniel's Harbour. Both calcite and dolomite phases occur as replacement and pore-filling cements and petrographic relations indicate that calcite C3 postdates all other calcite and dolomite generations (Plate. 3.2e).

Early dolomite (D1) is ~18.5% by abundance and typically consists of replacive, fabric retentive near-micritic to tightly packed non-planar mosaic crystals with irregular intercrystalline boundaries and range from < 4 to 30 μm (Plate. 3.1d). Dolomite D1 is almost nonporous (<1%) and exhibits dull CL. Stylolite-associated dolomites (Ds) range in size from 60 μm to 175 μm, is associated with stylolites and are cross-contaminated with the residual materials transported along pressure dissolution seams and stylolites. Dolomite Ds samples were excluded in other analyses due to the expected inconsistent signature overprints from insoluble residues and other elements associated with chemical compaction. Similar petrographic features were documented for D1 and Ds dolomites at Port au Choix and Port au Port sections (Knight et al. 2007; Greene 2008; Conliffe et al. 2012).

Dolomite D2 is the most abundant type of dolomite (making up ~ 72% of Catoche carbonates by abundance) and consists of coarse equant euhedral to subhedral crystals ranging from 70 μm to 1 mm. Crystals often have cloudy cores with clear rims under plane polarized light and undulose extinction under crossed polars as well as concentric zoned luminescence under cathodoluminoscope (Plate. 3.1e-f). It is fabric destructive and likely replaced calcite C1 and/or D1 dolomite. Intercrystalline porosity with visual estimates up to 12% is associated with D2 dolomite and pores are occasionally lined with kerogen that gives off a blue luminescence under the UV luminoscope (Plate. 3.2c-d) and fluorescence spectra with peaks at 490-495nm (Fig 3.1).

Similar features were documented in D2 dolomites at Port au Choix and Port au Port Peninsula (Knight et al. 2007; Greene 2008; Conliffe et al. 2012).

The latest dolomite generation (D3), is ~16.3% by abundance and typically consists of pore-filling, coarse, subhedral to anhedral crystals of saddle dolomite, which are up to 3 mm and show undulose extinction (Plate. 3.2a). Dolomite D3 is generally restricted to vugs and joints and subhedral crystals often appear zoned under crossed polarized light and cathodoluminoscope (Plate. 3.2a-b). Intercrystalline and vuggy porosity are occasionally associated with D3 particularly with its subhedral crystals. Similar features were also documented in the D3 dolomites in the equivalent sections at Port au Choix and Port au Port peninsula (Knight et al. 2007; Greene 2008; Conliffe et al. 2012).

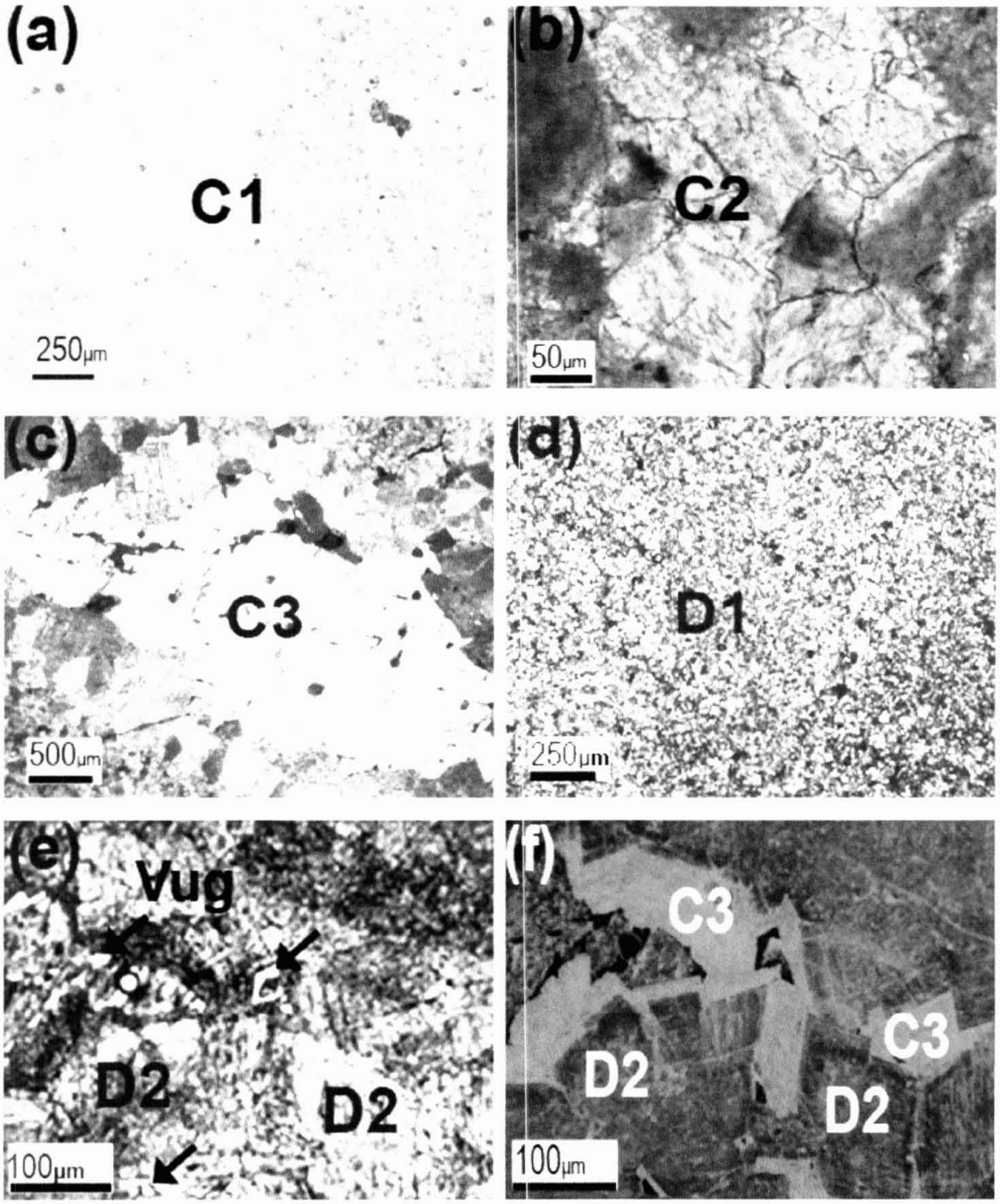

Plate 3.1. Photomicrographs of petrographic features of Catoche carbonates in the investigated core showing (a) C1 calcite (crossed polars; Sample 4-118), (b) C2 calcite (crossed polars; Sample 4-100), (c) C3 calcite (crossed polarized light; Sample 6-4), (d) D1 dolomite (crossed polars; Sample 6-16), (e) Rhombs of D2 dolomite showing cloudy core with clear rim and intercrystalline pores (arrows) associated with D2 (plane polarized light; Sample 6-4), (f) Cathodoluminescence image of (plate 3.1e) showing concentric zonation CL in D2 and bright orange CL of C3.

(a)
100μm
(b)
D3
50μm
(c)
100μm
(d)
100μm
200μm

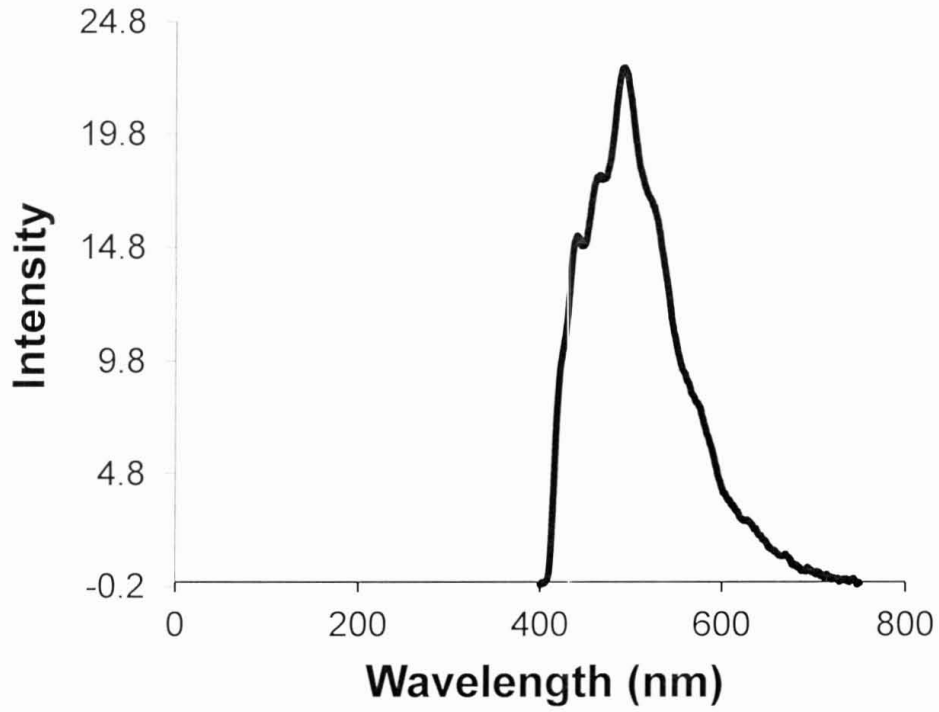

Fig 3.1. Fluorescence spectra of kerogen material in intercrystalline pores of D2 dolomite in Catoche carbonates

3.1.1 Fluid inclusion

Primary fluid inclusions were examined in dolomite generations D2, D3 and calcite C3. However, no measureable inclusions were available in D1, and calcites C1 and C2. All microthermometric measurements were performed on primary two-phase (liquid + vapor) inclusions that occurred in clusters. Care was taken to examine inclusions hosted in the core of crystals or aligned parallel to growth direction as such inclusions are known to retain their primary signatures (Goldstein and Reynolds 1994). Homogenization temperatures were measured before freezing to avoid stretching of the inclusions by ice formation, an issue described by Lawler and Crawford (1983). Fluid inclusions in dolomites D2 and D3 show consistent liquid: vapor ratios (~ 0.95), however, fluid inclusions in D3 are generally larger in size (> 20 μm) relative to those in D2 (Plate 3.3 a-b). The majority of inclusions in the latest calcite cement (C3) were too small to produce reliable results for melting points (and invariably salinity) although some measurements of T_h were obtained. Microthermometric measurements of homogenization temperature (T_h, the minimum estimate of entrapment temperature), initial melting temperature (T_i), and final melting temperature of ice (T_m (ice)) with estimated salinity (Bodnar 2003) were taken from dolomites D2, D3 and calcite C3. The results are summarized in Appendix 2, Table 3.1 and Figure 3.2(a-d). Fluid inclusions in D2 range in size from 2 μm to ~ 20 μm and in D3 from 2 μm to ~ 35 μm. Some inclusion clusters showed evidence of post-entrapment leaking and therefore data were only collected from inclusions that had relatively consistent liquid: vapor ratios and narrow homogenization temperature ranges (usually less than 15°C).

The mean values of T_h for the respective generations of Catoche dolomites is highest at Daniel's Harbour (Table 3.1), with values of 126.6 ± 12.8°C, n = 97 and 174.1 ± 7.6 °C, n = 29

for dolomites D2 and D3 respectively. These temperatures are considerably higher than those of their equivalent dolomites from Port au Choix (D2 = 109 ± 13 °C, n = 42, D3 = 118 ± 10 °C, n=16) and Port au Port (D2 = 106±11 °C, n=42, D3 = 112 ± 21 °C, n =29) sections (Conliffe et al. 2012). The mean salinity of fluid inclusions associated with D2 (Table 3.1), is similar at Daniel's Harbour (23.2 ± 1.4 eq wt % NaCl, n = 60) and Port au Choix (22 ± 2.4 eq wt % NaCl n = 17) and are higher relative to their counterpart at Port au Port (16.5 ± 1.6 eq wt % NaCl, n = 8). On the other hand, the salinity of fluid inclusions in D3 is similar at Daniel's Harbour (21.3 ± 0.6 eq wt % NaCl, n = 27) and Port au Port (20.7 ± 2.7 eq wt % NaCl, n = 10) but higher relative to its counterpart at Port au Choix (14 ± 1.8 eq wt % NaCl, n = 11, Conliffe et al. 2012). Fluid inclusions in calcite C3 have a higher mean T_h but lower salinity at Port au Port relative to Port au Choix (116 °C, 13.7±4.2 eq wt % NaCl and 102 °C, 23.6 ± 1.1 eq wt % NaCl), respectively, (Table 3.1).

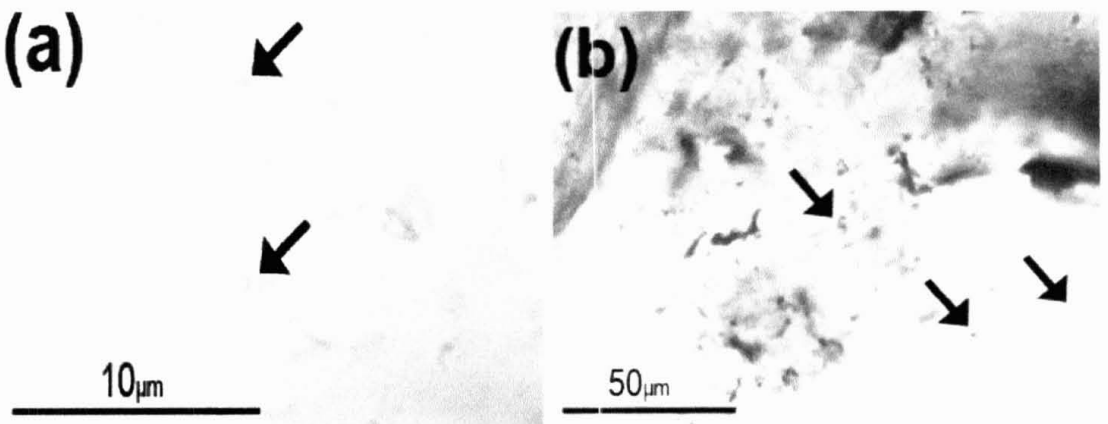

Plate 3.3. Photomicrographs showing distribution of fluid inclusions. (a) Biphase inclusion in D3 (arrows). (b) Biphase inclusion in D2 (arrows).

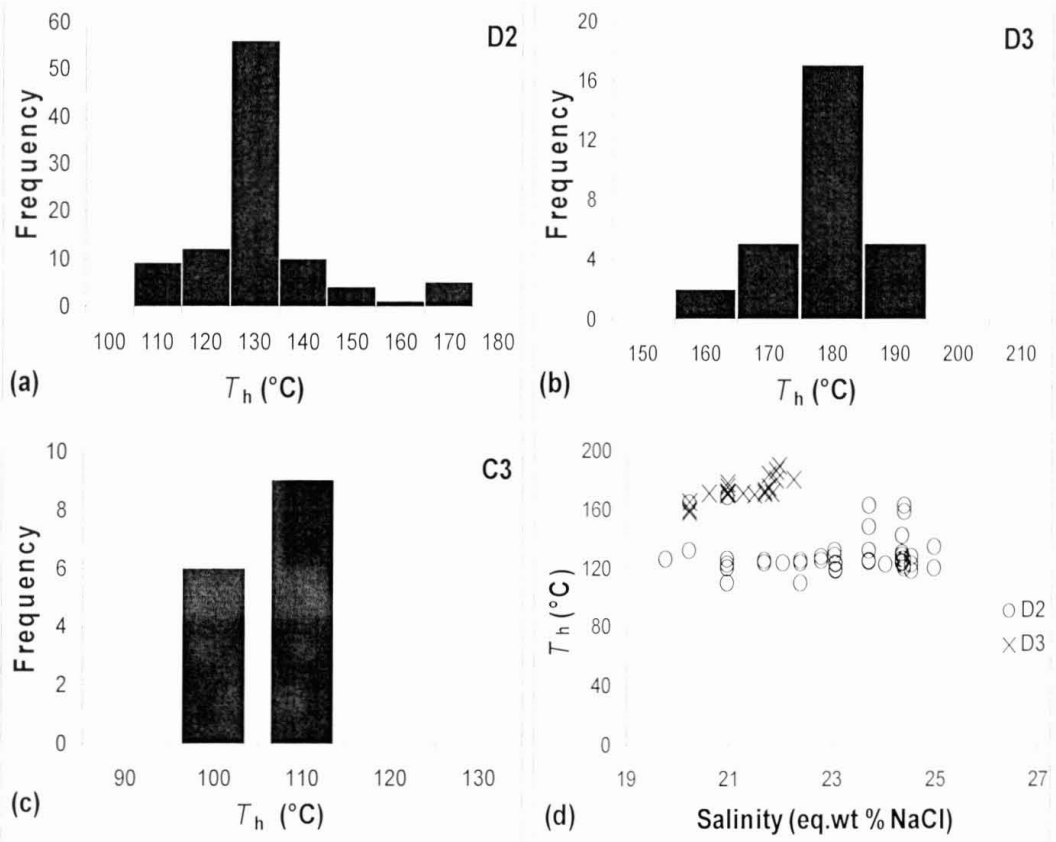

Fig 3.2. Plots of the microthermometric data from primary two-phase fluid inclusions trapped in D2, D3 and C3 of the Catoche Formation at Daniels Harbour showing (a) histogram of homogenization temperature of D2, (b) Histogram of homogenization temperature of D3, (c) Histogram of homogenization temperature of C3, and (d) Scatter diagram of estimated salinity (Bodnar, 2003) vs. homogenization temperature of D2 and D3

Table 3.1. Summary Statistics of microthermometric measurements in the Catoche Formation carbonates at Daniels Harbour (current study), and at Port au Choix and Port au Port (Conliffe et al, 2012).

Daniels Harbour (Northern Peninsula)

Host Mineral		T_i (°C)	$T_{m\ (ice)}$ (°C)	Eq. wt% NaCl	T_h (°C)
D2	n	7	60	60	97
	Mean	-52.3	21.2	23.2	126.6
	S.D	2.6	2	1.4	12.8
	Max	-48	-16.4	25	168
	Min	-55	-24	19.8	102
D3	n	5	27	27	29
	Mean	-54.3	-18.5	21.3	174.1
	S.D	3	0.8	0.6	7.6
	Max	-50	-17	22.2	190
	Min	-58	-19.8	20.2	158
C3	n				15
	Mean				101.3
	S D				5.2
	Max				108
	Min				92

Port au Choix (Northern Peninsula)

Host Mineral		T_i (°C)	$T_{m\ (ice)}$ (°C)	Eq. wt% NaCl	T_h (°C)
D2	n	4	17	17	42
	Mean	-54.9	-19.7	22	109
	S.D	0.5	3.4	2.4	13
	Max	-54.2	-13.6	25.5	134
	Min	-55.3	-24.8	17.4	87
D3	n	6	11	11	16
	Mean	-53.1	10.1	14	118
	S.D	1	1.8	1.8	10
	Max	-51.7	-7.8	18.4	140
	Min	-54.4	-14.6	11.5	109

C3	n	5	14	14	20
	Mean	-52.8	-21.8	23.6	102
	S D	1.7	1.6	1.1	15
	Max	-51.2	-19.7	25	129
	Min	-55.2	-24	22.2	72

Port au Port Peninsula

Host Mineral		T_i (°C)	$T_{m\ (ice)}$ (°C)	**Eq. wt% NaCl**	T_h (°C)
D2	n	3	8	8	42
	Mean	-49.8	-12.6	16.5	106
	S.D	0.7	1.7	1.6	11
	Max	-49	-10.2	19.1	132
	Min	-50.3	-15.6	14.1	90
D3	n	4	10	10	29
	Mean	-51	-17.8	20.7	112
	S.D	2.3	3.5	2.7	21
	Max	-49.6	-11.2	24.5	147
	Min	-54.5	-23.2	15.7	85
C3	n	5	20	20	29
	Mean	-46.9	-10.2	13.7	116
	S D	13.3	3.9	4.2	60
	Max	-23.2	-5	19.1	205
	Min	-53.7	-15.6	7.9	52

3.2 Geochemistry

3.2.1 Major and trace elements

Table 3.2 summarizes the major and trace element concentrations of the Catoche carbonates at Daniel's Harbour and other locations across western Newfoundland. Elemental geochemical data for calcite C2 was excluded because C2 is rare and found only mixed with calcite C1, such that it was impossible to micro sample without cross contamination. The results indicate that D1 and D2 are less calcitic on the Northern Peninsula at Daniels Harbour ($CaCO_3$; D1 = 51.6 ± 2%, *n*=15, D2 = 51.9 ± 2%, *n*=35) and Port au Choix ($CaCO_3$; D1 = 57.9 ± 2%, *n*=13, D2 = 55.6 ± 1%, *n*=20), compared to their counterparts at Port au Port (D1 = 60.9 ± 5%, *n*=5 and D2 = 61.7 ± 2%, *n*=11). Also, the Northern Peninsula sections have a lower mean Sr concentration (Daniel's Harbour; D1 = 47.3 ± 2.5 ppm, *n*=15 and D2 = 36.4 ± 8 ppm, *n*=35, Port au Choix; D1 = 70 ± 43 ppm, *n*=13 and D2 = 31 ± 4 ppm, *n*=20) relative to their counterparts at Port au Port (D1 = 106 ± 60 ppm, *n*=5 and D2 = 68 ± 21 ppm, *n*=11). Dolomite D2 generally has similar Fe concentration at all locations although it is slightly enriched on the Northern Peninsula relative to those at Port au Port whereas the mean Mn concentration is lower in carbonates of the former locality (Conliffe et al. 2012).

3.2.2 Carbon and oxygen isotopes

Table 3.2 summarizes the isotopic composition of Catoche Formation carbonates at Daniel's Harbour and other locations in western Newfoundland. At Daniel's Harbour, mean $\delta^{13}C$ values decreased from -0.5 ‰ ± 0.3 VPDB in calcite C1 to -3.7‰ ± 0.9 VPDB in C3 but there is no significant change in the mean $\delta^{18}O$ values of the calcites. On the contrary, the mean $\delta^{13}C$ and $\delta^{18}O$ values of the dolomites exhibit no strong trends (Table 3.2). Catoche dolomites at Port au

Port are slightly more positive in their $\delta^{13}C$ and $\delta^{18}O$ values (Conliffe et al. 2012) relative to their counterparts on the Northern Peninsula (Table 3.2). No significant correlation was found between the Mn/Sr ratios and the $\delta^{13}C$ values of the dolomites in the Daniel's Harbour section (Fig 3.3a-c) as well at the Port au Choix and Port au Port sections (Conliffe et al. 2012).

3.2.3 Rare earth elements (REE)

Table 3.3 is the summary statistics of the REE concentrations of Arenig seawater and Catoche carbonates at Daniel's Harbour (Appendix 1). Mean ΣREE values are lowest in calcite C1 (5.4 ± 1.1 ppm, n = 8), invariable between dolomite D1 (11.9 ± 4.8 ppm, n = 15) and D2 (10.6 ± 3.9 ppm, n = 35) but increased in dolomite D3 (20.7 ± 16.4 ppm, n = 12) to the highest mean value.

Table 3.4 summarizes the statistics of the Ce and Eu anomaly calculations (Bau and Dulski 1996) as well as Th/U and V/Sc ratios for the respective phases of Catoche carbonates. Calcite C1 has the lowest mean Ce anomaly with a value of 0.68 ± 0.06, whereas dolomite D3 has the highest mean Ce anomaly with a value of 0.88 ± 0.06. Mean Ce anomaly values for all the other carbonates fall between these values. A narrow mean Eu anomaly range is displayed by the carbonates of the Catoche Formation, which range from 0.67 ± 0.08 in C1 to 0.70 ± 0.11 in D3. Calcite C1 has the lowest mean V/Sc ratio with a value of 2.89 ± 1.43, whereas dolomite D3 has the highest mean V/Sc ratio with a value of 5.70 ± 4.16. Mean V/Sc ratio values for all the other carbonates fall between these values. Mean Th/U ratios are 0.21 ± 0.04, 1.19 ± 0.78, 0.96 ± 0.51 and 0.94 ± 0.58 for C1, D1, D2 and D3 respectively.

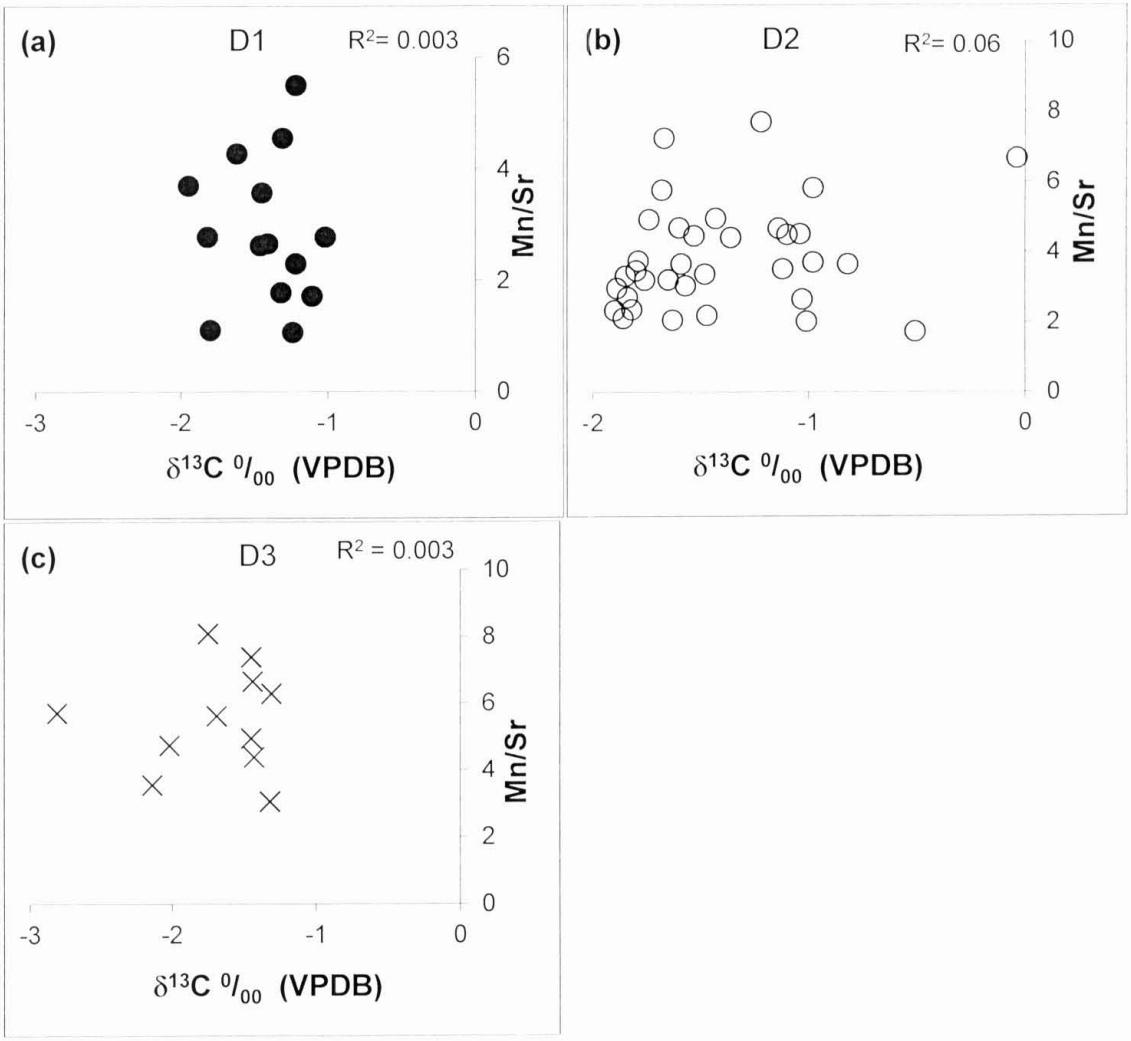

Fig 3.3. Scatter diagrams of $\delta^{13}C$ vs Mn/Sr for (a) D1, (b) D2, and (c) D3 dolomites of the Catoche Formation in the investigated core section showing insignificant correlations.

Table 3.2. $CaCO_3$, $MgCO_3$, Mn, Sr, Fe, $\delta^{18}O$ and $\delta^{13}C$ statistics for Catoche Formation carbonates in the investigated core section at Daniels Harbour and equivalent sections at Port au Choix and Port au Port (Conliffe et al., 2012).

Daniel's Harbour (Northern Peninsula)

Phase		$CaCO_3$ % (ppm)	$MgCO_3$% (ppm)	Fe (ppm)	Mn (ppm)	Sr (ppm)	$\delta^{18}O$ ‰(VPDB)	$\delta^{13}C$ ‰(VPDB)
C1	n	8	8	8	8	8	8	8
	Mean	98	2	114	18	271	-9.3	-0.5
	S.D	2	2	43	5	26	0.3	0.3
	Max	99.2	6.7	214	27	303	-8.7	-0.03
	Min	93.3	0.8	73	13	222	-9.7	-0.99
C3	n	1	1	1	1	1	4	4
	Value	95	5	205	149	17	-9.6	-3.7
	S.D						0.2	0.9
	Max						-9.3	-2.8
	Min						-10	-4.8
D1	n	15	15	15	15	15	17	17
	Mean	51.6	48.4	1445	103	47	-9.0	-1.3
	S.D	2	2	695	28	25	1	0.4
	Max	55.2	50.6	3082	141	126	-6.8	-0.3
	Min	49.4	46.5	720	47	26	-10.4	-2
D2	n	35	35	35	35	35	52	52
	Mean	51.9	48.1	1684	131	36	-9.5	-1.4
	S.D	2	2	1096	50	8	0.8	0.4
	Max	57.7	50.5	4493	342	52	-7.9	-0.04
	Min	49.5	42.3	531	43	27	-11.6	-2
D3	n	12	12	11	12	12	15	15
	Mean	51.9	48.1	1784	198	39	-10.5	-1.7
	S.D	1	1	618	55	9	1.3	0.4
	Max	53.7	49.6	3299	280	57	-7.9	-1.3
	Min	50.4	46.3	810	97	26	-13.2	-2.8

Port au Choix (Northern Peninsula)

Phase		$CaCO_3$ % (ppm)	$MgCO_3$% (ppm)	Fe (ppm)	Mn (ppm)	Sr (ppm)	$\delta^{18}O$ ‰(VPDB)	$\delta^{13}C$ ‰(VPDB)
C1	n	13	13	13	13	13	13	13
	Mean	97.3	2.7	1607	53	362	-8.5	-1.7
	S.D	2	2	626	17	61	0.6	0.5
	Max	98.8	6.1	2874	79	482	-7.9	-1.1
	Min	93.9	1.2	822	36	290	-9.7	-2.7
D1	n	13	13	13	13	13	13	13
	Mean	57.9	42.1	4001	100	70	-8.7	-0.8
	S.D	2	2	1939	40	43	1.3	0.5
	Max	62.1	45	7389	183	161	-6.6	0.1
	Min	55	38	1721	56	31	-10.3	-1.7
D2	n	20	20	20	20	20	20	20
	Mean	55.6	44.4	1751	178	31	-9.2	-0.9
	S.D	1	1	1008	90	4	1.2	0.4
	Max	57	46.5	5600	435	40	-6.9	-0.2
	Min	53.5	43	853	62	26	-10.7	-1.4
D3	n	4	4	4	4	4	4	4
	Mean	60.9	39.1	14934	316	64	-7.3	-1.2
	S.D	2	2	10287	115	13	1	0.4
	Max	63.8	40.6	29279	485	83	-6.1	-0.7
	Min	59.5	36.2	4881	240	52	-8.5	-1.5

Port au Port Peninsula

Phase		$CaCO_3$ % (ppm)	$MgCO_3$% (ppm)	Fe (ppm)	Mn (ppm)	Sr (ppm)	$\delta^{18}O$ ‰(VPDB)	$\delta^{13}C$ ‰ (VPDB)
C1	n	5	5	5	5	5	14	14
	Mean	99.4	0.6	394	98	211	-7.9	-0.7
	S.D	0.4	0.4	253	158	166	0.6	0.5
	Max	99.7	1.2	777	379	486	-6.9	-0.1
	Min	98.8	0.3	174	15	84	-8.7	-2.2
C3	n	8	8	8	8	8	15	15
	Mean	99.1	0.9	402	798	122	-8.4	-2.6
	S.D	1	1	244	963	87	2.4	2.4
	Max	99.8	3.2	813	2282	303	-2.3	0.4
	Min	96.8	0.2	109	11	41	-11.8	-7.4

D1	n	5	5	5	5	5	5	5
	Mean	60.9	39.1	1706	140	106	-6.1	-0.7
	S.D	5	5	465	114	60	0.7	0.2
	Max	66	44.8	2248	342	206	-5.4	-0.5
	Min	55.2	34	1175	67	61	-6.9	-1
D2	n	11	11	11	11	11	26	26
	Mean	61.7	38.3	1589	209	68	-7	-0.8
	S.D	2	2	1001	190	21	0.5	0.3
	Max	63.7	41.5	3354	741	108	-5.7	-0.4
	Min	58.5	36.3	490	60	46	-7.8	-1.4
D3	n	1	1	1	1	1	1	1
	Value	63	37	1178	186	65	-7.5	-0.8

Table 3.3. Summary of rare earth element concentration of Catoche carbonates at Daniel's Harbour

PHASE		La (ppb)	Ce (ppb)	Pr (ppb)	Nd (ppb)	Sm (ppb)	Eu (ppb)	Gd (ppb)	Tb (ppb)	Dy (ppb)	Ho (ppb)	Er (ppb)	Tm (ppb)	Yb (ppb)	Lu (ppb)	ΣREE (ppm)
D1	n	15	15	15	15	15	15	15	15	15	15	15	15	15	15	15
	Mean	2476	4900	599	2268	412	88	436	57	298	56	171	22	135	20	12
	S.D	973	2071	248	925	169	34	157	22	106	21	61	8	45	8	5
	Max	4597	9456	1156	4373	769	158	736	97	524	102	280	38	223	38	22
	Min	1438	2562	340	1285	222	47	233	26	140	22	81	9	67	8	7
D2	n	35	35	35	35	35	35	35	35	35	35	35	35	35	35	35
	Mean	2299	4244	525	2001	367	78	377	54	282	55	161	21	131	19	11
	S.D	837	1769	206	755	127	26	129	17	90	17	52	6	41	7	4
	Max	4452	8127	955	3654	648	127	750	102	522	102	301	35	247	36	20
	Min	1204	2020	241	1062	203	42	218	34	168	25	89	9	69	8	6
D3	n	12	12	12	12	12	12	12	12	12	12	12	12	12	12	12
	Mean	3858	8985	1137	4224	724	163	699	85	380	67	190	23	136	22	21
	S.D	2733	7514	971	3577	572	101	518	56	212	35	96	12	65	9	16
	Max	10269	26917	3491	12991	2049	344	1909	210	775	129	357	48	261	37	60
	Min	1276	2476	307	1113	202	55	202	33	166	25	73	7	42	8	6
CI	n	8	8	8	8	8	8	8	8	8	8	8	8	8	8	8
	Mean	1280	1821	248	1003	201	45	231	34	196	42	124	18	105	16	5
	S.D	242	360	58	214	52	12	58	9	56	14	31	5	36	4	1
	Max	1692	2418	350	1354	297	66	326	49	289	68	178	25	158	24	7
	Min	917	1233	164	708	155	29	174	24	136	26	89	10	66	11	4
C3	n	1	1	1	1	1	1	1	1	1	1	1	1	1	1	1
	Value	6889	11276	1256	4534	632	137	644	68	295	56	180	24	183	25	26
Arenig Seawater Brach shells	n	4	4	4	4	4	4	4	4	4	4	4	4	4	4	4
	Mean	362	812	100	373	57	14	61	5	27	5	16	2	15	1	2
	S.D	151	256	34	135	20	6	27	3	9	2	9	2	10	2	1
	Max	545	1025	138	557	85	19	98	9	39	8	27	5	25	4	3
	Min	202	506	63	234	42	7	38	3	19	3	8	0.3	4	0.3	1

Table 3.4. Summary statistics of Ce $(Ce/Ce^*)_{SN}$ and Eu $(Eu/Eu^*)_{CN}$ anomaly analysis (based on the equations by Bau and Dulski, 1996), as well as ratios of Th/U and V/Sc for Catoche carbonates at Daniel's Harbour.

Phase		Ce^*_{SN} anomally	Eu^*_{CN} anomally	Th/U	V/Sc
C1	n	8	8	8	8
	Mean	0.68	0.67	0.21	2.89
	S.D	0.06	0.08	0.04	1.43
	Max	0.76	0.76	0.28	5.71
	Min	0.60	0.52	0.13	1.56
D1	n	15	15	15	15
	Mean	0.85	0.67	1.19	2.89
	S.D	0.05	0.05	0.78	1.34
	Max	0.94	0.79	2.79	5.22
	Min	0.77	0.59	0.37	0.57
D2	n	35	35	31	34
	Mean	0.81	0.65	0.96	2.98
	S.D	0.06	0.05	0.51	1.22
	Max	0.91	0.75	2.25	5.86
	Min	0.70	0.56	0.34	0.64
D3	n	12	12	11	11
	Mean	0.96	1.21	0.94	5.70
	S.D	0.07	0.56	0.58	4.16
	Max	1.04	2.91	2.01	11.24
	Min	0.83	0.78	0.08	0.69

3.3 Fluids-Inclusion Gas Analysis

Results of fluid inclusion gas analysis carried out on each carbonate phase of the Catoche Formation at Daniels Harbour, are as shown in Appendix 3. The weighted mean ratio of CO_2/CH_4 varied from 0.03 to 0.08 in calcite C1, 0.10 to 0.32 in D1, 0.07 to 0.14 in D2 and 0.58 to 1.36 in D3, while the corresponding weighted mean ratio of N_2/Ar varied from 132.4 to 143.2, 80.1 to 103, 90.9 to 105.5 and 54.4 to 66.2, respectively.

CHAPTER FOUR

INTERPRETATIONS AND POROSITY DISTRIBUTION

4.1. Dolomite Petrography

The fine crystalline fabric-retentive nature and dull cathodoluminescence of the dolomicrite (D1) suggest early dolomitization of marine limemud at near-surface conditions in shallow burial settings prior to compaction. This is consistent with the presence of microstylolites that cut through D1 and the occurrence of D1 as dolomicrite intraclasts directly above the St. George unconformity (Lane, 1990). The very low porosity associated with D1 (visual estimates < 1%) suggests that dolomitization was extensive and occurred under open system conditions with sufficient supply of Mg^{2+} ions such that dolomicrite occluded every available pore present. This agrees with the suggested origin for D1 in the Catoche Formation at Port au Choix and Port au Port (Greene, 2008; Conliffe et al., 2012).

The fabric destructive nature and larger crystal sizes of D2 (70 μm - 1mm), compared with D1 (dolomicrite), suggest a later stage of replacive dolomitization that started with increased temperature and pressure (Warren, 2000). The cloudy core with clear rims, undulose extinction and zoned CL images of D2 indicates variations in chemistry and redox conditions of the dolomitizing fluids as well as an increase in temperature during the course of crystallization (e.g., Rameil, 2008; Kırmacı, 2008). This is consistent with the mean T_h (126.6 ± 12.8 °C, n=97) for D2 and suggests deeper burial relative to D1. The presence of undulose extinction has been linked in some earlier studies to sulphate reduction (Radke and Mathis, 1980), however no evidence has been found in the Catoche dolomites to support this process. The generally higher mean T_h measurements from Catoche dolomites on the Northern Peninsula relative to its

counterparts at Port au Port, may reflect relatively deeper settings for the former location (Table 3.1).The high intercrystalline porosity associated with D2 indicates dolomitization under a closed to semi-closed system with limited external supply of Mg^{2+} ions such that no extra dolomite occluded the developed intercrystalline pores. These pores are often filled or lined with kerogen that exhibits blue UV luminescence (Plate. 3.2c-d; e.g., Roedder, 1984; Gillespie and Burden, 2010). Micro-spectroscopic analysis of the kerogen material shows fluorescence with peaks at 490-495nm (Fig. 3.1). This strongly suggests the presence of light hydrocarbons with API > 45 (Gillespie and Burden, 2010). Also, the spectroscopic profile is identical to that of known crude oil samples from within the Jeanne d'Arc Basin, off the coast of eastern Newfoundland (Gillespie and Burden, 2010).

The mean T_h of D3 (174.1 ± 7.6 °C, n=29), coupled with its limited distribution, imply development at the very late stages of diagenesis at higher temperature relative to D2. The generally higher mean T_h values for dolomites on the Northern Peninsula suggest hotter fluids and/or possible deeper burial settings relative to those documented for the equivalent Port au Port Peninsula section (Table 3.1).

Despite the difference in the ranges of T_h values, the considerable overlap in the salinity and measured T_h values of fluid inclusions associated with D2 and D3 (Fig. 3.2a,-b and d, Table 3.2) suggests that they likely formed from fluids of similar composition but at different temperatures in a closed system or possibly from the same fluids that circulated during burial in a close to semi closed system. This is consistent with the occurrence of intercrystalline pores in D3 similar to those commonly associated with D2. A similar overlap in salinity and T_h was documented by Conliffe et al (2012) in dolomites at Port au Choix and Port au Port.

4.2 Major and Trace Elements

The mean values of $CaCO_3$ and $MgCO_3$ concentrations of D1 at Daniel's Harbour (Table 3.2) indicates near-stoichiometric dolomite (Appendix 1) with mean Sr concentration of 47 ± 25ppm (< 550 ppm; Tucker and Wright, 1990). This suggests a coeval open system with an abundant supply of Mg ions or alteration of a precursor Mg- rich polymorph of $CaCO_3$ in an open system (e.g., Sperber et al., 1984; Azmy et al., 2001, 2008) rather than a hypersaline sabkha origin (Lane, 1990). This is consistent with the absence of evaporite beds in the Catoche and surrounding formations (cf. Meyers et al., 1997; Lu and Meyers, 1998; Azmy et al., 2001, 2008) and lack of moldic porosity within the Catoche Formation (Land, 1967; Matthews, 1974; Longman, 1980; James and Choquette, 1984; Moore, 1997). Consistency in near stoichiometry and narrow ranges of Sr, Mn, and Fe variations in dolomites D1 to D3 (Table 3.2) probably reflects localized circulation of fluids of similar compositions through crustal rocks, which got hotter with subsequent dolomitization events during diagenesis. The occurrence of non-stoichiometric calcian dolomite at Port au Choix and Port au Port suggests possibly less fluid mobility and/or a relatively limited supply of Mg^{2+} (e.g., Sperber et al., 1984).

Iron (Fe) and Manganese (Mn) concentrations are indicators of redox conditions during dolomitization (e.g. Azmy and Lavoie, 2009; Azmy et al., 2008, 2010; Conliffe et al., 2009, 2012). The general increase in the mean values of Fe and Mn concentrations from calcite C1 to C3 and D1 to D3 at Daniel's Harbour (Table 3.2) reflects a decrease in oxidizing conditions from the earliest dolomite generation (D1) to the latest generation (D3). The relatively higher Fe content of D1 at Port au Choix, compared with other locations, is probably due to the influence of terrestrially derived fluids (riverine input) rather than reducing conditions since most petrographic and geochemical evidences support formation at or near the surface (Greene, 2008;

Conliffe et al., 2012). The slightly higher Fe content of D2 dolomite on the Northern Peninsula suggests reduced oxidizing conditions consistent with deeper burial settings and higher T_h values (Table 3.1).

Although it has different petrographic features, D3 at Daniel's Harbour is geochemically similar to D2 (Table 3.2). This may suggest that both D2 and D3 formed from similar or possibly the same diagenetic fluids, which supports the overlap in their salinity and T_h values (Table 3.1). A similar relationship between D2 and D3 has been documented at Port au Port and is akin to non-saddle and saddle D2 dolomite at Port aux Choix (Table 3.2, Conliffe et al., 2012).

4.3 Carbon and Oxygen Isotopes

The $\delta^{13}C$ and $\delta^{18}O$ values of C1 and most of D1, are within range of values of the best preserved carbonates precipitated from Arenig seawater (Fig. 4.1), suggesting a high degree of preservation of its primary isotopic signatures particularly those of carbon (cf. Veizer et al., 1999; Shields et al., 2003). This is supported by the lack of correlation between Mn/Sr and $\delta^{13}C$ values (Fig 3.3a-c). The overlap in $\delta^{13}C$ values of dolomites D1 and D2 with those of calcite C1 suggests that C1 was likely the precursor for these dolomite generations as diagenetic fluids generally have low dissolved CO_2 (low pCO_2; Land, 1992), which makes resetting of C-isotope signatures difficult in many cases. Also, the considerable overlap in the $\delta^{13}C$ signature of dolomites D2 and D3 coupled with the lack of correlation between Mn/Sr and $\delta^{13}C$ in all generations of dolomite (Figs. 3.3a-c and 4.1), implies that deposition of the kerogen material, sometimes lining intercrystalline pores associated with D2, occurred after D2 but prior to D3 rather than contemporaneous with either dolomite precipitation, i.e. dolomitization was not influenced by carbon from organic matter. The variations in the mean $\delta^{13}C$ and $\delta^{18}O$ values of

Catoche dolomites at Daniel's Habour are consistent with diagenetically closed or semi closed system conditions. The significant overlap in $\delta^{18}O$ values of dolomites D1 to D3 with many values of the best preserved carbonates precipitated from Arenig seawater (Fig. 4.1), suggests that dolomitizing fluids might have originated from modified Arenigian or slightly older seawater.

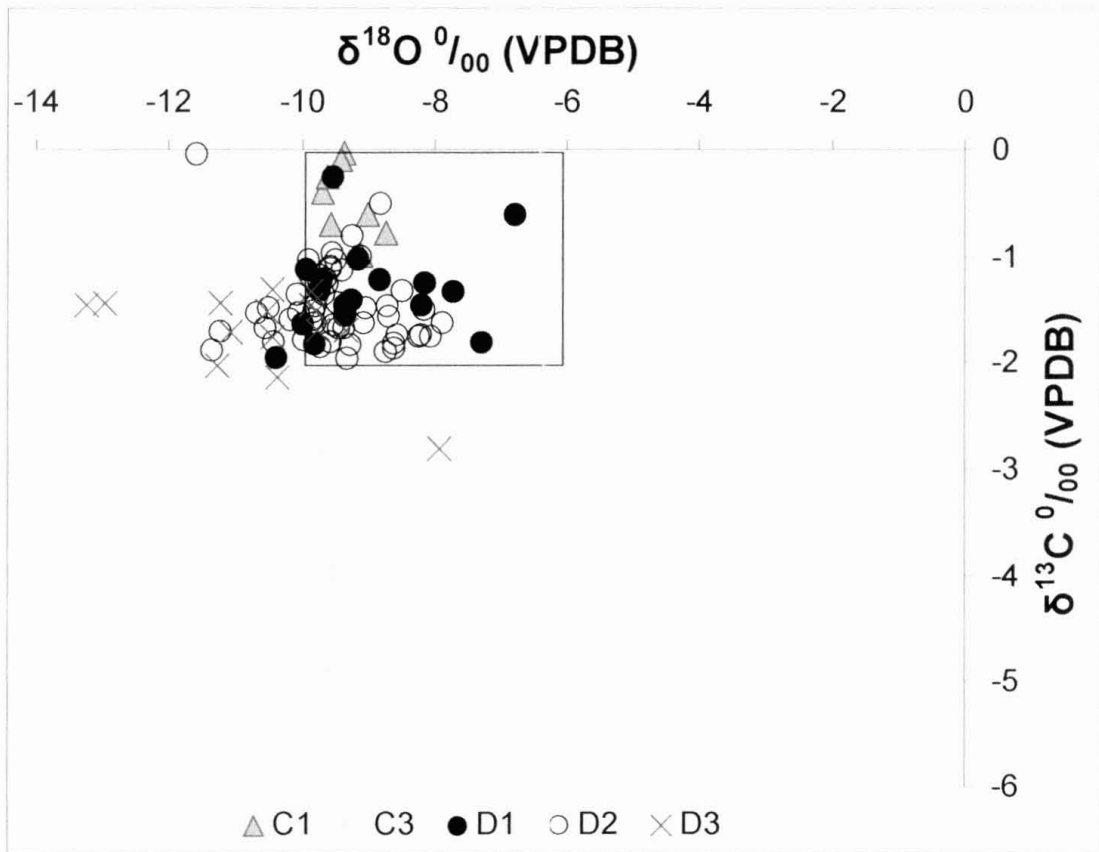

Fig 4.1. Scatter diagram of $\delta^{18}O$ vs. $\delta^{13}C$ for the different Catoche carbonate phases. The square represents the range of isotopic composition of best preserved carbonates precipitated from Arenig seawater (cf. Veizer et al. 1999 and Shields et al. 2003).

Dolomitization requires a large supply of Mg-rich fluids such as seawater. Thus, the isotopic composition of oxygen in dolomites is ultimately influenced by that of the dolomitizing fluid and the temperature of dolomitization (Land, 1992). Therefore, the $\delta^{18}O$ composition of dolomitizing fluids can be determined, if the temperature of dolomitization is known (Land, 1983). Homogenization temperatures of primary liquid-vapor fluid inclusions, nature of rock fabric and fossil content can be used as proxies for temperature of dolomitization (Goldstein and Reynolds, 1994). The fabric-retentive texture of D1 coupled with the near-micritic grain size and occurrence of fenestral and stromatolitic lime mudstones (Knight et al., 2007) along with the absence of evaporite interbeds in the Catoche Formation, reflect warm (~20°C), possibly humid, tropical conditions similar to present-day ones. The best preserved $\delta^{18}O$ values of carbonates (low-Mg calcite brachiopod shells), that precipitated from Arenig seawater during the time of deposition of the Catoche Formation are between -8.2 and -10.1‰ (VPDB; Shields et al., 2003; Bassett et al., 2007). This may reflect precipitation from tropical seawater with a mean $\delta^{18}O$ value of ~ -7.2‰ (SMOW) and values between approximately -6.2 to -8.2‰ (SMOW) at 20°C (Hayes and Grossman, 1991). The dolomicritic crystal size suggests that D1 (the earliest dolomite), was formed during an early stage of diagenesis at near-surface conditions (temperatures ~ 25 to 30 °C, cf. Goldstein and Reynolds, 1994). Therefore, the $\delta^{18}O$ signatures of D1 at Daniel's Harbour (-9.02 ± 1‰ (VPDB), n=17. Table 3.2) suggest that $\delta^{18}O$ values of the dolomitizing fluid were approximately between -10 and -11.2‰ (VSMOW) with a mean of about -10.6 ‰ (VSMOW; Fig. 4.3, Shields et al., 2003; Bassett et al., 2007). The difference between the average $\delta^{18}O$ compositions of seawater and meteoric waters in modern tropical environment is ~ 4‰ (SMOW, Clark and Fritz, 1997). Assuming that the difference in $\delta^{18}O$ compositions between the Arenig meteoric and seawaters was similar to that of the modern

environment, the mean $\delta^{18}O$ value of Arenig meteoric water would be -11.2‰ (SMOW), (i.e. ~ 4‰ lower than -7.2‰). Thus, the estimated $\delta^{18}O$ values of the dolomitizing fluids which formed D1 falls within the calculated mean range of Arenig meteoric (-11.2 ‰, SMOW) and sea water (-7.2 ‰, SMOW). This suggests that dolomitization occurred by mixed waters possibly in a mixing zone environment (e.g., Azmy et al., 2009; Greene, 2008; Conliffe et al., 2012), which is consistent with the low Sr and high Fe contents coupled with the lack of evaporite beds in the Catoche Formation. Applying the above approach at the same temperature to D1 at Port au Choix (Greene, 2008) and Port au Port (Conliffe et al., 2012), suggests that $\delta^{18}O$ value of fluids that precipitated D1 varied from -9.7 to -10.8 ‰ (VSMOW) and -7.0 to -8.2 ‰ (VSMOW), respectively. Thus, the dolomitizing fluids for D1 were more enriched in ^{18}O on the Port au Port peninsula relative to the Northern Peninsula, which suggest that dolomitizing fluids on the Northern Peninsula had a higher Arenig meteoric water content compared to their counterpart on the Port au Port Peninsula (Conliffe et al., 2012). This is consistent with lower Sr and higher Fe concentrations of D1 on the Northern Peninsula (Table 3.2, Appendix 1). On the other hand, the estimated $\delta^{18}O$ composition of dolomitizing fluids for dolomites D2 and D3 in the Daniel Harbour section is more enriched (+2.1 to +8.1‰ and +5.8 to +8.1‰, VSMOW respectively) relative to D1 dolomitizing fluids (Fig. 4.2), which is normal for fluids formed at higher temperatures of deeper burial. Deep-basinal brines are usually highly saline and enriched in ^{18}O irrespective of age and location (Goldstein and Reynolds 1994; Azmy et al., 2001; Lonnee and Machel, 2006). Thus, T_h and salinity measurements coupled with the $\delta^{18}O$ signatures of the dolomitizing fluids for dolomites D2 and D3 reflect a hydrothermal origin (Conliffe et al., 2010). This is consistent with the postulated origin of dolomites D2 and D3 at Port au Choix and Port au Port (Greene, 2008; Conliffe et al., 2012). The overlap in estimated $\delta^{18}O$ values of dolomitizing

fluids for dolomites D2 and D3 (Fig 4.2) at the Daniel's Harbour section implies that both generations likely precipitated from similar fluids or possibly the same fluid that circulated in the crustal rocks under closed system conditions (e.g., Azmy et al., 2009; Conliffe et al., 2012), which is also supported by the invariant mean salinity values for both dolomites D2 and D3 (Table 3.1). A similar overlap has been reported for dolomites D2 and D3 at Port au Choix (Greene, 2008).

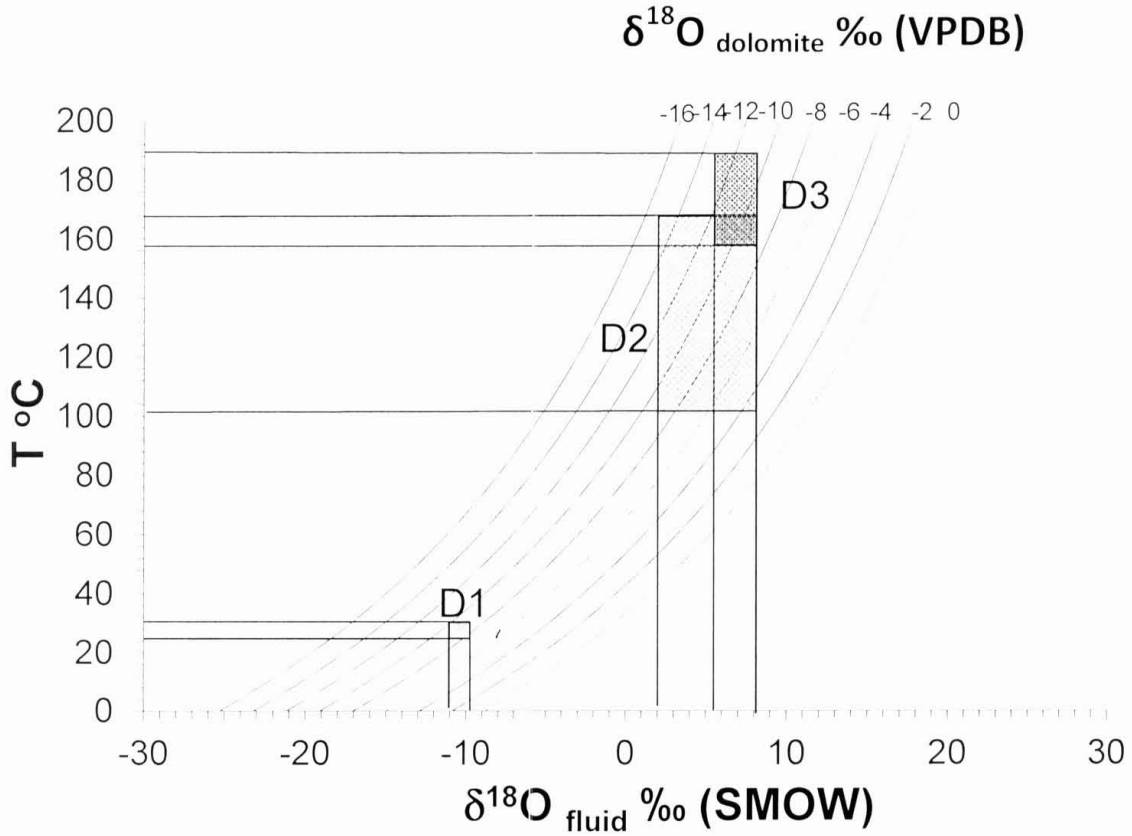

Fig 4.2. Temperature (T) vs. $\delta^{18}O_{dagenetic\ fluid}$ for various $\delta^{18}O_{\ dolomite}$ values that were reconstructed from the following equation: $10^3 \ln \_ = 3.2 * 10^6 T^{-2} - 3.3$ (Land, 1983). The vertical bars indicate the ranges or $\delta^{18}O$ fluid based on the ranges of $\delta^{18}O$ values and homogenization Temperature (T_h) of each identified dolomite generation.

The slightly lower $\delta^{13}C$ values of dolomites at Daniel's Harbour relative to their counterparts at other locations (Table 3.2) are most likely controlled by the precursor carbonate (C1). The higher $\delta^{13}C$ values for calcite C1 at Daniel's Harbour (-0.48 ‰ (VPDB) ± 0.34, n=13) and at Port au Port (-0.7 ‰ (VPDB) ± 0.5, n=14), compared with those at Port au Choix, is consistent with calcites that initially had a higher proportion of high magnesium calcite (Romanek et al., 1992; Swart and Eberli, 2005; Weissert et al., 2008). Generally speaking, the insignificant variations in the mean $\delta^{13}C$ values among the equivalent dolomite generations at all three locations suggests possible regional circulation of diagenetic fluids with similar compositions across western Newfoundland rather than regional mixing with magmatic fluids (e.g., Lavoie et al., 2010). The diagenetic fluids probably became hotter during circulation through crustal rocks of deeper settings.

The lack of correlation between $\delta^{13}C$ and Mn/Sr values particularly for the near-micritic and fabric retentive D1 at Daniel's Harbour (Fig. 3.2a), implies that the $\delta^{13}C$ values are near primary and the reconstructed $\delta^{13}C$ profile (Fig. 1.2) is suitable for chemostratigraphic correlations (e.g., Azmy and Lavoie, 2009; Azmy et al., 2010). A similar result was reported for the Port au Choix and Port au Port carbonates (Greene, 2008; Conliffe et al., 2012). Figure 1.2 shows the $\delta^{13}C$ profile of Catoche dolomites at the three locations across western Newfoundland. The $\delta^{13}C$ profiles show a common negative shift at the top and a similar but broader one at the middle that can be utilized for refining stratigraphic correlation of the formation across the area.

4.4 Rare Earth Elements (REE)

Using the mean REE concentrations (Table 3.3) and shale normalized (REE_{SN}) values of the best preserved brachiopods (low-Mg calcite) precipitated during the Arenig as a proxy for

Arenig seawater (Azmy et al., 2011), a plot of the mean (REE / REE_{SN}) values for Catoche carbonates and Arenig seawater are shown in Figure 4.3. The shale normalized patterns of the Catoche calcites and dolomites have similar and parallel profiles that mimic those of Arenig well preserved low-Mg calcite brachiopod shells. This trend suggests that the REE composition of diagenetic dolomites is at least partially controlled by that of the precursor carbonate and that the parent fluids which deposited these dolomites likely contained Arenig seawater. The pattern for calcite C1 shows enrichment in total REE contents (5 ± 1ppm, n=8)) relative to that of the brachiopods (2 ± 1ppm, n=4). This reflects the influence of alteration despite the petrographic preservation of micritic grain size and fabric. However, it is noteworthy that despite the reset in the REE composition, calcite C1 may retain its near-primary $\delta^{13}C$ signature due to the low pCO_2 in diagenetic fluids. The micritic grain size of C1 suggests that alteration occurred at near-surface conditions (i.e. in an oxidizing environment) with low water-rock ratio, which accounts for its negative Ce anomaly (Figs 4.3, 4.4a and Table 3.4) and preserved $\delta^{13}C$ values (Fig. 4.1). The similarities between calcite C1 and dolomite D1 in their shale normalized REE profiles (Fig. 4.3), $\delta^{13}C$ signatures (Fig. 4.1), ΣREE contents (Table 3.3) and fabric preservation coupled with < 550 ppm Sr concentrations for D1 (Table 3.2), are strong evidence of support for calcite C1 as the precursor for dolomite D1 and thus, the Catoche dolomicrites are not syngenetic and therefore cannot be hypersaline sabkha dolomites as was previously believed (e.g., Lane, 1990). Also, the occurrence of REE normalized pattern of calcite C1 between those of the Arenigian well-preserved (low-Mg calcite) brachiopods (lower) and the dolomicrite (upper) supports the scenario of deposition of D1 at very early stage of diagenesis from solutions that were likely a mixture of Arenig meteoric and marine waters.

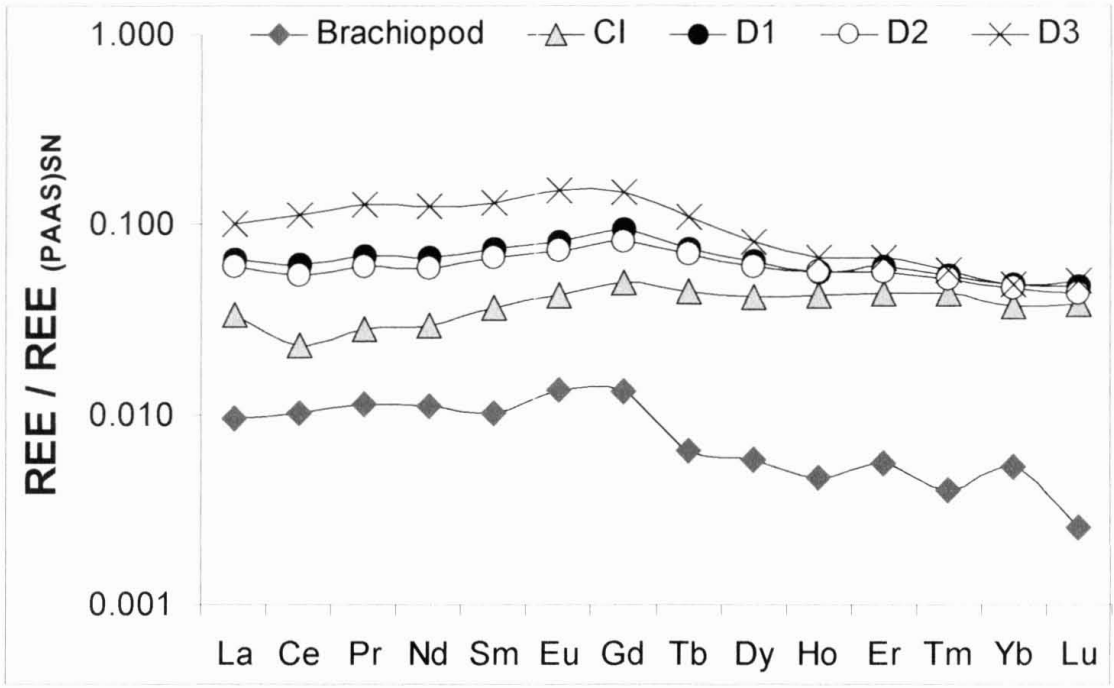

Fig 4.3 Mean shale-normalized (PAAS) values of REE concentrations of best preserved Arenig brachiopod shells and the respective phases of Catoche carbonates.

Insignificant variation in the mean $\delta^{13}C$ values of calcite C1 and the dolomites (Table 3.2), regardless of slight increase in ΣREE of the dolomites relative to calcite C1 (Table 3.3), suggests low water-rock interaction ratios as the carbon isotopic composition of dolomite reflects the nature of the precursor carbonate unless the process of dolomitization occurs in conditions of high water-rock interaction ratios such that diagenetic solutions have enough dissolved CO_2 to reset the C-isotope signature of the precursor carbonate (Tucker and Wright, 1990; Boggs, 2009).

Ce and La anomalies of the Catoche dolomites and calcite C1 cluster around unity (Fig. 4.4a-d), which suggests that they were diagenetically altered in REE equilibrium with their respective diagenetic fluids. Hence, observed variations in REE_{SN} and ΣREE of the respective carbonate

phases reflect evolution of fluid composition during diagenesis. Furthermore, La anomaly is minor whereas Ce anomaly is mostly negative (Fig. 4.4a-d). The normalized REE patterns of Catoche dolomites (D1, D2, and D3) are almost identical and parallel to each other with those of D1 and D2 almost superimposed (Fig. 4.3), coupled with insignificant variations in their respective ΣREE contents (Table 3.3), strongly supports the suggested scenario of circulation of basinal fluids of similar composition (or possibly same composition), through crustal rocks during burial and excludes the involvement of magmatic fluids or fluids of other origins in dolomitization (e.g., Azmy et al., 2008, 2009, 2011; Azmy and Conliffe, 2010; Conliffe et al., 2010; Lavoie et al., 2010).

All Ce anomaly values (Table 3.4), suggest oxic to suboxic fluid conditions during the formation/diagenesis of Catoche dolomites and calcite C1 whereas Eu anomalies expressed as $(Eu/Eu^*)_{CN}$ are consistent with low temperatures (< 250 °C) for the diagenetic fluids that precipitated the dolomites and calcite (e.g. Möller, 2000; Wilde et al., 1996; Bau and Dulski, 1996), which is supported by petrographic features, elemental compositions and fluid inclusion analyses of the respective carbonates. Calculated Eu anomalies coupled with fluid inclusion analysis of Catoche dolomites D2 and D3 and calcite C3, strongly suggest that temperature(s) of dolomitization and latest calcite precipitation was < 200 °C as positive Eu anomaly only occurs at temperatures above 250 °C (Bau and Dulski, 1996; Möller, 2000), which supports the exclusion of magmatic fluids.

Low mean Th/U (between ~1 and 2, Table 3.4) and V/Sc (> 2, Table 3.4) ratios (Wignall and Twitchett, 1996; Kimura and Watanabe, 2001), support suboxic fluid conditions during formation/diagenesis of Catoche dolomites, which is consistent with the interpretations obtained from Ce and Eu anomalies. The petrographic and geochemical data, coupled with Ce anomaly

and V/Sc ratios for calcite C1 (mainly microbial lime mudstone), indicates oxic to slightly suboxic fluid conditions for the limemud. The low mean Th/U ratio of C1 is therefore unlikely caused by anoxic depositional condition but probably due to the activities of bacteria and biodegradation of organic materials as such processes are known to cause U enrichment in sediments (Barnes and Cochran, 1990; Zheng et al., 2002; Thomas and Barry. 2004). This suggests that the reduction process for U^{6+} (which causes U enrichment in sediments), is not a simple inorganic reaction as it may involve particle surfaces for catalysis, specific enzymes produced by bacteria and humic acids from biodegradation of organic materials in sediments (Barnes and Cochran, 1990; Zheng et al., 2002; Thomas and Barry. 2004; Nicolas et al., 2006).

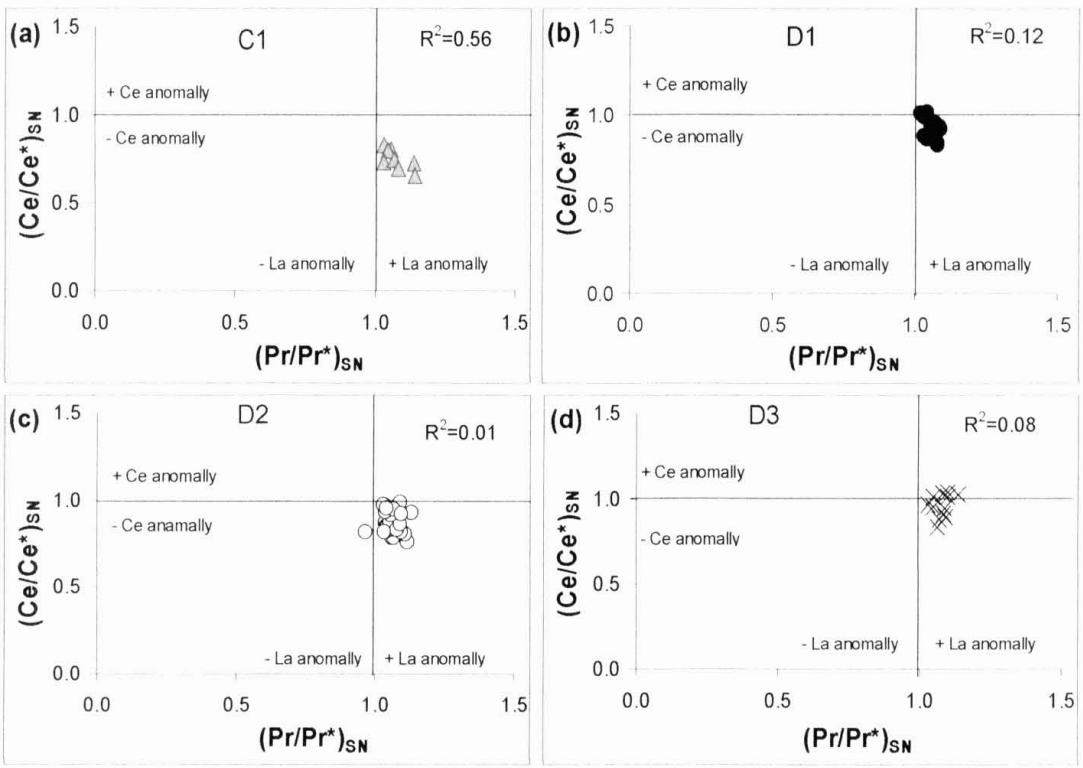

Fig 4.4. Ce and La anomalies (La = $(Pr/Pr^*)_{SN}$) plots for (a) C1, (b) D1, (c) D2, and (d) D3. The values, with few exceptions, cluster close to the unity lines.

4.5 Fluid Inclusion Gas Analyses

Figure 4.5a-b exhibits the plots of CO_2/CH_4 against N_2/Ar ratios for Catoche carbonate inclusion gases at Daniel's Harbour. The data points plot well inside the crustal zone and precludes the involvement of magmatic fluid(s) in the dolomitization process. Rather, Crustal (basinal) fluids which evolved from meteoric waters are present in all generations of Catoche dolomites (Fig 4.5a). The evolution of meteoric waters likely occurred via mixing with seawater as meteoric waters do not have enough Mg^{2+} to cause dolomitization. Calcite C1 plots within the organic field; which implies that there is sufficient organic nitrogen to increase the N_2/Ar ratio above that of air-saturated water. This is consistent with elevated methane levels in the fluid inclusion gas analyses of C1 (Appendix 3) as nitrogen and methane are by-products of protein decay. Release of methane via organic decay also explains why source fluids associated with C1 appear to be more reduced relative to the dolomites (Fig 4.5a-b). Data points of inclusion gases of dolomites D1 and D2, which plot slightly into the organics field, are likely relics of calcite C1. This suggests that calcite C1 is the precursor for these dolomites and is consistent with the overlap in their $\delta^{13}C$ values (Fig. 4.1), similarities in normalized REE profiles (Fig. 4.3) and overlap in values of inclusion gases (Fig. 4.5b). This indicates that D2 likely originated from the recrystallization of D1 and direct dolomitization of calcite C1. All data points plot within the crustal section, which is consistent with low water-rock interaction ratios.

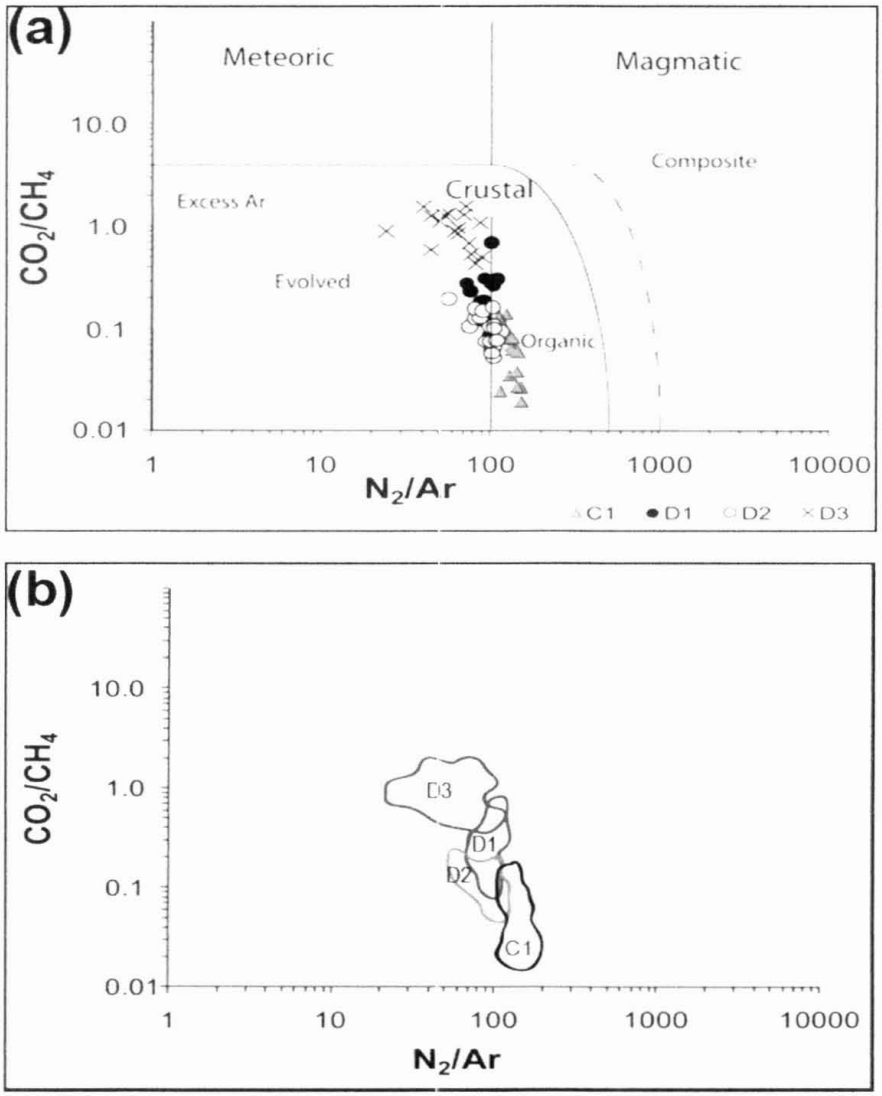

Fig 4.5. Plots of gas analysis of Catoche Formation fluid inclusion gases showing (a) Scatter diagram of CO_2/CH_4 vs N_2/Ar, and (b) data fields for the respective Catoche carbonates showing overlap.

4.6 Diagenetic Environments of Catoche Carbonates

The Catoche carbonates were deposited in warm shallow marine conditions. Petrographic and geochemical features observed suggest that the sediments were affected by diagenesis in the marine, meteoric and shallow burial environments. Calcites C1 and C2 likely precipitated in oxic conditions of the phreatic zone in a marine environment whereas D1 precipitated in oxic conditions of the mixed shallow phreatic zone of a meteoric environment. High salinity, low temperature (< 200) basinal fluids likely derived from the circulation of fluids of the mixed phreatic zone through crustal rocks, deposited D2, D3 and C3 in suboxic conditions of a shallow burial environment

4.7. Variations in Porosity Distribution

Porosity (ϕ) is a key parameter in reservoir characterization and plays an important role in the evolution of hydrocarbon reservoirs. Ultraviolet fluorescence from micro spectroscopy analyses (Plate 3.2c-d, Fig 3.1) coupled with the occurrence of kerogen materials often associated with D2 dolomite of the Catoche Formation at Daniel's Harbour and other locations (e.g. Conliffe et al., 2012), refers to early emplacement of hydrocarbons prior to the precipitation of D3. The preserved porosity in the Catoche Formation is mainly secondary and occurs in dolomites (Fig.1.2), suggesting that it is directly related to the dolomitization process (e.g., Dravis, 1992; Esteban and Taberner, 2003; Wierzbicki et al., 2006; Azmy et al., 2009; Conliffe et al., 2009; Azmy and Conliffe, 2010). Porosity is mostly of the intercrystalline variety (apparent long axes of pores ~50 to 600 μm) and mainly associated with D2 but also occasionally occurs among the subhedral crystals of D3. Dissolution vugs (up to 2.5 mm) and stylolitic pores also occur in the formation. Some of the intercrystalline pores and vugs are filled with D3 and C3, but frequently with kerogen. The calcite C3 cement likely originated from late-

stage non-ferroan Ca-rich fluids that were emplaced after D3. Depleted $\delta^{18}O$ values measured in calcite C3 (Table 3.2) are consistent with the suggested late-stage mid to deep burial origin (Azmy et al., 2009). Intercrystalline porosity likely developed during dolomitization in closed to semi-closed conditions due to the difference in molar crystal volume of dolomite compared to its precursor calcite. The decrease in volume of the resulting dolomite is thus accompanied by porosity development (Warren, 2000); hence volume change is consistent with dolomitization of a precursor calcite while no significant volume change is expected during recrystallization of dolomicrite. If dolomitization operated under completely open system conditions, resulting pores from volume change would be occluded with dolomite cements (cf. Lucia and Major, 1994). Dissolution and the resultant vugs generally occur in response to a significant change in the chemistry of pore fluids such as changes in salinity, temperature, or partial pressure of CO_2 while stylolites develop in response to compaction pressures. Stylolites may increase the permeability of carbonates by acting as conduits for fluid transport (Moore, 1997). Petrographic and geochemical features of the Catoche D2 are similar to those documented for Rhaetian (Upper Triassic) dolomites of the Sorrento Peninsula (Southern Italy; Iannace et al., 2011)

Distribution of porosity in the Catoche Formation is controlled by the relative degree of D2 dolomitization with visual estimates of porosity (ϕ) varying between < 1 to 12 % in the Daniel's Harbour sequence. Similar porosities were observed in the Catoche carbonates at Port au Port and Port au Choix. On the Port au Port Peninsula, porous horizons (visual estimate of ϕ = 4 to 10%) are generally thin (< 5 m) but greater than 5 m at Daniel's Harbour and Port au Choix. This suggests that D1 dolomitization was relatively more pervasive on the Port au Port Peninsula relative to Northern Peninsula (Conliffe et al., 2012), leaving only thin horizons of undolomitized limestone to be dolomitized in later stages of diagenesis and thus host

intercrystalline porosity. Figure 1.2 shows the distribution of porosity in the Catoche Formation at all three locations. Previous studies of the Catoche dolomites reveal that porous intervals are usually dominated by calcian D2 dolomites. This lead authors to suggest that such porous D2 horizons likely resulted from a one-step dolomitization of a precursor calcite (lime mudstones) while non-porous D2 intervals formed by recrystallization of D1 (e.g., Conliffe et al., 2012; Azmy and Conliffe, 2010; Azmy et al., 2008, 2009; Greene, 2008). Porous D2 horizons at Daniel's Harbour are slightly more calcian (mean $CaCO_3$ for porous horizons = 52% ppm ± 2) compared with non-porous D2 horizons (mean $CaCO_3$ for non-porous horizons = 51 %ppm ± 1). The porous ($\phi \geq 4$ %) horizons of the Catoche Formation at Daniel's Harbour) occur in 4 layers (Fig. 1.2). Three are about 4 m thick, approximately 6 m, 120 m and 150 m from the top of the section whereas the fourth is about 40 m thick approximately 70 m from the top of the section. Similarly, the equivalent section at Port au Port has 4 porous intervals about 12 m, 4 m, 8 m and 8 m thick at approximately 24 m, 44 m, 48 m and 74 m respectively from the top of the section. In contrast, the porous intervals are in the first ~50 m of the section at Port au Choix. This may suggest that the Catoche porous zones occur at different stratigraphic levels and are not continuous across western Newfoundland, which is contrary to the reported distribution pattern of porous zones in the underlying Watts Bight Formation (Azmy and Conliffe, 2010). However, the porous zones in the Catoche are associated with hydrothermal dolomites and characterized by broad negative $\delta^{13}C$ shifts (Fig. 1.2) that were likely caused by sea-level change and associated carbon cycling changes (Azmy et al., 2009; Azmy and Lavoie, 2009; Azmy and Conliffe, 2010), a common case in the carbonate sequence of the St. George Group in western Newfoundland.

CHAPTER FIVE

CONCLUSIONS

Petrographic examination of the Catoche Formation carbonates from boreholes 12i/4-1 and 12i/6-121 at Daniel's Harbour on the Northern Peninsula of western Newfoundland reveals three distinct generations of dolomite, from the oldest to the youngest, replacive dolomicrite (D1), replacive and vug filling eu- to subhedral zoned dolomite (D2) and sub- to anhedral pore-filling saddle dolomite (D3). Dolomite D2 (with some subhedral D3) is characterized mostly by intercrystalline porosity (ϕ < 1 to 12%) and zoned crystals.

Trace element and stable isotope geochemistry coupled with fluid inclusion gas analyses of the dolomites and microthermometric measurements on the trapped primary two-phase fluid inclusions, suggest that D1 formed at an early stage of diagenesis and likely from fluids consisting of a mixture of Arenig marine and meteoric waters under open system conditions. In contrast, dolomites D2 and D3 formed at mid to deep burial settings from hydrothermal fluids under suboxic and closed to semi closed system conditions during later stages of diagenesis.

The ΣREE contents, REE_{SN} profiles, Ce and Eu anomalies, as well as geochemical and gas inclusion analyses, reflect the evolution of the diagenetic fluids throughout the sediments burial history and support formation under oxic to suboxic conditions from hot hydrothermal (< 200 ^{o}C) basinal fluids that were circulated through crustal rocks but excludes contributions from magmatic fluids.

Stratigraphic levels of porous horizons in the Catoche Formation at Daniel's Harbour do not correlate with their equivalent levels in sections at Port au Choix and Port au Port (separated by ~30 and 230 km, respectively), which suggests that pore zones are discontinuous across western

Newfoundland, but are associated with broad negative $\delta^{13}C$ shifts on the C-isotope profiles of those sections. The porosity associated with D2 coupled with appropriate thermal maturation, occurrences of suitable traps, and evidences of hydrocarbon accumulation as well as the documented seeps of oil in some of the outcrops at Port au Choix, suggest that the Catoche dolomites are potential reservoirs and suitable hydrocarbon targets.

REFERENCES

Alibo, D.S., and Nozaki, Y., 1999. Rare earth elements in seawater: particle association, shale normalization and Ce oxidation. Geochimica et Cosmochimica Acta, 63, 363–372.

Azmy, K., Veizer, J., Misi, A., De Olivia, T., and Dardenne, M., 2001. Isotope stratigraphy of the Neoproterozoic carbonate of Vazante Formation, Sao˜ Francisco Basin, Brazil. Precambrian Research, 112, 303–329.

Azmy, K., Lavoie, D., Knight, I. and Chi, G., 2008. Dolomitization of the Aguathuna Formation carbonates of Port au Port Peninsula in western Newfoundland, Canada: implications for a hydrocarbon reservoir. Canadian Journal of Earth Sciences, 45, 795–813.

Azmy, K., Knight, I., Lavoie, D. and Chi, G., 2009. Origin of the Boat Harbour dolomites of St. George Group in western Newfoundland, Canada: implications for porosity controls. Bulletin of Canadian Petroleum Geology, 57, 81–104.

Azmy, K., and Lavoie, D., 2009. High-resolution isotope stratigraphy of the Lower Ordovician St. George Group of western Newfoundland, Canada: implications for global correlation. Canadian Journal of Earth Sciences, 46, 403–423.

Azmy, K., and Conliffe, J., 2010. Dolomitization of the lower St. George Group on the Northern Peninsula in western Newfoundland: implications for lateral distribution of porosity. Bulletin of Canadian Petroleum Geology 58(4), 1-14.

Azmy, K., Brand .U., Sylvester .P., Gleeson S.A., Logan .A., and Bitner M.A., 2011.

Biogenic and abiogenic low-Mg calcite (bLMC and aLMC): Evaluation of seawater-REE composition, water masses and carbonate diagenesis. Chemical Geology, 280, 180-190

Baker P.A., and Kastner M., 1981, Constraints on the formation of sedimentary

dolomites; *Science*, 213, 214 – 216

Baker, D., and Knight, I., 1993. The Catoche dolomite project, Anticosti Basin, eastern

Canada: CERR Report, Memorial University of Newfoundland, St. John's, Nfld., 174 p.

Banner, J.L., Hanson, G.N., and Meyers, W.J., 1988. Rare earth element and Nd isotopic

variations in regionally extensive dolomites from the Burlington–Keokuk Formation (Mississippian): implications for REE mobility during carbonate diagenesis. Journal of Sedimentary Petrology, 58, 415–432.

Barnes, C.E., and Cochran, J.K., 1990. Uranium removal in oceanic sediments and the oceanic U balance. Earth Planet. Sci. Lett., 97, 94–101.

Barton, E.D., and Bau, M., Alexander, B., 2006. Preservation of primary REE patterns

without Ce anomaly during dolomitization of Mid-Paleoproterozoic limestone and the potential re-establishment of marine anoxia immediately after the 'Great Oxidation Event'. South African Journal of Geology, 109, 81–86.

Bassett, D., Macleod, K.G., Miller, J.F., and Ethington, R.L., 2007. Oxygen isotopic

composition of biogenic phosphate and the temperature of early Ordovician seawater. Palaios, 22, 98–103.

Bathurst, R. G. C, 1975. Carbonate Sediments and their Diagenesis, Developments in Sedimentology, 12, Elsevier, Amsterdam: 658p.

Bau, M., and Dulski, P., 1996. Distribution of yttrium and rare-earth elements in the Penge and Kuruman iron-formations, Transvaal Supergroup, South Africa. Precambrian Research, 79, 37-55.

Bau, M., Koschinsky, A., Dulski, P., and Hein, J.R., 1996. Comparison of the partitioning behaviours of yttrium, rare earth elelements, and titanium between hydrogenetic marine ferromanganese crusts and seawater. Geochimica et Cosmochimica Acta, 60, 1709–1725.

Bodnar, R.J., 2003. Interpretation of data from aqueous-electrolyte fluid inclusions. In: I. Samson, A. Anderson and D. Marshal (eds.). Fluid Inclusions: Analyses and Interpretation. Mineralogical Association of Canada. Short Course Series, 32, 81–100.

Boggs, S.,Jr. and Krinsley, D. 2006. Application of Cathodoluminescence Imaging to the Study of Sedimentary Rocks. New York, Cambridge University Press, 165 p.

Boggs, .S. Jr. 2009. Petrology of Sedimentary rocks. University press, Cambridge, UK

Boyce, W.D., 1989: Early Ordovician trilobite faunas of the Boat Harbour and Catoche Formations (St. George Group) in the Boat Harbour-Cape Norman area, Great Northern Peninsula, western Newfoundland. Newfoundland Dept. of Mines and Energy, Geol. Surv. Branch report, 89-2, 169

Carpenter, A.B. 1980. The chemistry of dolomite formation: stability of dolomites: In Concepts and models of dolomitization (Edited by D.H Zenger, J.B Dunham, R.L Ethington) SEPM Spec, 28, 1 - 9.

Cawood, P.A., McCausland, P.J.A. and Dunning, G.R., 2001. Opening Iapetus: Constraints from Laurentian margin in Newfoundland. Geological Society of America Bulletin 113, 443–453.

Choquette, P.W. and James, N.P., 1987. Limestones — the burial diagenetic environment. In: Mcllreath, LA., Morrow, D.W. (Eds.), Diagenesis. Geosci. Can. Repr. Ser., 4: 75-112.

Clark, I.D., and Fritz, P., 1997. Environmental isotopes in hydrogeology. Lewis Publisher, Boca Raton, Fla., 328 p.

Coleman, M.L., Walsh, J.N. and Benmore, R.A., 1989. Determination of both chemical and stable isotope composition in milligram-size carbonate samples. Sedimentary Geology, 65, 233–238.

Conliffe, J., Azmy, K., Knight, I. and Lavoie, D., 2009. Dolomitization in the Lower Ordovician Watts Bight Formation of the St. Georges Group, western Newfoundland. Canadian Journal of Earth Sciences, 46, 247–261

Conliffe, J., Azmy, K., Gleeson, S.A., and Lavoie, D., 2010. Fluids associated with hydrothermal dolomitization in St. George Group, western Newfoundland, Canada. Geofluids 9, 1–16.

Conliffe, J., Azmy, K., and Greene, M., 2012. Hydrothermal Dolomites in the Lower Ordovician Catoche Formation. Marine and Petroleum geology 30, 161-173.

Compton, J. S., 1988. Degree of supersaturation and precipitation of organogenic dolomite. *Geology*, 16. 318 – 321

Cooper, M., Weissenberger, J., Knight, I., Hostad, D., Gillespie, D., Williams, H., et al. 2001. Basin evolution in western Newfoundland: new insights from hydrocarbon exploration. American Association of Petroleum Geologists (AAPG) Bulletin, 85, 393–418.

Davies, G.R. and Smith, L.B., 2006. Structurally controlled hydrothermal dolomite reservoir: an overview. The American Association of Petroleum Geologists Bulletin, 90, 1641–1690.

Dravis, J.J., 1992. Burial dissolution in limestones and dolomites — criteria for recognition and discussion of controls: a case study approach (part 1): Upper Jurassic Haynesville limestones, east Texas; part 2: Devonian Upper Elk Point dolomites, western Canada: American Association of Petroleum Geologists–Canadian Society of Petroleum Geologists Short Course on Subsurface Dissolution Porosity in Carbonates, Calgary, Canada, 171 p.

Emerson, S.R., and Huested, S.S., 1991, Ocean anoxia and the concentrations of molybdenum and vanadium in seawater: Marine Chemistry, 34, 177–196.

Esteban, M. and Taberner, C., 2003. Secondary porosity development during late burial

In carbonate reservoirs as a result of mixing and/or cooling of brines. Journal of Geochemical Exploration, 78-79, 355–359.

Faure G., and Mensing T. M., 2005. Isotope principles and applications. 3rd edn. John Wiley & Sons, NJ.

Folk R.L and Land L.S. (1975). Mg/Ca ratios and salinity, two controls over

crystallization of dolomites. American Association of Petroleum Geologists Bulletin, 59, 60–68.

Fowler, M.G., Hamblin, A.P., Hawkins, D., Stasiuk, L.D. and Knight, I. 1995.

Petroleum geochemistry and hydrocarbon potential of Cambrian and Ordovician rocks of western Newfoundland. Bulletin of Canadian Petroleum Geology, 43, 187–213

Giggenbach, W. F., 1986, "The use of gas chemistry in delineating the origin of fluids

discharges over the Taupo Volcanic Zone: A review," International Volcanological Congress, Hamilton, New Zealand, Proceedings Symposium 5, 47-50.

Gillespie, H. and Burden, E.T. 2010 Fluorescence microspectroscopy as a proxy to

determining the thermal maturation and API gravity of naturally occurring crude oils. Internal report CREAIT Network, Memorial University of Newfoundland. 9pp.

Goldstein, R.H., and Reynolds, T.J., 1994. Systematics of fluid inclusions in diagenetic

minerals. Society for Sedimentary Geology (SEPM) Short Course, Tulsa, Okla.

Greene, M., 2008. Multiple generations of dolomitization in the Catoche formation of Port au Choix Newfoundland. Unpub ished M.Sc. thesis, Memorial University of Newfoundland, St. John's Newfoundland.

Hanson, G.N., 1980. Rare Earth Elements in petrogenetic studies of igneous systems. Ann. Rev. Earth Planet. Sci., 8, 371-406.

Hayes, P.D., and Grossman, EX., 1991. Oxygen isotopes in meteoric calcite cements as indicators of continental paleoclimate: Geology, 19, 441-444.

Haywick, D.W., 1984. Dolomite within the St. George Group (Lower Ordovician), western Newfoundland. Unpublished M.Sc. thesis, Memorial University of Newfoundland, St. John's Newfoundland

Hsu, K.J. and Siegenthaler, C. 1969. Preliminary experiments on hydrodynamic movement induced by evaporation and their bearing on the dolomite problem. Sedimentology, 12, 11-25

Iannace. A., Cupuano, M., and Galluccio. L., 2011. "Dolomites and dolomites" in Mesozoic platform carbonates of the Southern Apennines: Geometric distribution, petrography and geochemistry. Palaeogeography, Palaeoclimatology, Palaeoecology 310 (2011) 324–339

James, N. P. and Choquette, P. W., 1984. Diagenesis 9 - Limestones - The meteoric diagenetic environment. Geosci. Can., 11, 161-194

James, N.P., and Choquette, P.W., 1988. Limestones - the meteoric diagenetic environment. In: Mellreath, I.A., Morrow, D.W. (Eds.), Diagenesis. Geosci. Can. Repr. Ser., 4, 35-73.

James, N.P., Stevens, R.K., Barnes, C.R. and Knight, I., 1989. Evolution of a Lower Paleozoic continental-margin carbonate platform, northern Canadian Appalachians. In: P. D. Crevello, J. L. Wilson, J. F. Sarg and J. F. Read (Eds.). Controls on Carbonate Platform and Basin Development, Society of Economic Paleontologists and Mineralogists Special Publication, 44, 123–146.

Ji, Z., and Barnes, C.R., 1989: Conodont paleontology and biostratigraphy of the St. George Group, Lower Ordovician, western Newfoundland. Annual Mtg. Geol. Assoc. Can. , Montreal, Prog. with abstr., p. A15.

Ji, Z., 1989. Lower Ordovician conodonts From the St. George Group of Port au Port Peninsula, Western Newfoundland. Unpubl. Ph.D. thesis, Memorial University of Newfoundland.

Kamber, B.S., and Webb, G.E., 2001. The geochemistry of late Archean microbial carbonate: implications for ocean chemistry and continental erosion history. Geochimica et Cosmochimica Acta 65, 2509–2525.

Kimura, H., and Watanaba, Y., 2001. Ocean anoxia at the Precambrian-Cambrian boundary: Geology, 29 (11), 995–998;

Kırmacı, M.Z., 2008. Dolomitization of the late Cretaceous–Paleocene platform carbonates, Gölköy (Ordu), eastern Pontides, NE Turkey. Sedimentary Geology, 20, 289–306.

Knight I., 1986. Ordovician sedimentary strata of the Pistolet Bay and Hare Bay area, Great Northern Peninsula. In: current research. Newfoundland Department of Energy and Mines, report 86-1, 147-160

Knight I., 1987. Geology of Roddickton (12i/16) map area. In current research. Newfoundland department of energy and mines, mineral development division. Report 87-1, 343-357

Knight I., and James N P., 1987. The stratigraphy of the Lower Ordovician St. George Group western Newfoundland: The interaction between eustasy and tectonics. Can. Journal of Earth Sciences, 24, 1927-1951

Knight, I. 1991. Geology of Cambro-Ordovician rocks in the Port Saunders (NTS 12I/11), Castors River (NTS 12I/15), St. John Island (NTS 12I/14), and Torrent River (NTS 121/10) map areas. Newfoundland Department of Mines and Energy, Mineral Development Division, Report 91-4, 138 p.

Knight, I., James, N.P., and Lane, T.E. 1991. The Ordovician St. George Unconformity, northern Appalachians: the relationship of plate convergence at the St. Lawrence Promontory to the Sauk/Tippecanoe sequence boundary. Geological Society of

America Bulletin,103,1200–1225.

Knight I., 1994. The Geology of Cambrian-Ordovician platform rocks of the Psadena map area (NTS 12H/4). In: current research. Newfoundland Department of Energy and Mines. Report 97-1, 211-235

Knight I. 1997. Ordovician dolomite reservoirs of the Port aux Choix area, Western Newfoundland: Report to Hunt Oil and Pan-Canadian Petroleum. 88 p.

Knight, I., Azmy, K.,Greene, M. and Lavoie, D. 2007. Lithostratigraphic setting of diagenetic, isotopic, and geochemistry studies of Ibexian and Whiterockian carbonates of the St. George and Table Head groups in western Newfoundland. Current Research Newfoundland and Labrador. Department of Natural Resources Geological Survey. Report 07-1, 55–84.

Knight, I., Azmy, K., Boyce, D. and Lavoie, D. 2008. Tremadocian carbonates of the lower St. George Group, Port au Port Peninsula, western Newfoundland: Lithostratigraphic setting of diagenetic, isotopic, and geochemistry studies. Current Research. Newfoundland and Labrador. Department of Natural Resources Geological Survey. Report 08-1, 1–43.

Kretz, .R. 1982. A model for the distribution of trace elements between calcite and dolomite. geochim. Cosmochim. Acta 46, 1979-1981

Land, L. **S.,** 1967. Diagenesis of skeletal carbonates. J. Sediment. Petrol., 37, 914-930

Land, L.S. 1980. The isotope and trace element geochemistry of dolomites: the state of the art: In Concepts and models of dolomitization (Edited by D.H Zenger, J.B Dunham, R.L Ethington) SEPM Spec, 28, 87 - 110.

Land, L.S. 1983. The application of stable isotopes to studies of the origin of dolomite and to problems of diagenesis of clastic sediments. In Society for Sedimentary Geology (SEPM) Short Course Notes 10. Edited by M.A. Arthur, T.F. Anderson, I.R. Kaplan, J. Veizer, and L.S. Land. pp. 4.1–4.22.

Land, L.S. 1985. The origin of massive dolomite: J. Geol. Educ., 33, 112-125

Land, L.S. 1992. The dolomite problem: Stable and radiogenic isotope clues, In: N. Clauer and S. Chaudhuri (eds.). Isotopic Signature of Sedimentary Records. Lecture Notes in Earth Science, 43, 49–68.

Lane, T.E. 1990. Dolomitization, brecciation and zinc mineralization and their paragenetic stratigraphic and structural relationships in the upper St. George Group (Ordovician) at Daniel's Harbour, western Newfoundland. Unpublished Ph.D. thesis, Memorial University of Newfoundland, St. John's, Nfld.

Lavoie, D., Chi, G., Brennan-Alpert, P. and Betrand, R. 2005. Hydrothermal dolomitization in the Lower Ordovician Romaine Formation of the Anticosti Basin: significance for hydrocarbon exploration. Bulletin of Canadian Petroleum Geology, 53, 454–471

Lavoie, D., Morin, C., Urbatsch, M., and Davis, W.J., 2010. Massive dolomitization of a pinnacle reef in the Lower Devonian West Point Formation (Gaspé Peninsula, Quebec): an extreme case of hydrothermal dolomitization through fault-focused circulation of magmatic fluids. American Association of Petroleum Geologists Bulletin, 94, 513–531.

Lawler, J.P., and Crawford, M.L., 1983: Stretching of fluid inclusions resulting from a low-temperature microthermometric technique. Econ. Geol. 78, 527-529.

Lindholm, R.C., and Finkelman, R.B., 1972. Calcite staining: semiquantitative determination of ferrous iron. Journal of Sedimentary Petrology, 42, 239-242.

Lippmann, F. 1973. Sedimentary Carbonate Minerals, pp 228. Springer-Verlag, Berlin

Longman, M. W., 1980. Carbonate diagenetic textures from near surface diagenetic environments. Am. Assoc. Petrol. Geol. Bull., 64, 461-487.

Lonnee, J., and Machel, H.G., 2006. Pervasive dolomitization with subsequent hydrothermal alteration in the Clarke Lake gas field, Middle Devonian Slave Point Formation, British Columbia, Canada. American Association of Petroleum Geologists Bulletin, 90, 1739–1761.

Lu, F.H., and Meyers, W.J., 1998. Massive dolomitization of Late Miocene carbonate platform: a case of mixed evaporate brines with meteoric water, Nijar, Spain. Sedimentology, 45, 263–277.

Machel, H.G. 1985. Cathodoluminescence in calcite and dolomite and its chemical interpretation. Geoscience. Canada, 12, 139-147.

Machel G.-G., and Mountjoy E.W., 1986, Chemistry and environment of dolomitization-A reappraisal; *Earth sciences* Rev., 23, 175 – 222

Machel, H-G. and Burton, E. A., 1991. Factors governing cathodoluminescence in calcite and dolomite, and their implications for studies of carbonate diagenesis. In: Luminescence Microscopy: Quantitative and Qualitative Aspects (Ed. by C. E. Barker & O. C. Kopp), Soc. econ. Palaeont. Miner., Dallas, Short Course, 25, 37-57.

Machel, H-G., Mason, R., Mariano, A. N. and Mucci, A., 1991. Causes and emission of luminescence in calcite and dolomite. In: Luminescence Microscopy: Quantitative and Qualitative Aspects (Ed. by C. E. Barker & O. C. Kopp), Soc. econ. Palaeont. Miner., Dallas, Short Course, 25, 9-25.

Mackenzie, F.T and Piggot, J.D. 1981 Tectnic controls on Phanerozoic sedimentary rock cycling. Journal of Geology 138, 183-196

Mackenzie, F.T., Bischoff, W.D., Bishop, F.c., Loijens, M., Schoonmaker, J., and Wollast, R. 1983. Magnesian calcite: low temperature occurrence, solubility and solid solution behaviour. (Edited by R.J Reeder) Reviews in mineralogy 11, 94-144. Mineralogical society of America, Washington

Matte, D.H and Mountjoy E.W. 1980. Burial dolomitization of the upper Devonian Miette

buildup, Jasper national part, Alberta: In Concepts and models of dolomitization (Edited by D.H Zenger, J.B Dunham, R.L Ethington) SEPM Spec, 28, 259 - 297.

Matthews, R. K., 1974. A process approach to diagenesis of reefs and reef associated limestones. In: L. F. Laporte (Ed.), Reefs in Time and Space. SEPM Spec. Pub, 18 953-960, 234-256.

McLennan, S.M., 1989. Rare earth elements in sedimentary rocks: influence of provenance and sedimentary processes. In: Lipin, B.R., McKay, G.A. (Eds.), Geochemistry and Mineralogy of Rare Earth Elements: Mineral. Soc. Am. Rev. Miner., 21, 169–200.

Meyers, W.J., Lu, F.H., and Zachariah, J.K. 1997. Dolomitization by mixed evaporative brines and freshwater, Upper Miocene carbonates, Nijar, Spain. Journal of Sedimentary Research, 67, 898–912.

Möller, P. 2000: Rare earth elements and yttrium as geochemical indicators of the source of mineral and thermal waters. In: I. Stober and K. Bucher (eds): Hydrology of crystalline rocks. Kluwer Acad. Press, 227-246.

Moore, C. H., 1997. Carbonate diagenesis and porosity. Developments in sedimentology 46. Elsevier science B.V. Amsterdam Netherlands

Morrow, D.W. 1982(b). Diagenesis 2. Dolomite –Part 2. Dolomitization models and ancient

dolostones. Geosciences Canada, 9, 5-13

Muir, A., Lock, D., and Von der Borch, C.C. 1980. Coorong model for penecontemporaneous dolomites formation in the Middle Proterozoic McArthur Group, Northern territory, Austrailia. In Concepts and models of dolomitization (Edited by D.H Zenger, J.B Dunham, R.L Ethington) SEPM Spec, 28, 51 - 67.

Nicolas, T., Thomas, J.A., Timothy, L., and Armelle, R., 2006. Trace metals as paleoredox and paleoproductivity proxies: An update. Chemical Geology, 232, 12-32

Norman, D.I., and Blamey, N.J.F., 2001. Quantitative analysis of fluid inclusion volatiles by a two mass spectrometer system. In: Noronha, F., Doria, A., Guedes, A. (Eds.), European Current Research On Fluid Inclusions, Porto 2001 (XVI ECROFI): Faculdidade de Ciencias do Porto, Departamento de Geologia, Memoria, 7, 341–344.

Norman, D.I., and Moore, J.N., 1999. Methane and excess N2 and Ar in geothermal fluid inclusions. Proceedings: Twenty-fourth workshop of geothermal reservoir engineering, Stanford University, Stanford, California, January 22–24, pp. 233–240.

Norman, D.I., Moore, J.N., Yonaka, B., and Musgrave, J., 1996. Gaseous species in fluid inclusions: a tracer of fluids and in indicator of fluid processes. Proceedings: Twenty-first workshop of geothermal reservoir engineering, Stanford University, Stanford, California, pp. 233–240.

Norman, D.I., Moore, J.N., and Musgrave, J., 1997. More on the use of fluid inclusion gaseous species as tracers in geothermal systems. Proceedings: Twenty-second workshop on Geothermal reservoir engineering, Stanford University, Stanford, California, pp. 419–426.

Norman, D.I., Blamey, N.J.F., and Moore, J.N., 2002. Interpreting geothermal processes and fluid sources from fluid inclusion organic compounds and CO_2/N_2 ratios. Proceedings, Twenty-Seventh Workshop on Geothermal Reservoir Engineering, Stanford University, Stanford, California. . 419–426.

Nothdurft, L.D., Webb, G.E., and Kamber, B.S., 2004. Rare earth element geochemistry of Late Devonian reefal carbonates, Canning Basin, Western Australia: confirmation of a seawater REE proxy in ancient limestones. Geochimica et Cosmochimica Acta 68, 263–283.

Parry W.T., and Blamey, N.J.F., 2010. Fault fluid composition from fluid inclusion measurements, Laramide age Uinta thrust fault, Utah. Chemical Geology, 278, 105-119

Radke, B.M., and Mathis, R.L. 1980. On the formation and occurrence of saddle dolomite. Journal of Sedimentary Petrology, 50, 1149–1168.

Rameil, N. 2008. Early diagenetic dolomitization and dedolomitization of Late Jurassic and earliest Cretaceous platform carbonates: a case study from the Jura Mountains (NW Switzerland, E France). Sedimentary Geology, 212,

70–85.

Roedder, E., 1984. Fluid inclusions. Mineralogical Society of America. Reviews in Mineralogy 12, 644.

Romanek, C. S., E. L.Grossman., and J.W.Morse., 1992. Carbon isotopic fractionation in synthetic aragonite and calcite – Effects of temperature and precipitation rate. – Geochimica et Cosmochimica Acta, 56, 419–430.

Scherer, M., and Seitz, H., 1980. Rare earth element distribution in Holocene and Pleistocene corals and their redistribution during diagenesis. Chemical Geology 28, 279–289.

Shaw, H.F., and Wasserburg, G.J., 1985. Sm–Nd in marine carbonates and phosphates: implications for Nd isotopes in seawater and crustal ages. Geochimica et Cosmochimica Acta 49, 503–518.

Shepherd T.J, Rankin A.H., and Alderton D.H.M. 1985. A practical guide to fluid inclusions. Blackie, London.

Shields, G.A., Carden, G.A.F., Veizer, J., Meidla, T., Rong, J., and Li, R.-Y. 2003. Sr, C, and O isotope geochemistry of Ordovician brachiopods: a major isotopic event around the Middle–Late Ordovician transition. Geochimica et Cosmochimica Acta, 67, 2005–2025.

Sholkovitz, E., and Shen, G.T., 1995. The incorporation of rare-earth elements in modern coral. Geochimica et Cosmochimica Acta 59, 2749–2756.

Smith, L.B. 2006. Origin and reservoir characteristics of Upper Ordovician Trenton-Black River hydrothermal dolomite reservoirs in New York. Bulletin of the American Association of Petroleum Geologists, 90, 1691–1718

Sperber, C.M., Wilkinson, B.H., and Peacor, D.R. 1984. Rock composition, dolomite stoichiometry, and rock/water reactions in dolomitic carbonate rocks. Journal of Geology, 92(6), 609-622

Stockmal, G.S., Slingsby, A. and Waldron, J.W.F. 1998. Deformation styles at the Appalachian structural front, western Newfoundland: implications of new industry seismic reflection data. Canadian Journal of Earth Sciences, 35, 1288–1306.

Swart, P. K., and Eberli. G., 2005. The nature of the delta C-13 of periplatform sediments: Implications for stratigraphy and the global carbon cycle. – Sedimentary Geology, 175, 115–129.

Taylor, S.R., and S.M. McLennan. 1985. The Continental Crust: Its Composition and Evolution. Oxford, UK: Blackwell Scientific Publications.

Thomas, J.A., and Barry, M.J., 2004. Trace-element behavior and redox facies in core shales of Upper Pennsylvanian Kansas-type cyclothems. Chemical Geology, 206, 289-318

Tucker, M.E., and Wright, V.P. 1990. Carbonate Sedimentology. Blackwell Publishing, Oxford, UK.

Veizer, J., Lemieux, J., Jones, B., Gibling, M.R., and Savelle, J. 1978. Paleosalinity and dolomitization of the lower Paleozoic carbonate sequence , somerset and prince of wales islands, Artic Canada. Canadian Journal of Earth Sciences, 15, 1448–1461.

Veize, J. 1983b. Trace element and isotopes in carbonate minerals. Mineral. Soc. Am. Rev. in Mineral 11, 265-299

Veizer, J., Ala, D., Azmy, K., Bruckschen, P., Bruhn, F., Buhl, D.,et al. 1999. 87Sr/86Sr,^{18}O and $_{}^{13}$C evolution of Phanerozoic seawater. Chemical Geology, 161, 59–88.

Von der Borch, C.C. 1976. Stratigraphy and formation of Holocene dolomite carbonate deposits of the Coorong area, south Australia, journal for sedimentary petrology, 46, 952-966

Von der Borch, C.C and Jones, J.B. 1976. Spherular modern dolomites from the Coorong area, South Australia. Sedimentology 23, 587-591

Von der Borch C.C and Lock, D. 1976. Geological significance of Coorong dolomites. Sedimentology 26, 813-824

Warren J. 2000. Dolomite: Occurrence, evolution and economically important associations. Earth-Science Reviews, 52, 1-81.

Webb, G.E., and Kamber, B.S., 2000. Rare earth elements in Holocene reefal microbialites: a new shallow seawater proxy. Geochimica et Cosmochimica Acta 64, 1557–1565.

Webb, G.E., Nothdurft, L.D., Kamber, B.S., Kloprogge, J.T., and Zhao, J.-X. 2009. Rare earth element geochemistry of scleractinian coral skeleton during meteoric diagenesis: a before and-after sequence through neomorphism of aragonite to calcite. Sedimentology 56, 1433–1463

Weissert .H., Michael .J., and Michael .S. 2008. Chemostratigraphy. Newsletter on Stratigraphy 42, 145-179.

Whitaker, F.F., Smart, P.L., Vahrenkamp, V.C., Nicholson, H., and Wogelius, R.A. 1994. Dolomitization of near normal seawater? Field evidence from the Bahamas: In Dolomites ((Edited by Tucker and Zenger)) - a Volume in Honour of Dolomieu: international association of sedimentologists special publication 21, 111-132.

Wierzbicki, R., Dravis, J. J., Al-Aasm, I. and Harland, N. 2006. Burial dolomitization and dissolution of Upper Jurassic Abenaki platform carbonates, Deep Panuke reservoir, Nova Scotia, Canada. American Association of Petroleum Geologists Bulletin, 90, 1843–1861.

Wignall, P.B., 1994, Black shales: New York, Oxford University Press, 127 p.

Wignall, P.B., and Twitchett, R.J., 1996, Oceanic anoxia and the end Permian mass extinction: Science, 272, 1155–1158.

Wilde, P., Quinby-Hunt .S.M., and Erdtmann .B.D. 1996. The whole-rock cerium anomaly: a potential indicator of eustatic sea-level changes in shales of the anoxic facies. Sedimentary Geology, 101, 43-53

Wilson, J.L., Medlock, P.L., Fritz, R.D., Canter, K.L. and Geesaman, R G.

1992. A review of Cambro-Ordovician breccias in North America. In: M. P.

Candelaria and C. L. Reed (eds.). Paleokarst, karst-related diagenesis and

reservoir development. SEPM-Permian Basin Section, Publication 92-33,

19–29.

Yvonne, V. L., Crisógono, V., Rolf W., and Judith .M. 2000. Role of Sulfate Reducing Bacteria during Microbial Dolomite Precipitation as Deduced from Culture Experiments. *Journal of Conference Abstracts* 5(2), 1038

Zheng, Y., Anderson, R.F., van Geen, A., and Fleisher, M.Q., 2002. Remobilization of authigenic uranium in marine sediments by bioturbation. Geochim. Cosmochim. Acta 66, 1759– 1772.

Zhong, S., and Mucci, A., 1995. Partitioning of rare earth elements (REEs) between calcite

and seawater solutions at 25 °C and 1 atm, and high dissolved REE concentrations. Geochimica et Cosmochimica Acta 59, 443–453.

APPENDIX 1

SAMPLES WITH DESCRIPTION, CORE ID, DEPTH, ELEMENTAL, ISOTOPIC AND REE COMPOSITION OF CATOCHE CARBONATES

Sample ID	Core No	Depth (m)	$CaCO_3$ % (ppm)	$MgCO_3$% (ppm)	Fe 54 (ppm)	Mn (ppm)	Sr (ppm)	$\delta^{13}C$ ‰ (VPDB)	$\delta^{18}O$ ‰ (VPDB)
4-102-C1	12i/4-1	340.3	97.86	2.14	113.9	14.18	295.3	-0.99	-9.10
4-106-C1	12i/4-1	344.3	98.87	1.13	102.3	12.72	302.7	-0.60	-9.00
4-108-C1	12i/4-1	346.3	98.87	1.13	104.9	12.52	291.6	-0.78	-8.72
4-110-C1	12i/4-1	348.3	98.45	1.55	114.3	23.41	270.0	-0.40	-9.69
4-114-C1	12i/4-1	352.3	98.91	1.09	73.30	16.16	260.4	-0.70	-9.56
4-118-C1	12i/4-1	356.3	99.20	0.80	81.05	16.11	251.2	-0.10	-9.42
4-120-C1	12i/4-1	358.3	93.30	6.70	214.9	26.75	222.5	-0.03	-9.36
4-124-C1	12i/4-1	362.3	98.79	1.21	106.9	19.27	272.6	-0.25	-9.61
6-4-C3	12i/6-121	5.2	94.96	5.04	205.3	148.8	16.74	-3.23	-9.96
6-54.5-C3	12i/6-121	54.7						-2.80	-9.51
6-64-C3	12i/6-121	64.2						-4.83	-9.43
4-80-D1	12i/4-1	318.3	50.44	49.56	1596	60.72	54.81	-1.80	-7.29
4-81.5-D1	12i/4-1	319.8	49.64	50.36	1160	76.09	42.67	-1.32	-7.73
4-89.5-D1	12i/4-1	327.8	53.50	46.50	2397	103.2	59.98	-1.11	-9.94
4-92-D1	12i/4-1	330.3	53.32	46.68	1396	70.82	66.25	-1.24	-8.16
4-96-D1	12i/4-1	334.3						-1.54	-9.37
4-104-D1	12i/4-1	342.3	55.24	44.76	1403	47.26	125.8	-0.60	-6.78
4-120-D1	12i/4-1	358.3						-0.26	-9.53
6-16-D1	12i/6-121	17.2	50.82	49.18	720	117.2	42.14	-1.02	-9.16
6-20-D1	12i/6-121	21.2	49.59	50.41	814.7	122.3	26.81	-1.31	-9.74

Sample ID	Core No	Depth (m)	$CaCO_3$ % (ppm)	$MgCO_3$% (ppm)	Fe 54 (ppm)	Mn (ppm)	Sr (ppm)	$\delta^{13}C$ ‰ (VPDB)	$\delta^{18}O$ ‰ (VPDB)
6-24-D1	12i/6-121	25.2	49.40	50.60	971.6	141.3	25.65	-1.22	-9.71
6-60-D1	12i/6-121	60.2	49.62	50.38	748.9	97.90	42.50	-1.22	-8.84
6-64-D1	12i/6-121	64.2	49.66	50.34	768.8	107.3	40.30	-1.45	-9.36
6-66-D1	12i/6-121	66.2	53.44	46.56	901.1	125	34.91	-1.41	-9.27
6-72-D1	12i/6-121	72.2	53.47	46.53	1920	134	50.99	-1.46	-8.21
6-74-D1	12i/6-121	74.2	52.45	47.55	3082	102.8	36.96	-1.82	-9.82
6-92.5-D1	12i/6-121	92.7	51.95	48.05	2067.	119.3	32.20	-1.95	-10.39
6-126-D1	12i/6-121	126.2	50.93	49.07	1724	118.7	27.73	-1.62	-9.98
4-86.5-D2	12i/4-1	324.8	53.55	46.45	1254	91.45	30.80	-1.89	-11.36
4-88-D2	12i/4-1	326.3						-1.53	-10.66
4-122-D2	12i/4-1	360.3	57.75	42.25	4493	342.2	51.23	-0.04	-11.59
4-126-D2	12i/4-1	364.3	54.74	45.26	696.6	42.72	38.81		
6-4-D2	12i/6-121	5.2	51.03	48.97	926.1	100.8	37.96	-1.03	-9.90
6-10D2	12i/6-121	11.2	49.55	50.45	849.3	133.9	29.76	-1.10	-9.57
6-12-D2	12i/6-121	13.2	50.56	49.44	628.3	112.8	30.82	-0.82	-9.22
6-13-D2	12i/6-121	14.2	50.45	49.55	1182	212.5	27.56	-1.22	-9.64
6-14-D2	12i/6-121	15.2	50.33	49.67	531.2	114.6	32.55	-1.12	-9.57
6-18-D2	12i/6-121	19.2	50.38	49.62	1109	134.4	29.73	-1.04	-9.48
6-22-D2	12i/6-121	23.2	50.36	49.64	1059	119.6	27.07	-1.36	-10.07
6-26-D2	12i/6-121	27.2	52.24	47.76	1099	137.8	27.78	-1.26	-9.62
6-28-D2	12i/6-121	29.2						-1.18	-9.73
6-30-D2	12i/6-121	31.2	52.12	47.88	884.9	146.1	31.22	-1.25	-9.74
6-37.5-D2	12i/6-121	37.7	51.68	48.32	1054	183.6	31.47	-1.52	-9.82

Sample ID	Core No	Depth (m)	$CaCO_3$ % (ppm)	$MgCO_3$% (ppm)	Fe 54 (ppm)	Mn (ppm)	Sr (ppm)	$\delta^{13}C$ ‰ (VPDB)	$\delta^{18}O$ ‰ (VPDB)
6-40-D2	12i/6-121	40.2	52.54	47.46	1045	81.56	47.03	-0.51	-8.81
6-45-D2	12i/6-121	45.2	51.74	48.26	1156	114.9	30.95	-0.98	-9.54
6-46.5-D2	12i/6-121	46.7	52.05	47.95	844.0	87.50	43.29	-1.01	-9.11
6-48-D2	12i/6-121	48.2	50.36	49.64	1062	128.8	27.43	-1.60	-9.83
6-52-D2	12i/6-121	52.2	53.09	46.91	705.5	113.0	51.51	-1.47	-8.71
6-54-D2	12i/6-121	54.2						-1.33	-8.48
6-54.5-D2	12i/6-121	54.7	52.11	47.89	728.4	100.4	48.71	-1.63	-9.06
6-56.5-D2	12i/6-121	56.7	52.20	47.80	1030	115.1	35.86	-1.65	-9.51
6-68-D2	12i/6-121	68.2	51.29	48.71	655.7	103.0	38.01	-1.84	-9.26
6-70-D2	12i/6-121	70.2						-1.80	-9.56
6-74-D2	12i/6-121	74.2	50.73	49.27	1551	112.6	33.91	-1.85	-9.70
6-76-D2	12i/6-121	76.2						-1.97	-9.32
6-78-D2	12i/6-121	78.2						-1.74	-8.20
6-80-D2	12i/6-121	80.2	52.14	47.86	1888	107.9	45.90	-1.90	-8.72
6-82-D2	12i/6-121	82.2	52.34	47.66	4240	103.3	48.87	-1.86	-8.59
6-84-D2	12i/6-121	84.2						-1.76	-8.22
6-88-D2	12i/6-121	88.2	51.83	48.17	3046	111.2	47.09	-1.82	-8.60
6-90-D2	12i/6-121	90.2						-1.63	-7.86
6-94-D2	12i/6-121	94.2	52.89	47.11	4231	131.6	35.11	-1.79	-9.97
6-96-D2	12i/6-121	96.2	52.83	47.17	3136	144.3	45.06	-1.76	-8.05
6-98-D2	12i/6-121	98.2	51.85	48.15	2723	196.1	27.05	-1.67	-10.54
6-100-D2	12i/6-121	100.2	51.76	48.24	2218	118.2	32.26	-1.59	-10.16
6-100-D2B	12i/6-121	100.2	51.11	48.89	1827	117.9	33.97	-1.80	-10.42

Sample ID	Core No	Depth (m)	$CaCO_3$ % (ppm)	$MgCO_3$% (ppm)	Fe 54 (ppm)	Mn (ppm)	Sr (ppm)	$\delta^{13}C$ ‰ (VPDB)	$\delta^{18}O$ ‰ (VPDB)
6-104-D2	12i/6-121	104.2						-1.55	-9.34
6-106-D2	12i/6-121	106.2	51.41	48.59	2107	175.3	35.56	-1.74	-8.56
6-108-D2	12i/6-121	108.2						-1.67	-9.44
6-110-D2	12i/6-121	110.2						-1.70	-11.22
6-112-D2	12i/6-121	112.2	50.41	49.59	2839	102.1	30.26	-1.48	-10.50
6-116-D2	12i/6-121	116.2	52.75	47.25	2182	171.2	29.68	-1.68	-9.35
6-120-D2	12i/6-121	120.2						-1.62	-9.79
6-122-D2	12i/6-121	122.2						-1.47	-9.78
6-124-D2	12i/6-121	124.2	51.96	48.04	2297	144.1	32.29	-1.53	-10.04
6-128-D2	12i/6-121	128.2	52.13	47.87	1678	140.4	46.17	-1.57	-8.68
6-130-D2	12i/6-121	130.2						-1.50	-8.16
4-86.5-D3	12i/4-1	324.8	50.53	49.47	1678	146.4	49.47	-1.51	-10.51
6-4-D3	12i/6-121	5.2	51.72	48.28	1641	172.7	30.22	-2.81	-7.93
6-10-D3	12i/6-121	11.2	51.04	48.96	810.0	147.8	26.30	-1.69	-9.33
6-22-D3	12i/6-121	23.2	53.19	46.81	1620	250.6	30.97	-1.75	-10.45
6-37.5-D3	12i/6-121	37.7						-1.51	-9.78
6-45-D3	12i/6-121	45.2	53.70	46.30	1580	235.3	37.44	-1.31	-10.44
6-46.5-D3	12i/6-121	46.7	52.53	47.47	1818	270.4	40.64	-1.44	-11.23
6-60-D3	12i/6-121	60.2	52.05	47.95	2061	280.1	37.93	-1.45	-9.86
6-76-D3	12i/6-121	76.2	52.28	47.72	1511	189.2	39.94	-2.02	-11.27
6-92.5-D3	12i/6-121	92.7	52.16	47.84	1404	96.51	27.16	-2.14	-10.37
6-98-D3	12i/6-121	98.2	51.37	48.63	65.46	173.2	56.72	-1.32	-9.86
6-100-D3	12i/6-121	100.2	50.43	49.57	2199	210.1	42.43	-1.45	-13.24

Sample ID	Core No	Depth (m)	$CaCO_3$ % (ppm)	$MgCO_3$% (ppm)	Fe 54 (ppm)	Mn (ppm)	Sr (ppm)	$\delta^{13}C$ ‰ (VPDB)	$\delta^{18}O$ ‰ (VPDB)
6-116-D3	12i/6-121	116.2						-1.70	-11.08
6-120-D3	12i/6-121	120.2						-1.69	-9.76
6-124-D3	12i/6-121	124.2	52.29	47.71	3299	197.1	44.95	-1.43	-12.96

Sample ID	La (ppb)	Ce (ppb)	Pr (ppb)	Nd (ppb)	Sm (ppb)	Eu (ppb)	Gd (ppb)	Tb (ppb)	Dy (ppb)	Ho (ppb)	Er (ppb)	Tm (ppb)	Yb (ppb)	Lu (ppb)
4-102-C1	1136	1819	224.1	900.7	170.0	29.2	177.2	27.0	135.8	26.0	88.8	10.3	65.7	10.5
4-106-C1	1229	1905	242.2	956.8	196.0	37.7	228.3	30.4	178.9	35.8	116.4	15.6	125.0	18.8
4-108-C1	1249	1911	242.3	975.4	159.9	40.4	207.0	31.6	181.7	35.0	107.3	17.5	92.2	15.0
4-110-C1	917.4	1233	163.7	708.0	155.1	37.4	192.2	24.0	163.3	35.6	107.0	13.3	78.8	12.1
4-114-C1	1399	1969	265.2	1081	203.5	50.9	240.2	37.3	190.7	40.4	125.3	17.2	99.9	16.3
4-118-C1	1121	1415	197.3	812.4	167.1	42.8	173.5	27.6	151.6	37.3	103.2	16.1	67.3	14.4
4-120-C1	1692	2418	349.7	1354	297.4	65.7	325.8	47.2	289.1	67.9	177.6	25.2	158.1	23.8
4-124-C1	1495	1895	297.7	1237	259.8	59.2	307.6	49.1	274.7	58.2	163.6	25.3	150.3	20.2
6-4-C3	6889	11276	1256	4535	632.5	136.8	644.0	67.5	295.1	55.6	180.5	24.1	183.4	25.3
6-54.5-C3	3597	5873	639.4	2338	350.2	111.3	393.0	52.0	250.1	45.9	144.8	12.6	96.7	16.1
4-80-D1	2357	4988	564.0	2083	324.8	83.9	402.1	47.6	232.6	46.3	131.6	17.0	114.3	16.3
4-81.5-D1	1673	3785	439.4	1626	278.1	61.9	311.0	35.1	215.6	34.5	109.4	14.0	92.7	12.8
4-89.5-D1	3732	7553	893.0	3176	607.3	133.3	615.5	86.8	438.4	82.1	248.5	32.3	189.7	29.3
4-92-D1	3104	6990	814.5	3156	588.1	120.1	573.6	79.9	379.4	74.7	234.2	30.3	166.3	27.3
4-104-D1	4082	7838	991.8	3767	654.2	143.7	736.4	97.2	523.9	102.4	279.8	37.7	223.0	38.4
6-16-D1	2149	3758	484.9	1858	347.8	82.0	403.6	58.3	320.1	59.5	173.2	24.9	134.5	19.7
6-20-D1	1845	3558	457.4	1845	362.1	74.2	399.4	57.2	322.2	64.6	202.5	25.2	152.7	22.6
6-24-D1	1479	2562	340.2	1350	227.7	54.2	300.4	40.6	231.9	44.5	159.9	18.2	119.8	17.0
6-60-D1	2484	4224	505.6	1933	374.3	76.1	409.9	52.1	269.4	51.8	159.2	17.5	121.6	16.7
6-64-D1	2260	4064	497.9	1983	333.9	72.4	390.7	48.6	280.0	54.7	161.2	17.3	135.6	19.0
6-66-D1	1793	3288	409.1	1619	329.1	64.0	330.8	44.1	216.7	50.3	127.2	19.6	103.7	18.5
6-72-D1	4597	9456	1156	4373	769.0	158.3	734.3	94.8	432.6	72.7	263.1	29.9	197.4	27.3
6-74-D1	1808	3600	442.9	1583	266.1	63.7	282.2	34.9	180.9	30.4	104.5	15.0	67.3	12.8
6-92.5-D1	2337	4934	632.8	2379	490.0	90.5	417.2	57.9	280.9	50.6	136.1	19.6	132.9	21.4
6-126-D1	1438	2906	356.3	1285	222.4	46.6	233.4	25.9	140.3	22.2	81.5	8.7	68.2	7.6
4-86.5-D2	2310	3740	423.9	1543	305.9	57.3	288.2	38.0	184.4	34.8	101.1	12.4	69.9	9.9
4-122-D2	2842	4545	667.0	2721	572.0	127.1	620.7	84.7	490.8	94.4	278.7	34.1	198.8	30.8
4-126-D2	1885	3151	431.0	1779	363.0	82.5	430.3	60.2	384.3	75.0	240.2	30.1	170.7	27.7
6-4-D2	1748	3014	366.6	1394	224.8	52.7	261.4	41.3	206.6	46.7	122.5	14.2	107.9	10.2
6-10D2	1612	2766	350.1	1416	271.4	61.8	251.4	40.1	225.9	47.7	141.7	20.6	104.6	20.9
6-12-D2	2002	3398	424.6	1689	366.7	73.6	368.7	52.9	311.2	62.0	194.4	22.9	135.3	23.7

Sample ID	La (ppb)	Ce (ppb)	Pr (ppb)	Nd (ppb)	Sm (ppb)	Eu (ppb)	Gd (ppb)	Tb (ppb)	Dy (ppb)	Ho (ppb)	Er (ppb)	Tm (ppb)	Yb (ppb)	Lu (ppb)
6-13-D2	1345	2020	240.5	1062	203.0	46.0	218.5	36.0	168.0	40.9	121.5	15.7	116.1	8.4
6-14-D2	1648	2473	318.0	1260	277.7	62.0	281.3	50.0	241.8	52.2	161.1	22.1	114.7	13.5
6-18-D2	1811	2808	375.6	1533	286.6	66.2	337.1	53.7	291.1	56.1	166.6	22.5	106.6	21.2
6-22-D2	1596	2853	364.5	1409	276.0	59.7	281.2	48.4	250.8	53.1	151.4	22.8	140.0	22.3
6-26-D2	1224	2065	285.4	1110	246.2	63.5	262.7	44.1	244.7	54.2	155.9	19.6	123.0	16.2
6-30-D2	1254	2047	266.5	1121	233.3	54.2	255.6	42.2	282.0	55.4	165.5	22.0	125.8	17.1
6-37.5-D2	1509	2509	306.5	1193	241.2	46.5	246.9	43.4	247.0	47.8	152.3	15.1	103.0	14.7
6-40-D2	2739	4921	648.4	2634	536.0	109.5	537.3	85.7	464.1	92.1	284.1	33.7	247.0	35.4
6-45-D2	1392	2256	290.5	1084	209.9	42.1	231.9	35.6	201.0	39.4	117.8	15.8	119.4	15.1
6-46.5-D2	4452	7696	955.0	3654	648.4	127.4	749.6	102.4	522.2	101.9	301.0	35.4	236.0	36.5
6-48-D2	1669	2841	372.6	1484	255.5	54.8	287.3	44.8	238.6	45.4	138.5	20.2	99.6	15.6
6-52-D2	2767	4665	606.0	2340	460.3	95.2	474.7	76.2	421.4	81.4	220.3	30.6	170.7	28.7
6-54.5-D2	2392	4133	511.2	1846	350.2	67.0	385.7	58.5	289.3	55.3	183.8	25.7	161.9	23.9
6-56.5-D2	2304	3388	399.2	1532	253.4	57.4	307.8	41.3	235.2	47.5	120.0	15.0	121.7	20.5
6-68-D2	2202	4042	471.7	1711	271.0	63.1	290.5	35.8	179.0	32.3	88.5	9.5	69.2	9.3
6-74-D2	2266	5301	680.7	2549	452.6	96.8	433.8	58.3	270.5	45.4	125.8	16.1	113.7	13.8
6-80-D2	3665	7302	854.1	3163	542.9	118.6	509.0	70.5	316.1	61.6	174.4	24.2	152.1	25.1
6-82-D2	3203	6202	730.3	2776	495.8	103.6	477.5	62.8	292.2	57.4	155.8	18.8	133.0	17.9
6-88-D2	3318	6636	786.0	2826	506.4	100.9	503.4	58.2	309.8	59.4	175.4	23.5	146.5	18.3
6-94-D2	2109	4564	558.2	2236	403.5	75.9	396.4	56.9	228.1	50.3	149.0	23.7	135.5	20.4
6-96-D2	3231	6455	753.4	2819	430.6	102.0	439.0	58.3	276.3	55.8	143.8	18.1	127.9	17.2
6-98-D2	1688	3252	392.9	1380	227.9	52.8	231.0	33.9	167.6	25.2	95.2	14.2	71.1	10.5
6-100-D2	1905	3895	468.9	1761	348.0	74.4	322.5	46.3	218.1	46.9	129.6	16.3	110.3	11.2
6-100-D2B	2881	5507	637.3	2336	348.6	75.5	379.5	49.0	225.0	44.5	123.1	13.1	96.7	11.5
6-106-D2	3364	6916	838.6	3100	523.6	124.2	531.5	72.6	355.8	63.3	175.8	23.6	190.9	21.4
6-112-D2	1205	2764	371.3	1498	281.0	56.9	269.0	38.5	250.5	45.0	131.5	17.7	123.4	15.0
6-116-D2	1943	3950	500.1	1719	330.5	75.1	300.2	44.5	185.6	35.1	99.7	16.2	89.7	11.1
6-124-D2	3030	6325	761.8	2745	500.4	95.6	466.3	60.7	320.2	53.3	144.5	21.5	117.4	17.9
6-128-D2	3963	8127	953.1	3614	593.5	116.1	570.9	80.6	386.0	74.1	189.4	23.3	151.4	19.6
4-86.5-D3	1969	4031	482.2	1817	315.3	68.0	285.7	34.4	166.4	30.2	90.5	10.9	71.5	11.3
6-4-D3	2462	4497	564.8	2144	387.4	87.0	417.3	56.9	305.6	59.4	180.2	21.9	148.7	25.3

Sample ID	La (ppb)	Ce (ppb)	Pr (ppb)	Nd (ppb)	Sm (ppb)	Eu (ppb)	Gd (ppb)	Tb (ppb)	Dy (ppb)	Ho (ppb)	Er (ppb)	Tm (ppb)	Yb (ppb)	Lu (ppb)
6-10-D3	2782	4386	534.8	1996	376.9	93.7	443.3	60.2	342.1	70.2	209.3	25.7	144.8	23.5
6-22-D3	1438	2920	399.0	1582	283.1	64.0	303.0	45.5	216.7	42.9	142.4	19.6	101.6	19.9
6-45-D3	1276	2476	306.6	1113	201.8	54.7	202.1	32.7	170.0	31.2	85.1	13.5	72.6	12.5
6-46.5-D3	3622	9955	1388	5180	1013	253.0	921.7	118.3	540.4	92.5	252.8	32.7	181.2	31.8
6-60-D3	7337	18192	2248	8239	1351	257.8	1364	160.4	711.0	129.1	356.6	47.9	261.3	37.3
6-76-D3	3591	7887	898.1	3222	471.9	290.5	469.6	48.7	180.8	25.3	72.6	7.0	41.5	8.2
6-92.5-D3	2151	4698	607.5	2299	442.6	105.0	461.7	60.5	331.2	59.9	175.7	18.9	133.3	24.6
6-98-D3	3068	6366	755.6	2929	516.9	141.8	533.7	61.3	273.8	48.0	126.4	14.3	82.2	12.4
6-100-D3	6328	15491	1967	7173	1280	194.7	1075	126.6	544.9	91.7	231.8	28.5	177.9	25.0
6-124-D3	10269	26918	3491	12991	2049	344.4	1909	210.5	774.9	118.1	353.7	35.4	211.6	31.8

APPENDIX 2

FLUID INLUSION DATA FOR CATOCHE CARBONATES AT DANIEL'S HARBOUR

Sample ID	Host Mineral	Occurrence	Degree of fill	T(m) first	Tm (H_2O)	Freezing point depression	Eq wt % NaCl (Bodnar 2003)	$T_{(h)}$
4-86.5	D3	cluster	0.95	-52	-19.2	19.2	21.82	171
4-86.5	D3		0.95		-18	18	20.97	171
4-86.5	D3		0.95		-17.5	17.5	20.60	171
4-86.5	D3		0.95		-18	18	20.97	175
4-86.5	D3		0.95		-17	17	20.22	160
4-86.5	D3	cluster	0.95	-56	-19.1	19.1	21.75	175
4-86.5	D3		0.95		-19	19	21.68	173
4-86.5	D3		0.95		-18.7	18.7	21.47	170
4-86.5	D3		0.95		-19	19	21.68	171
4-86.5	D3		0.95		-19	19	21.68	171
4-86.5	D3		0.95		-19	19	21.68	171
4-86.5	D3	cluster	0.95	-54	-19.4	19.4	21.96	190
4-86.5	D3		0.95		-19.4	19.4	21.96	190
4-86.5	D3		0.95		-19.1	19.1	21.75	184
4-86.5	D3		0.95		-19.3	19.3	21.89	186
4-86.5	D3		0.95	-56	-19.1	19.1	21.75	184
4-86.5	D3		0.95		-19.3	19.3	21.89	180
4-86.5	D3	cluster	0.95	-58	-18	18	20.97	178
4-86.5	D3		0.95		-18.4	18.4	21.26	171
4-86.5	D3		0.95		-19	19	21.68	171
4-86.5	D3		0.95		-19.8	19.8	22.24	180
4-86.5	D3		0.95			0		178
4-86.5	D3		0.95			0		174
6-120	D3	cluster	0.95	-50	-17	17	20.22	165
6-120	D3		0.95		-18	18	20.97	170

Sample ID	Host Mineral	Occurrence	Degree of fill	T(m) first	Tm (H_2O)	Freezing point depression	Eq wt % NaCl (Bodnar 2003)	$T_{(h)}$
6-120	D3		0.95		-17	17	20.22	158
6-120	D3		0.95		-18	18	20.97	172
6-120	D3		0.95		-18	18	20.97	170
6-120	D3		0.95		-18	18	20.97	170
4-86.5	D2	Cluster	0.95	-54	-23	23	24.34	124
4-86.5	D2		0.95		-23	23	24.34	124
4-86.5	D2		0.95		-22.5	22.5	24.02	122
4-86.5	D2		0.95		-23	23	24.34	124
4-86.5	D2		0.95		-22.5	22.5	24.02	122
4-86.5	D2		0.95		-23	23	24.34	123
6-26	D2	Cluster	0.95	-55	-23	23	24.34	123
6-26	D2		0.95		-22	22	23.70	125
6-26	D2		0.95		-23	23	24.34	126
6-26	D2		0.95		-18	18	20.97	120
6-26	D2		0.95		-21	21	23.05	128
6-26	D2		0.95			0		126
6-26	D2	Cluster	0.95	-52	-20	20	22.38	125
6-26	D2		0.95		-21	21	23.05	132
6-26	D2		0.95		-23	23	24.34	130
6-26	D2		0.95			0		126
6-26	D2		0.95			0		138
6-26	D2	Cluster	0.95	-52	-23	23	24.34	126
6-26	D2		0.95		-23	23	24.34	128
6-26	D2		0.95		-21	21	23.05	128
6-26	D2		0.95		-23	23	24.34	142
6-26	D2		0.95			0		148
6-26	D2		0.95			0		130
6-2	D2	Cluster	0.95	-55	-20	20	22.38	123
6-2	D2		0.95		-19.5	19.5	22.03	123

Sample ID	Host Mineral	Occurrence	Degree of fill	T(m) first	Tm (H_2O)	Freezing point depression	Eq wt % NaCl (Bodnar 2003)	$T_{(h)}$
6-2	D2		0.95		-20	20	22.38	123
6-2	D2		0.95		-21	21	23.05	128
6-2	D2		0.95			0		135
6-2	D2		0.95			0		138
6-2	D2		0.95			0		138
6-2	D2	Cluster	0.95	-48	-19	19	21.68	123
6-2	D2		0.95		-19	19	21.68	125
6-2	D2		0.95		-20	20	22.38	125
6-2	D2		0.80			0		128
6-2	D2		0.80			0		128
6-2	D2		0.80			0		134
6-8	D2	cluster	0.95		-21	21	23.05	119
6-8	D2		0.95		-21	21	23.05	123
6-8	D2		0.95			0		123
6-8	D2		0.95			0		125
6-8	D2		0.95			0		120
6-8	D2	cluster	0.95		-23	23	24.38	120
6-8	D2		0.95		-23	23	24.38	120
6-8	D2		0.95		-22	22	23.7	125
6-8	D2		0.95			0		125
6-8	D2		0.95			0		125
6-124	D2	cluster	0.95		-21	21	23.05	118
6-124	D2		0.95		-22	22	23.7	125
6-124	D2		0.95		-24	24	24.96	120
6-124	D2		0.95			0		134
6-124	D2		0.95			0		126
6-124	D2		0.95			0		148
6-124	D2	cluster	0.95		-22	22	23.7	148
6-124	D2		0.95		-24	24	24.96	134

Sample ID	Host Mineral	Occurrence	Degree of fill	T(m) first	Tm (H_2O)	Freezing point depression	Eq wt % NaCl (Bodnar 2003)	$T_{(h)}$
6-124	D2		0.95		-22	22	23.7	132
6-124	D2		0.95			0		130
6-124	D2	cluster	0.95		-22	22	23.7	124
6-124	D2		0.95		-21	21	23.05	122
6-124	D2		0.95			0		121
6-124	D2		0.95			0		122
6-124	D2		0.95			0		121
6-120	D2	cluster	0.95		-23	23	24.38	120
6-120	D2		0.95			0		113
6-120	D2		0.95			0		118
6-120	D2		0.95			0		128
6-120	D2	cluster	0.95		-23	23	24.38	121
6-120	D2		0.95		-23	23	24.38	126
6-120	D2		0.95					110
6-120	D2		0.95					128
6-120	D2		0.95					128
6-120	D2		0.95					128
6-120	D2	cluster	0.95		-23	23	24.38	158
6-120	D2		0.95		-23	23	24.38	162
6-120	D2		0.95		-22	22	23.7	162
6-120	D2		0.95					162
6-120	D2		0.95		-17	17	20.22	164
6-120	D2		0.95		-18	18	20.97	168
6-124	D2	cluster	0.95		-20.6	20.6	22.78	125
6-124	D2		0.95		-20.6	20.6	22.78	125
6-124	D2		0.95		-20.6	20.6	22.78	127
6-124	D2		0.95		-20.6	20.6	22.78	127
6-124	D2		0.95		-17	17	20.22	132
6-124	D2		0.95		-18	18	20.97	126

Sample ID	Host Mineral	Occurrence	Degree of fill	T(m) first	Tm (H_2O)	Freezing point depression	Eq wt % NaCl (Bodnar 2003)	$T_{(h)}$
6-124	D2		0.95		-16.4	16.4	19.76	126
6-124	D2	Cluster	0.95		-23.3	23.3	24.52	118
6-124	D2		0.95		-23.3	23.3	24.52	127
6-124	D2		0.95		-18	18	20.97	122
6-124	D2		0.95		-18	18	20.97	109
6-124	D2		0.95		-20	20	22.38	109
6-124	D2		0.95		-18	18	20.97	109
6-124	D2		0.95		-23.3	23.3	24.52	122
8-8	D2	Cluster	0.95					102
6-8	D2		0.95					104
8-9	D2		0.95					102
6-9	D2		0.95					102
8-10	D2		0.95					102
6-10	D2		0.95					112
4-106	C3	cluster						98
	C3							103
	C3							103
	C3							98
	C3							103
	C3	Cluster						108
	C3							108
	C3							108
	C3							103
	C3							105
	C3	cluster						92
	C3							92
	C3							98
	C3							103
	C3							98

APPENDIX 3

RESULTS OF FLUID INCLUSION GAS ANALYSIS

Sample	4-94 C1						Weighted
Crush#		8692b	8692c	8692d	8692e	8692f	8692g	Mean
H2		0.000	0.000	0.000	0.000	0.000	0.000	0.000
He		0.001	0.001	0.001	0.001	0.001	0.001	0.001
CH4		5.389	7.312	8.762	9.186	10.83	6.766	8.818
H2O		94.20	92.04	90.47	90.10	88.27	92.88	90.48
N2		0.263	0.377	0.422	0.458	0.590	0.218	0.435
O2		0.017	0.013	0.012	0.014	0.024	0.008	0.016
Ar		0.002	0.003	0.003	0.003	0.004	0.001	0.003
CO2		0.130	0.253	0.328	0.241	0.287	0.129	0.250

Sample	4-102 C1					Weighted
Crush#		8690b	8690c	8690d	8690e	8690f	Mean
H2		0	0	0	0	0	0
He		0.002	0.002	0.005	0.003	0.002	0.003
CH4		5.854	10.53	12.75	10.22	9.846	10.58
H2O		92.87	87.74	85.33	87.90	88.99	87.69
N2		0.398	0.707	0.905	0.929	0.489	0.769
O2		0.045	0.096	0.119	0.116	0.054	0.099
Ar		0.003	0.005	0.007	0.007	0.004	0.006
CO2		0.830	0.919	0.893	0.830	0.620	0.857

Sample	4-129 C1					Weighted
Crush#	8693a	8693b	8693c	8693d	8693e	Mean
H2	0	0	0	0	0	0
He	0.001	0.002	0.003	0.004	0.003	0.003
CH4	5.536	6.447	5.740	9.465	8.722	7.974
H2O	93.49	92.73	93.32	89.37	90.47	91.06
N2	0.172	0.168	0.230	0.302	0.237	0.242
O2	0.059	0.054	0.064	0.073	0.056	0.063
Ar	0.002	0.001	0.002	0.002	0.002	0.002
CO2	0.744	0.594	0.640	0.783	0.515	0.656

Sample	4-89.5 DI					Weighted
Crush#	8694a	8694b	8694c	8694d	8694e	Mean
H2	0	0	0	0	0	0
He	0.005	0.007	0.005	0.006	0.007	0.007
CH4	3.927	5.362	3.574	4.794	6.983	5.348
H2O	95.37	93.72	95.37	94.12	91.73	93.62
N2	0.341	0.532	0.374	0.466	0.552	0.494
O2	0.006	0.018	0.007	0.014	0.012	0.014
Ar	0.003	0.005	0.004	0.005	0.005	0.005
CO2	0.344	0.362	0.671	0.593	0.715	0.515

Sample	4-104 D1					Weighted
Crush#	8691a	8691b	8691c	8691d	8691e	Mean
H2	0	0	0	0	0	0
He	0.002	0.001	0.003	0.004	0.005	0.004
CH4	1.938	2.002	4.338	5.895	8.132	6.231
H2O	96.56	97.24	94.11	91.80	88.68	91.31
N2	0.143	0.202	0.289	0.396	0.580	0.437
O2	0.009	0.017	0.032	0.039	0.071	0.049
Ar	0.001	0.002	0.003	0.004	0.005	0.004
CO2	1.353	0.536	1.223	1.861	2.526	1.966

Sample	6-72 D1					Weighted
Crush#	8695a	8695b	8695c	8695d	8695e	Mean
H2	0	0	0	0	0	0
He	0.004	0.008	0.007	0.006	0.006	0.006
CH4	1.572	3.132	3.104	3.358	3.512	3.176
H2O	97.99	96.26	96.09	95.56	95.18	95.85
N2	0.111	0.186	0.188	0.196	0.208	0.190
O2	0.020	0.040	0.060	0.082	0.100	0.072
Ar	0.001	0.002	0.002	0.003	0.003	0.002
CO2	0.298	0.375	0.552	0.795	0.989	0.700

Sample	6-10 D2							Weighted
Crush#	8619a	8694b	8694c	8694d	8694e	8694f	8694g	Mean
H2	0	0	0	0	0	0	0	0
He	0.003	0.002	0.003	0.005	0.006	0.001	0.002	0.002
CH4	5.253	1.949	3.126	5.538	6.281	3.410	2.798	3.302
H2O	93.24	97.47	95.70	92.88	91.98	95.55	96.18	95.66
N2	0.552	0.243	0.409	0.615	0.669	0.437	0.396	0.411
O2	0.003	0.003	0.004	0.002	0.002	0.003	0.003	0.003
Ar	0.005	0.002	0.005	0.006	0.007	0.004	0.005	0.004
CO2	0.370	0.203	0.325	0.421	0.389	0.362	0.354	0.325

Sample	6-30 D2							Weighted
Crush#	8630a	8630b	8630c	8630d	8630e	8630f	8630g	Mean
H2	0	0	0	0	0	0	0	0
He	0.001	0.002	0.001	0.002	0.003	0.004	0.001	0.001
CH4	3.100	5.847	1.957	2.659	6.642	5.263	2.867	3.079
H2O	96.20	92.10	97.31	96.50	91.51	92.45	96.14	95.96
N2	0.238	0.429	0.164	0.205	0.494	0.432	0.333	0.266
O2	0.004	0.006	0.009	0.005	0.006	0.005	0.006	0.006
Ar	0.002	0.005	0.003	0.003	0.005	0.005	0.003	0.003
CO2	0.286	0.764	0.380	0.417	0.680	0.777	0.459	0.428

Sample	6-68 D2					Weighted
Crush#	8664a	8664b	8664c	8664d	8664e	Mean
H2	0.000	0.000	0.000	0.000	0.000	0.000
He	0.003	0.004	0.005	0.004	0.006	0.005
CH4	3.859	6.870	7.977	8.123	9.853	8.105
H2O	95.68	92.37	91.18	90.82	88.90	90.94
N2	0.200	0.376	0.349	0.405	0.447	0.386
O2	0.005	0.020	0.022	0.023	0.022	0.021
Ar	0.002	0.004	0.003	0.004	0.004	0.004
CO2	0.254	0.357	0.461	0.618	0.772	0.540

Sample	6-100 D3						Weighted
Crush#	8662a	8662b	8662c	8662d	8662e	8662f	Mean
H2	0	0	0	0	0	0	0
He	0.001	0.002	0.001	0.001	0.001	0.002	0.001
CH4	0.600	0.777	0.551	0.704	0.714	0.703	0.677
H2O	98.72	98.14	98.45	98.25	98.11	98.24	98.27
N2	0.122	0.219	0.108	0.105	0.068	0.086	0.103
O2	0.028	0.041	0.025	0.025	0.026	0.024	0.026
Ar	0.002	0.002	0.002	0.001	0.002	0.002	0.002
CO2	0.528	0.823	0.868	0.916	1.080	0.941	0.924

Sample	6-12 D3						Weighted
Crush#	8663a	8663b	8663c	8663d	8663e	8663f	Mean
H2	0	0	0	0	0	0	0
He	0.000	0.002	0.000	0.001	0.000	0.000	0.001
CH4	0.214	0.091	0.254	0.099	0.222	0.324	0.209
H2O	99.30	99.71	99.31	99.71	99.44	99.24	99.45
N2	0.346	0.115	0.268	0.074	0.165	0.241	0.184
O2	0.042	0.024	0.033	0.023	0.025	0.028	0.027
Ar	0.004	0.003	0.003	0.003	0.002	0.003	0.003
CO2	0.090	0.054	0.135	0.086	0.150	0.164	0.122

Sample	6-98 D3					Weighted
Crush#	8689a	8689b	8689c	8689d	8689e	Mean
H2	0	0	0	0	0	0
He	0.002	0.002	0.003	0.002	0.003	0.003
CH4	0.731	0.725	0.930	0.998	0.825	0.870
H2O	98.23	98.16	98.04	97.81	97.95	97.96
N2	0.178	0.146	0.209	0.175	0.114	0.151
O2	0.049	0.049	0.036	0.051	0.063	0.054
Ar	0.003	0.003	0.003	0.003	0.003	0.003
CO2	0.806	0.916	0.780	0.967	1.046	0.958